k

University of Stavanger

FACULTY OF SCIENCE AND TECHNOLOGY

MASTER THESIS

Study program/specialization:

Energy and Petroleum Engineering

The spring semester, 2022

Open access

Author:
Roy-Martin Nicholas

Roy. N

(Signature of the author)

Program coordinator:
Supervisor(s): Mesfin Belayneh
External supervisor(s): Espen Andreassen, **Equinor ASA**

Thesis title:

Analysis for model verification of Torque, Drag and Hydraulic Modules in Oliasoft Welldesign Software

Credits: 30

Keywords:
Torque
Drag
Buckling
Tension
ECD
Standpipe Pressure
Oliasoft^{TM}
Wellplan^{TM}

Number of pages: 86

+ Supplemental Appendices: 10

Date/year 15.06.2022

Stavanger

Acknowledgment

I would like to use this opportunity to thank the people that have contributed to the work of this thesis.

Firstly, I would like to thank Tore Weltzin, Leader D&W Tech – Equinor, for letting me work on the thesis in the Equinor office and for facilitating necessary arrangements.

Espen Andreassen, Leading Advisor Well Construction – Equinor, has been a tremendous help to me and has offered some of his extensive knowledge on topics related to the thesis as well as other facets of the business. For this, I am incredibly grateful. Thank you also for answering my software questions while I was working with the thesis at Equinor. In addition, I would like to thank all the Equinor Employees who contributed to my work on this thesis.

I also would like to thank Farzad Shoghl, Principal Engineer D&W Tech – Equinor, for all the help contributed in during this thesis, and for guiding me through the hydraulics part.

In addition, I would like to thank my family for support in the months spent working on the thesis. Especially my father who have given me a big helping hand from the beginning to the very end.

Finally, I would want to express my gratitude to Mesfin Belayneh, my faculty supervisor, for patiently guiding me through this process and for being so kind and helpful.

Abstract

Drilling through the subsurface is a complicated process that frequently results in technical challenges. Understanding and anticipating drilling problems, as well as their causes and planning remedies, are essential for achieving the objective effectively. Pipe sticking, lost circulation, wellbore deviation, pipe failures, borehole instability, mud contamination, formation damage, and hole cleaning are the most prevalent drilling difficulties. To understand the mechanical behavior of the drill string and the wellbore state, and hence to predict and prevent downhole issues, torque, and drag modelling is crucial. In the well-drilling sector, torque and drag have been modelled using the soft string and stiff string methods. This thesis will investigate torque and drag simulations in the wellbore and provide an overview of the Oliasoft Welldesign^{TM} (OWD) software and if it is in range of Equinor’s requirement

Also, the hydraulic module must be taken into consideration for understanding and anticipating challenges while drilling. This thesis will investigate how the Standpipe Pressure (SPP) and Equivalent Circulating Density (ECD) will be affected when drilling in different depths and directions. Finally, the results from OWD will be compared to Wellplan (WP) and real time drilling data to see if OWD can used in the Equinor systems.

The OWD simulation analysis comparing with the WP showed that

- The Oliasoft torque, effective tensions, and hydraulics well design module results are within the acceptable range set by Equinor.
- One out of the considered eight wells, the buckling limit exhibited about 15.4%deviation from WelllPlan^{TM} software. This thesis therefore suggests Equinor to do further investigation.

Contents

Acknowledgment I

Abstract II

List of figures VII

List of tables VIII

List of Abbreviations IX

1 Introduction 1

1.1 Motivation and Problem formulation 1
1.2 Objective 2
1.3 Research Methods 2

2 Theory 4

2.1 Torque and Drag – Oliasoft 4
  2.1.1 Basic torque and drag (Soft String) 4
  2.1.2 Semi stiff string model 5
  2.1.3 Friction – contact surface effect 6
  2.1.4 Mud effects 6
  2.1.5 Von Mises Stresses 8
  2.1.6 Bending stress 8
  2.1.7 Bending force – Stiff string emulation 8
  2.1.8 Buckling force limit 8
  2.1.9 Buckling types 10
  2.1.10 Buckling pitch and period 10

2.2 Torque and Drag – Wellplan 11
  2.2.1 Drag model 11
  2.2.2 Curvilinear Model 13
  2.2.3 Viscous Drag 14
  2.2.4 Torque on pipe 15
  2.2.5 Buoyed Weight 15

2.2.6 Pipe Wall Thickness Modification ... 16
2.2.7 Stiff String Model ... 17
2.2.8 Loading and Unloading Models ... 19
2.2.9 Buckling Limit Factor ... 20

2.3 Hydraulics – Oliasoft ... 23
2.3.1 Fluid mechanics flow equations ... 24
2.3.2 Pressure loss calculation in annulus ... 24
2.3.3 Pressure loss calculation in pipe ... 27
2.3.4 Pipe and annulus velocity ... 28
2.3.5 Equivalent Circulating Density (ECD) ... 28
2.3.6 Drill bit calculation ... 29
2.3.7 Hole cleaning ... 29

2.4 Hydraulics Model – Wellplan ... 31
2.4.1 Herschel-Bulkley Rheology Model ... 32
2.4.2 ECD ... 33
2.4.3 Pressure Loss in Annulus and Pipe ... 34
2.4.4 Bit Pressure Loss ... 37

3 Software Simulation and Field Data Comparisons ... 38

3.1 Torque and Drag ... 38
3.1.1 Valemon B-13 ... 38
3.1.2 14x13 5/8” Section – Drag simulation ... 43
3.1.3 12 ¼” drilling Section ... 45
3.1.4 9 7/8” Section ... 49
3.1.5 Oseberg Sør K-12 A ... 51
3.1.6 12” Section ... 51
3.1.7 8 ½” drilling Section ... 55
3.1.8 Kvitebjørn A-12 B ... 59
3.1.9 7” Liner Section ... 59
3.1.10 Gullfaks ... 61
3.1.11 9 5/8” Liner Section ... 61

3.2 Hydraulics ... 62

3.2.1 Valemon 62
3.2.2 12 ¼” Section 62

3.3 Oseberg Sør 64
3.3.1 12” Section 64
3.3.2 8 ½” Section 66

3.4 Summary of the Torque & Drag and Hydraulics 68
3.4.1 Torque & Drag 68
3.4.2 Pressure losses 68

4 Results Analysis and Verification 70

4.1.1 Rotating Off Bottom 70
4.1.2 Pulling Out Off the Hole 71
4.1.3 Running Into the Hole 71
4.1.4 Buckling limit 72
4.1.5 Yield limit 72
4.1.6 Torque 73
4.1.7 Standpipe Pressure 73
4.1.8 Equivalent Circulating Density 73

5 Conclusion 74

6 References 75

7 Appendix 77

7.1 Valemon 77
7.1.1 B-13 A: Drill 17 ½” section 77
7.1.2 B-13 A: Drill 12 ¼” section 78
7.1.3 B-13 A: Run 13 5/8”x14” casing 79
7.1.4 B-13 A: Run 9 5/8” casing 80

7.2 Oseberg Sør 81
7.2.1 K-12 AHT2: Drill 12 ¼” Section 81
7.2.2 K-12 AHT2: Drill 8 ½” Section 83

7.3 Kvitebjørn 84

7.3.1 A-12 B: Run 7” liner 84
7.4 Gullfaks: 85
7.4.1 C-21 A: Run 9 5/8” liner 85

List of figures

Figure 1.1: Summary of Reasearch programs employed in this thesis........................ 3
Figure 2.1: Illustration of forces operating on a segment in an inclined hole............... 12
Figure 2.2: Illustration of velocity vectors impacting on a drill string 12
Figure 2.3: The Stiff String Model in Torque and Drag Analysis [17]............................ 17
Figure 2.4: Inclined Beam Section [17] 18
Figure 2.5: Idealized Beam Section with End Loads Caused by Weight W [17]......... 19
Figure 2.6: Loading and unloading scenarios 19
Figure 3.1: Simulated ROB hookload vs real-time ROB data 39
Figure 3.2: Simulated RIH hookload data vs real-time RIH hookload data.................. 40
Figure 3.3: Simulated POOH hookload data vs real-time POOH hookload data........ 41
Figure 3.4: Simulated ROB torque data vs real-time ROB torque data........................ 42
Figure 3.5: Simulated RIH hookload data vs real-time RIH hookload data.................. 43
Figure 3.6: Simulated POOH hookload data vs real-time POOH hookload data........ 44
Figure 3.7: Simulated ROB hookload data vs real-time ROB hookload data 45
Figure 3.8: Simulated RIH hookload data vs real-time RIH hookload data.................. 46
Figure 3.9: Simulated POOH hookload data vs real-time POOH hookload data........ 47
Figure 3.10: Simulated ROB torque data vs real-time ROB torque data...................... 48
Figure 3.11: Simulated RIH hookload data vs real-time RIH hookload data 49
Figure 3.12: Simulated POOH hookload data vs real-time POOH hookload data...... 50
Figure 3.13: Simulated ROB hookload data vs real-time ROB hookload data............ 51
Figure 3.14: Simulated RIH hookload data vs real-time RIH hookload data 52
Figure 3.15: Simulated POOH hookload data vs real-time POOH hookload data...... 53
Figure 3.16: Simulated ROB torque data vs real-time ROB torque data...................... 54
Figure 3.17: Simulated ROB hookload data vs real-time ROB hookload data............ 55
Figure 3.18: Simulated RIH hookload data vs real-time RIH hookload data 56
Figure 3.19: Simulated POOH hookload data vs real-time POOH hookload data...... 57
Figure 3.20: Simulated ROB torque data vs real-time ROB torque data...................... 58
Figure 3.21: Simulated RIH hookload data vs real-time RIH hookload data 59
Figure 3.22: Simulated POOH hookload data vs real-time POOH hookload data...... 60
Figure 3.23: Simulated RIH hookload data vs real-time RIH hookload data 61
Figure 3.24: Simulated SPP data vs real-time SPP data... 63

Figure 3.25: Simulated ECD data vs real-time ECD data 64
Figure 3.26: Simulated SPP data vs real-time SPP data 65
Figure 3.27: Simulated ECD data vs real-time ECD data 66
Figure 3.28: Simulated SPP data vs real-time SPP data 67
Figure 4.1: Excel sheet containing ROB hookload data from OWD and WP and the percentage difference between them 70
Figure 4.2: Excel sheet containing ROB hookload data from OWD and WP and the percentage difference between them 71
Figure 4.3: Excel sheet containing ROB hookload data from OWD and WP and the percentage difference between them 71
Figure 4.4: Excel sheet containing ROB hookload data from OWD and WP and the percentage difference between them 72
Figure 4.5: Excel sheet containing ROB hookload data from OWD and WP and the percentage difference between them 72
Figure 4.6: Excel sheet containing ROB hookload data from OWD and WP and the percentage difference between them 73
Figure 4.7: Excel sheet containing ROB hookload data from OWD and WP and the percentage difference between them 73
Figure 4.8: Excel sheet containing ROB hookload data from OWD and WP and the percentage difference between them 73

List of tables

Table 2.1: Helical buckling scaling factors [17] 21
Table 2.2: Helical buckling Scaling factors and BLF [17] 23

List of Abbreviations

BHA	Bottom hole assembly
BLF	Buckling Limit Factor
ECD	Equivalent circulating density
FF	Friction Factor
lpm	Liter per minute
MD	Measured Depth
MW	Mud Weight
NCS	Norwegian Continental Shelf
OBM	Oil Based Mud
OP	Over pull
POOH	Pull out of Hole
P/U	Pick up
PWD	Pressure while drilling (ECD / ESD)
ROB	Rotation off bottom
ROP	Rate of penetration
RIH	Run into hole
RPM	Rotations per minute
RT	Real Time
SPP	Standpipe pressure
TVD	True Vertical Depth
WOB	Weight on bit
YS	Yield Stress

1 Introduction

As contemporary drilling becomes longer and more intricate, so does its complexity. It is more difficult to reach the target depth. Simulation software such as Wellplan (WP) is utilized not only in the planning phase, but also in real-time drilling to evaluate any issues that may arise during drilling and well operations. To reduce costs and risks in the oil business, it is important that the software is accurate.

This study's purpose is to analyze software model verification for the software Oliasoft Welldesign (OWD). This study will concentrate on torque, drag, and hydraulics modules. The results of OWD will be compared against WP, the software currently utilized by Equinor, and real-time drilling data. In addition, the variances will be discussed and evaluated in terms of OWD software validation.

1.1 Motivation and Problem formulation

Drilling is a cost factor for the industry. Prior to drilling, it is essential to perform appropriate designs in order to drill safely and reduce undesired expenditures. For instance, among others design activities:

- During well construction, tubulars should carry the loading without being failed. Moreover, the combined loading in the tubular should not cross the yield strength.
- In order to lift cutting all the way to the surface, the efficiency of the pump should be strong enough. Moreover, the well pressure should be precisely determined to make sure that well instability issues will not occur.

For the design and analysis, it is common to use software. For instance, for drilling - Landmark/**Wellplan^{TM}** module solve design issues such as: Torque and Drag, Hydraulics, Well Control, Stuck pipe, Swab/Surge can be mentioned. The Halliburton/Landmark software is widely used in the industry. The Landmark software modules are built independently. For instance, **Wellplan^{TM} module** (for drilling), **StressCheck^{TM} module** (for Casing/Tubing design and Cost analysis), **WelCat^{TM} module** (Casing, Tubing, Production, Multistring) design software, **Compass^{TM}** (Survey), and **Wellcost^{TM}** are just to mention. Equinor use Landmark software to design almost all the wells in the Norwegian Continental Shelf (NCS).

Oliasoft is a new company that aims to develop a software product. The software is a well design tool that provides similar features as the ones available in Landmark modules. The unique characteristics of Oliasoft is that the well planning calculations are designed in one single cloud application.

Equinor recently is considering the possible use of Oliasoft for designing wells. For this, before licensing and usage of the application, Equinor is interested in checking how the results obtained from the Oliasoft is similar with the one commonly used Landmark**/WellPlan^{TM} (WP)** software.

With the limited research period and with agreement with Equinor, this thesis will address issues to be analyzed with Landmark/**WellPlan^{TM} (WP)** and **Oliasoft Well Design** (**OWD**) such:

- ✓ The prediction of drill string mechanics.
- ✓ The prediction of hydraulics, ECD.

1.2 Objective

The primary objective of this thesis is to answer the research questions addressed in section §1.1. For this the activities are:

- ➢ Review the theory behind Oliasoft and WellPlan associated with drill string mechanics and hydraulics calculators
- ➢ Build simulation cases based on field used well and operational data to simulate drill string mechanics and Hydraulics Oliasoft and WellPlan
- ➢ Compare the simulation results obtained from the two simulators with the field data
- ➢ Finally, verification of the Oliasoft software through analysis obtained from the comparison with WellPlan and Field data. The performance of Oliasoft prediction will be assessed based on the percentile deviation from Wellplan in the torque and drag section, and Field data in the hydraulics section and check if the results are within the acceptable requirement set by Equinor.

1.3 Research Methods

Figure 1.1 displays the summary of the research program employed in this thesis work. The first part deals with the review of WellPlan^{TM} and Oliasoft^{TM} theories used to calculate the Torque and Drag, Stress in drill string and Hydraulics.

The second part deals with simulation studies conducted by WellPlan and Oliasoft to be compared with several Field dataset obtained from the NCS.

Finally, the results will be compared in order to verify the possible application of Oliasoft for Equinor well planning purpose.

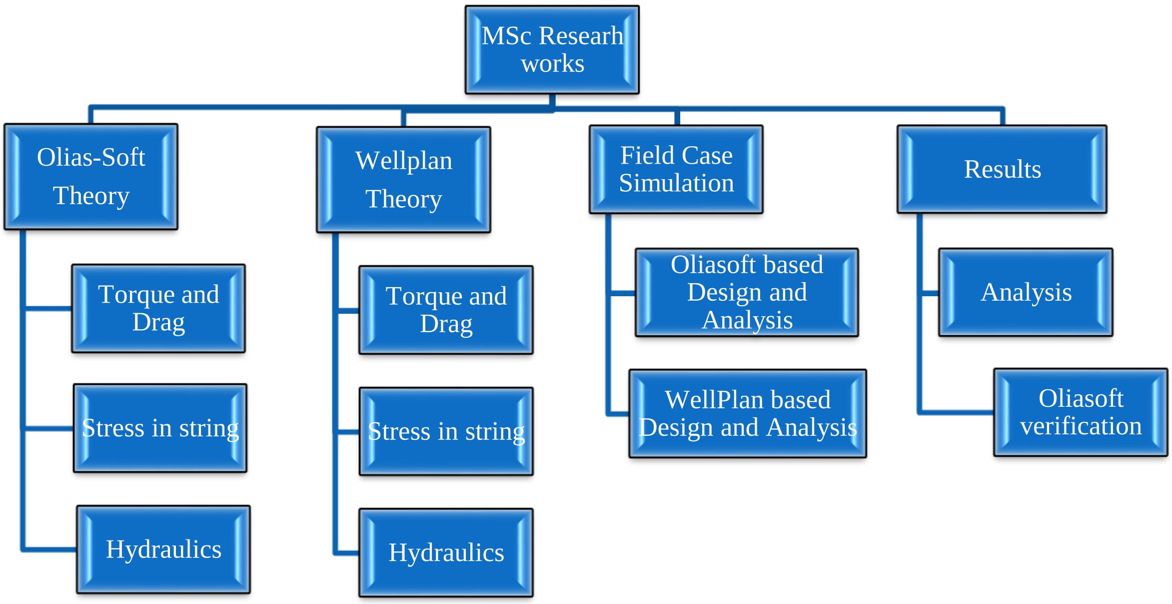

Figure 1.1: Summary of Reasearch programs employed in this thesis

2 Theory

To better understand the results given in both Oliasoft's Welldesign (OWD) and Landmark's Wellplan (WP) later in the thesis, one must look at the theory behind the different software's. First, there will be a briefing of the Torque & Drag section in both software's, then the Hydraulics section.

Hydraulic model which OWD are based on, has some differences and simplification with other hydraulic models which can be discussed. However, it will not be done in this study

2.1 Torque and Drag – Oliasoft

OWD includes among its models the so-called "soft string model" for torque and drag calculations. The "soft string model" was first described in [12] and assumes that the drill string in an inclined well is constantly resting on the bottom of the well bore. When a well is vertical, the drill string is positioned freely in the bore's center. Thus, the friction is determined by the string weight and geometry, the "weight on bit" (WOB), the angular velocity, the geometry of the well bore, and the material of the well bore wall. The "stiff string model" accounts for the fact that the drill string is stiff but elastic.

2.1.1 Basic torque and drag (Soft String)

The drill string's tip is the reference point for these calculations. It can either be a compressive force on the drill bit toward the bed rock (the WOB) and the assumed torque, or the drill string tip might be "hanging" freely within the well hole. This allows for the calculation of forces in the string. The side force depends on the tension or compression in the string and the geometry of the well bore. The function is:

$$\frac{dF_{\perp}}{dl} = \sqrt{(F_d sin\alpha \frac{d\phi}{dl})^2 + \left(F_d \frac{d\alpha}{dl} + g\frac{dm}{dl}\sin\alpha\right)^2} \qquad (1)$$

Where,

$dl = lenght\ of\ the\ element$
$F_d = tension\ from\ below\ the\ element$
$\alpha = inclination\ angle\ of\ the\ element$
$\phi = azimuth\ angle$
$dm = mass\ of\ the\ element$
$g = gravitatinal\ constant$

A simple study of equation (1) reveals that F_d can take both positive and negative values. The drill string is compressed by a negative tension. The side force is independent of the sign of the turn, $d\phi/dl$, but dependent on the sign of the build, $d\alpha/dl$. Thus, tension in the subsequent element can be determined by adding the weight and frictional force:

$$\frac{dF_d}{dl} = g\frac{dm}{dl}cos\alpha + \left(\mu\frac{dF_\perp}{dl} + \frac{dF_{mud}}{dl}\right)\sin\left(tan^{-1}\left(\frac{v}{r_p\omega_{rot}}\right)\right) \tag{2}$$

Where,

$\mu = friction\ coefficient$
$F_{mud} = frictional\ force\ on\ the\ pipe\ caused\ by\ mud\ flow$
$v = rate\ of\ penetration(ROP)$
$r_p = outer\ radius\ of\ drill\ string$
$\omega_{rot} = angular\ frequency\ of\ drill\ string$

To account for the fact that friction force is a vector, equation (2) is dependent on the ROP to rotation velocity ratio. This modification term for the frictional portion of the tension equation goes towards 1 when $f_{rot} \to 0$ and goes towards 0 when $v \to 0$.

The formula for torque is as follows:

$$\tau = \left(\mu F_\perp r_p + \tau_{mud}\right)\cos\left(tan^{-1}\left(\frac{v}{r_p\omega_{rot}}\right)\right) \tag{3}$$

Where, t_{mud} is the frictional torque on the pipe caused by relative movement of the mud on the pipe surface

The torque is basically proportional to the friction, since $v \ll r_p \cdot \omega_{rot}$ in most cases.

2.1.2 Semi stiff string model

In reference [2], Aadnoy developed a torque and drag model in which the frictional drag considers both build (changes in inclination) and turn (changes in azimuth). For each straight section, the Johancsik et al. standard model is applied; equation (2). The 3D model is dependent on the dogleg, $\Delta\theta$, and the change in drag over a component is as follows:

$$\Delta F_{top} = F_{low}\left(e^{\pm|\Delta\theta \cdot dl|} - \sigma_{rot}\right) + \frac{dm}{dl} \cdot d\mathrm{h}_{TVD} \tag{4}$$

$$\sigma_{rot} = \begin{cases} 0, if\ \omega_{rot} = 0 \\ 1, if\ \omega_{rot} > 1 \end{cases} \tag{5}$$

Where,

$F_{low} = force\ action\ on\ the\ low\ side\ of\ the\ section$

$\sigma_{rot} = stress$

When "dogleg filtering" asserts that the drill string can be straight within the open hole or casing section, the conventional "soft string model" is also employed. Similar to the method given by Tveitdal in [4], the filter is applied based on a purely geometric consideration.

2.1.3 Friction – contact surface effect

Maidla and Wojtanowicz [5] determined that friction between a rod and a flat surface differs from when the rod is lying inside a larger pipe. They offered a modification to K's friction:

$$d = \frac{\pi F_{\perp} r_{conn}}{12 E w_p} \tag{6}$$

$$Y = 0.5\,\frac{|r_b^2 - r_{conn}^2 + (r_b - r_{conn} + d)^2|}{r_b - r_{conn} + d} \tag{7}$$

$$X = \sqrt{|\ r_{conn}^2 - Y^2\ |} \tag{8}$$

$$\gamma = tan^{-1}\frac{X}{Y - r_b + r_{conn}} \tag{9}$$

$$K_{\mu} = \frac{2\gamma}{\pi\left(\frac{4}{\pi}\right) + 1} \tag{10}$$

2.1.4 Mud effects

As may be seen from equations (2) and (3), the mud contributes friction to the equation. The frictional forces induced by moving mud are evaluated in [6](Mitchell) and executed accordingly. This added friction produces modest modifications to the simulation, but Mitchell do endorse this strategy because it accounts for the higher drag. It is implemented as follows in OWD:

$$\frac{dF_{mud}}{dl} = \frac{dp}{dl}\frac{\pi(r_b^2 - r_p^2)r_p}{r_b - r_p} \tag{11}$$

$$\frac{d\tau_{mud}}{dl} = \tau_s 2\pi r_p^2 \tag{12}$$

Where,

$\frac{dp}{dl} = pressure\ drop$
$r_b = radius\ of\ open\ \mathrm{hole}$
$\tau_s = \mathrm{sh}ear\ stress\ in\ \mathrm{th}e\ mud$

$r_p = outer\ radius\ of\ drill\ string$

If the mud is not moving, these factors will be 0, and a simple order of magnitude analysis shows that in normal cases, we have the following:

$$\frac{dF_{mud}/dl}{dF_d/dl} \ll 1, \tag{13}$$

$$\frac{dF_{mud}/dl}{dm/dl} \ll 1, \tag{14}$$

$$\frac{d\tau_{mud}/dl}{dr/dl} \ll 1 \tag{15}$$

Regardless of whether the mud is moving, it will cause buoyancy in the element dm. The buoyant weight is the weight of an element in air minus the weight of the mud it displaces.

$$\frac{dm}{dl} = \rho_p \pi (r_p^2 - r_{in}^2)(1 - \frac{\rho_m^{out} r_p^2 - \rho_m^{in} r_{in}^2}{\rho_p (r_p^2 - r_{in}^2)}) \equiv \frac{dw}{gdl} \tag{16}$$

Where,

$\rho_p = density\ of\ pipe$
$\rho_{in}^{out} = density\ of\ mud\ in\ annulus$
$\rho_{min} = density\ of\ mud\ in\ pipe$
$r_{in} = inner\ rafius\ of\ pipe$

In a situation when the mud is not flowing, the density of the mud inside the pipe and in the annulus will be identical. However, if the mud is flowing, this will not be the case. This disparity between the internal and external pressures also plays a significant role in defining the buckling limits, which will be explored later.

The pressure losses, dp/dl, must be known along the entire flow path in order to calculate the pressure in the pipe and annulus. More about this in the “Hydraulics” section.

2.1.5 Von Mises Stresses

The Von Mises stress on the element dl is computed in a conventional manner. First, a three-dimensional stress matrix is calculated. As acceleration in the element is absent, the matrix is symmetrical. Therefore, the Von Mises stress can be found by solving this matrix. [16]

2.1.6 Bending stress

The bending stress is calculated from the compression of the drill string and its curvature coming from the curvature of the well bore: [16]

$$\sigma_{bend} = \frac{E}{2}(1 - \cos(\Delta\theta \cdot dl)) \tag{17}$$

Where,

E is Youngs Modulus for the material.

2.1.7 Bending force – Stiff string emulation

Stiff string modelling refers to the consideration of the drill string's stiffness. In OWD, an emulation of these effects is available. When the pipe is bent via a build or turn section, the bending force can be calculated. Since the connection usually has a larger outer diameter than the pipe body, it is also feasible to bend the pipe further so that not just the connectors touch the wall. Calculating the lateral force component from the dogleg of the drill string segment:

$$F_{\perp}^{bend} = \frac{4}{3}E\Delta\theta\left(r_p^3 - r_{in}^3\right) \cdot \sin\left(\Delta\theta \cdot dl\right) \tag{18}$$

The side forces, as computed by Equation (1), are a function of the string tension, therefore a portion of the lateral component will be absorbed by the material's elasticity (as long as one is below the material yield strength). OWD has the option to include these computations, so changing the normal force by the physical force required to bend a component.

2.1.8 Buckling force limit

Buckling limit calculations have been implemented as suggested by R. F. Mitchell [6]. The approach is to calculate the critical limit from:

$$F_c = \sqrt{\frac{4EIw_c}{r_c}} \tag{19}$$

$$I = \frac{\pi}{4}\left(r_p^4 - r_{in}^4\right) \tag{20}$$

$$r_c = r_b - r_p \tag{21}$$

$$\frac{dw_c}{dl} = (\frac{dF_\perp}{dl})_{F_d=F_c} \tag{22}$$

Where,

$E = Young's\ modulus$
$I = Second\ momemt\ of\ area$
$w_c = Contact\ force\ between\ pipe\ and\ bore\ wall$
$r_c = Radial\ clearance\ between\ pipe\ and\ bore\ wall$
$F_c = Critical\ force$

When the drill pipe is rotating, the contact force becomes:

$$w_f = \frac{w_c}{\sqrt{1-\mu^2}} \tag{23}$$

The implementation numerically solves this set of equations.

According to Mitchell in [6], the presence of mud creates axial stiffness. The equation that describes the addition of the extra stiffness to the force limit is:

$$F_{axial} = (p_{in} + \rho_{in}v_{in}^2)A_{in} - (p_{out} + \rho_{out}v_{out}^2)A_{out} \tag{24}$$

Where subscript in and out refers to inside and the outside of the drill pipe, respectively.

Where,

$v = Superficial\ velocity\ of\ the\ mud$
$p = Pressure$
$\rho = Density$

As seen by equation (22), the buckling force approaches zero as the inclination approaches zero. This is true if there is no support, and the length of the pipe is infinite ("Euler buckling"). According to Lubinski, Nwonodi, Adali, Tswenma in [7] and [8], this is to be computed as follows:

$$F_c = \sqrt[3]{w_b^2 \pi^2 EI} \tag{25}$$

2.1.9 Buckling types

If the buckling force limit is exceeded by compressive forces in the drill string, the implementation classifies the buckled state as:

$$1.38 \leq \frac{F_d}{F_c} < 2.60 \ - Lateral\ Buckling \tag{26}$$

$$2.60 \leq \frac{F_d}{F_c} < 3.88 \ - Semi\ \mathrm{h}elical\ Buckling \tag{27}$$

$$3.88 < \frac{F_d}{F_c} \ - Full\ \mathrm{h}elical\ Buckling \tag{28}$$

Where,

$$F_d = compressive\ forces\ in\ drill\ string$$

It is suggested to use $\sqrt{2}$ and $2\sqrt{2}$ for 1.38 and 2.6 in equations (29) and (30), but analytic solutions in [9] suggest these are the most correct numbers to use, thus they are kept as suggested by Mitchell.

2.1.10 Buckling pitch and period

When the algorithm finds that the drill string buckles, the pitch for the segment in question is also determined. When the lateral buckling criteria is met, the pitch is computed using the "beam-column" model by Huang [11] as recommended by Lubinski, Althouse and Logan in [10]. This is accomplished by calculating the length of the period for lateral buckling:

$$L = \frac{1}{K_{SF}} \cdot \sqrt[3]{\frac{n^2 \pi^2 EI}{w}} \tag{29}$$

where K_{SF} is a safety factor in the range 1.1 - 1.2 with default 1.15, and n is the number of sinusoidal half periods.

If the criterion for helical buckling is satisfied, the pitch, p , of the helix is calculated as follows:

$$p = \sqrt{\frac{8\pi^2 EI}{F_d}} \tag{30}$$

The maximum bending stress in this section of the buckled pipe is:

$$\sigma_{max} = \frac{r_b r_c F_d}{2I} \tag{31}$$

2.2 Torque and Drag – Wellplan

The **WellPlan™** software is the latest evolution in over 20 years of innovations in well-construction information solutions. Integrated together with Engineer's Desktop™ and Engineer's Data Model™ (EDM™) applications, it provides the one of the most complete and unparalleled well-engineering software tool kit in the industry. Torque and drag, hydraulics, centralization, swab & surge, and friction calibration capabilities available in the WellPlan™. Using the WellPlan™ software, one can analyze torque and drag, hydraulics, casing centralization, swab & surge, and underbalanced hydraulics.

Plan and analyze drilling, casing, and completion running operations, and assess the impact of predicted loads related to torque and drag. Main calculations are Tension, Torque, Side force, Fatigue, and Tri-axial Stress. The analysis allows users to know accurate forces acting along the string all the way down to the bottom of the well based on surface parameters. The software also accounts for the effect of hydraulic parameters like fluid properties, flow rate, diverse fluid columns, and pressures. Temperature effect on the string is also considered for the pipe stretch calculations. Riser-less and inner-string configurations are also modeled as well as the effect of stand-off devices like centralizers and friction reduction devices. [17]

2.2.1 Drag model

The side, or normal force, is a measurement of the force imposed on the string by the wellbore. The forces operating on a tiny segment of string lying in an inclined hole are depicted in the diagram below. In figure 2.1, the section is stationary. This illustration demonstrates that the normal force acts perpendicular to the inclined surface. The string's weight exerts a downward force in the direction of gravity.

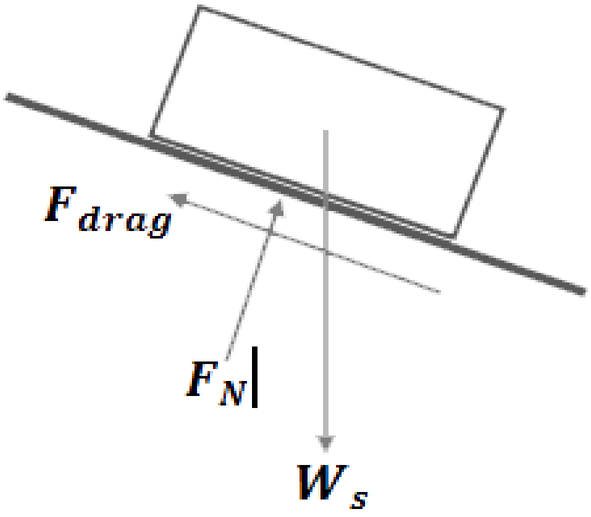

Figure 2.1: Illustration of forces operating on a segment in an inclined hole

The portion is also being acted upon by a second force, called the drag force. Always acting in the opposite direction of motion is the drag force. Because of drag, the piece does not slide down the inclined plane. The magnitude of the drag force is proportional to the normal force and the coefficient of friction between the inclined plane and the segment. The coefficient of friction describes the friction between the wellbore wall and string.

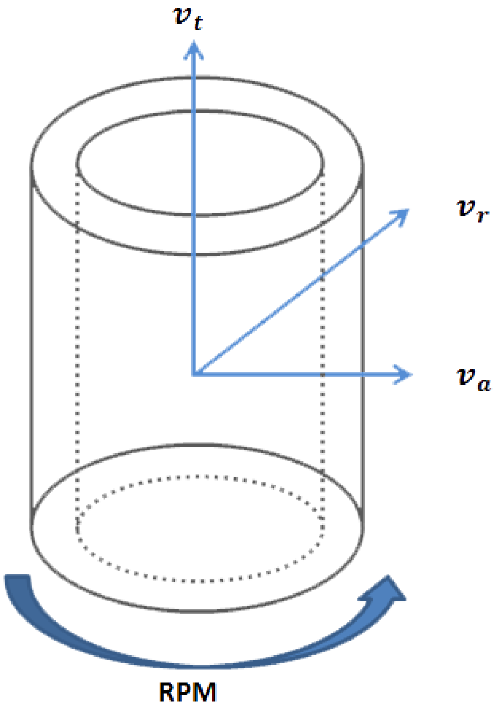

Figure 2.2: Illustration of velocity vectors impacting on a drill string

$$F_{drag} = \mu F_N \left(\frac{v_t}{v_r}\right) \tag{32}$$

$$v_r = \sqrt{v_t^2 + v_a^2} \tag{33}$$

$$T = r\mu F_N \left(\frac{v_a}{v_r}\right) \tag{34}$$

Where,

$F_{drag} = Drag\ force$
$F_N = Normal\ force$
$r = Radius\ of\ component$
$T = Torque$
$v_a = Angular\ speed$
$v_r = Resultant\ speed$
$v_t = Trip\ speed$
$\mu = Coefficient\ of\ friction\ (friction\ factor)$

Drag is the increased/decreases surface weight compared to the weight of a free-rotating drill string. Typically, this additional load is positive when pulling out of the hole and negative when running into the hole. The drag force is mostly caused by the drill string' s contact with the wellbore, which generates friction.

2.2.2 Curvilinear Model

For a torque drag analysis, the string is divided into 30-foot sections by the Landmark software Wellplan. The Straight Model assumes each section is of constant inclination. The Curvilinear Model considers the inclination (build or drop) change within each 30-foot section. In hole sections where there is an angle change, compression in the pipe through the doglegs causes extra side force. The additional side force acts to stabilize the pipe against buckling unless the pipe is dropping angle.

$$F_c > 2\left(\sqrt{\frac{EIW_c}{r_{cl}}}\right) \tag{35}$$

$$W_c = 2\left(\sqrt{(W_t sin\theta + F_c\epsilon') + F_c^2 sin^2\theta\epsilon'^2}\right) \tag{36}$$

Where,

$E = Young's\ modulus$
$F_c = Compressive\ axial\ force$
$I = Moment\ of\ inertia$
$r_{cl} = Radial\ clearance\ between\ wellbore\ and\ component$
$W_c = Contact\ load$
$W_t = Tubular\ weight\ in\ mud$
$\epsilon = Wellbore\ direction(azimuth)$
$\theta = Inclination$

2.2.3 Viscous Drag

Viscous drag is an additional drag force acting on the string due to hydraulic effects while tripping or rotating. The fluid forces are determined for "steady" pipe movement, and not for fluid acceleration effects.

The additional force due to viscous drag is calculated as follows. Note that this drag force is added to the drag force calculated using drag force calculations.

$$\Delta F_{vd} = \frac{\pi \Delta p_{loss}(d_h^2 - d_p^2)d_p}{4(d_h - d_p)} \tag{37}$$

Where,

$\Delta F_{vd} = Additional\ force\ due\ to\ viscous\ drag$

$d_h = Hole\ diameter$
$d_p = Pipe\ diameter$

$\Delta p_{loss} = Annular\ pressure\ loss\ calculated\ according\ to\ selected\ rhelogical\ model$

There are no direct computations of fluid drag due to pipe rotation. The method shown here is derived from the analysis of the Fann Viscometer given in Applied Drilling Engineering[22].

The shear rate in the annulus due to pipe rotation is computed using the following equation.

$$\gamma = \frac{4\pi\left(\frac{N}{60}\right)}{d_p^2\left(\frac{1}{d_p^2} - \frac{1}{d_h^2}\right)} \tag{38}$$

Given the shear rate, the shear stress is computed directly from the viscosity equations for the fluid type. The 479 in the equations below is a conversion from Centipoise to equivalent lbs/100 ft 2.

Bingham Plastic:

$$\tau = \tau_0 + \frac{\mu_p \gamma}{479} \tag{39}$$

Power Law:

$$\tau = \frac{K\gamma^n}{479} \tag{40}$$

Herschel Bulkley :

$$\tau = \tau_z + \frac{K\gamma^2}{479} \tag{41}$$

Where,

$K = Consistency\ index$
$L_d = Length\ of\ string$
$N = Rotary\ speed\ (RPM)$
$n = Flow\ behavior\ index$

$\mu_p = Plastic\ viscosity$
$\gamma = Shear\ rate\ in\ the\ annulus\ due\ to\ pipe\ rotation$
$\tau = Shear\ stress\ computed\ from\ the\ viscosity\ equation\ for\ the\ fluid\ rheological\ model$
$\tau_0 = Yield\ point$
$\tau_z = Zero\ gel\ yield$

2.2.4 Torque on pipe

No consideration is made to laminar or turbulent flow in this derivation. Additionally, the combined hydraulic effects of trip movement and rotation are ignored, which would accelerate the onset of turbulent flow.

Given the shear stress at the pipe wall (in lb/100 ft 2), **the torque** on the pipe is computed from the surface area of the pipe and the torsional radius.

$$\Delta T = \frac{\tau 2\pi L_d (\frac{d_p}{24})^2}{100} \tag{42}$$

In the case of rotational torque, the forces are equal and opposite between the pipe and the hole, although we are interested in the torque on the pipe and not the reaction from the hole.

Where,

$\mathrm{d_p} = \mathrm{Pipe\ diameter}$

$\mathrm{L_d} = \mathrm{Length\ of\ string}$

$\Delta\mathrm{T} = \mathrm{Calculated\ pipe\ torque}$

$\tau = \mathrm{Shear\ stress\ computed\ from\ the\ viscosity\ equation\ for\ the\ fluid\ rheological\ mode}$

2.2.5 Buoyed Weight

The surface pressure and mud densities are used to calculate the pressure inside and outside of the string. These pressures are used to calculate the buoyed weight of the string, which is used to calculate the forces and stresses acting on the string.

$$W_{buoy} = W_{air} - W_{fluid} \tag{43}$$

$$W_{fluid} = W_{ma}A_e - W_{mi}A_i \tag{44}$$

For components with tool joints:

The constraints 0.95, and 0.5 are used to assume 95% of the component length is body, and 5% is tool joint.

$$A_e = \frac{\pi}{4}(0{,}95d_{bo}^2 + 0{,}05d_{bi}^2) \quad (45)$$

$$A_i = \frac{\pi}{4}(0{,}95d_{bi}^2 + 0{,}05d_{bi}^2) \quad (46)$$

For components without tool joints:

$$A_e = \frac{\pi}{4}d_{bo}^2 \quad (47)$$

$$A_i = \frac{\pi}{4}d_{bi}^2 \quad (48)$$

Where:

$A_e = External\ are\ of\ the\ component$
$A_i = Internal\ area\ of\ the\ component$
$d_{bi} = Inside\ diameter\ of\ body$
$d_{bo} = Outside\ diameter\ of\ body$
$d_{ji} = Inside\ diameter\ of\ tool\ joint$
$d_{jo} = Outside\ diameter\ of\ tool\ joint$
$W_{buoy} = Buoyed\ weight\ per\ foot\ of\ the\ component$
$W_{fluid} = Weight\ per\ foot\ of\ displaced\ fluid$
$W_{ma} = Annular\ mud\ weight\ at\ component\ depth\ in\ the\ wellbore$
$W_{mi} = Internal\ mud\ weight\ at\ component\ depth\ inside\ the\ component$

2.2.6 Pipe Wall Thickness Modification

Drill pipe wall thickness will be modified according to the class specified for the pipe on the String tab. The class specified indicates the wall thickness modification as a percentage of the drill pipe outside diameter.

The outside diameter will be modified as follows:

$$d_{co} = cd_{bo} + d_{bi}(1 - c) \quad (49)$$

Where,

$d_{bi} = Inside\ diameter\ of\ body$
$d_{bo} = Outside\ diameter\ of\ body$
$d_{co} = Calculated\ outside\ diameter\ (OD)\ based\ on\ pipe\ class$
c
$= Based\ on\ pipe\ class, and\ calculated\ by\ dividing\ the\ percentage\ wall\ thickness\ by\ 100$

2.2.7 Stiff String Model

The Stiff String model accounts for:

- Tubular stiffness in bending
- Tubular join to hole wall clearance
- Stiffness modified for compressive force
- Single point weight concentrations

It impacts the torque and drag results in:

- Side forces and all derived calculations (Torque and Drag)
- Bending stresses
- Pipe position in the hole

The calculations consider friction on wellbore contact when the pipe is not rotating. In rotating mode, the bucking thresholds resemble the results for the 'unloading/curvilinear' buckling model. When static friction is applied (non-rotating pipe) the buckling thresholds will resemble those from the "loading/curvilinear" buckling model.

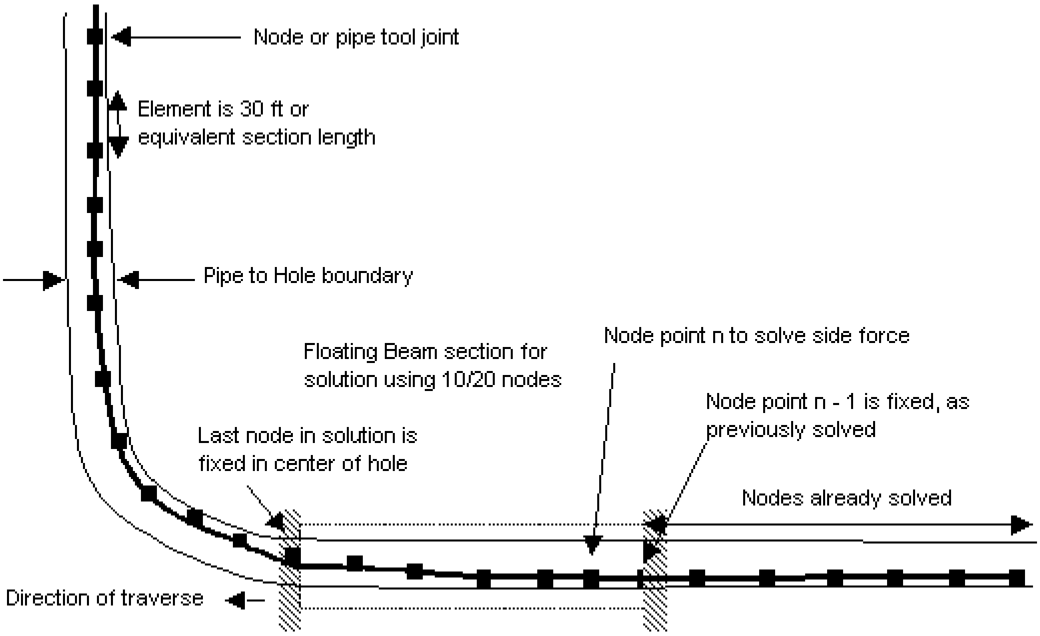

Figure 2.3: The Stiff String Model in Torque and Drag Analysis [17]

The Stiff String model traverses the string in the same manner as the Soft String model by selecting each component length or 30 inches of equivalent section. It computes the side force at the center point. This side force is used to compute the torque and drag change from one element to the next element. The detailed analysis of each node involved creating a local mesh of 10 to 20 elements around this node. The end nodes of the mesh are given the following end constraints (boundary conditions):

- If the model is at the bit or the top of the string, the node is a pivot and is free to rotate.
- If the end node has been previously solved in the traverse, then the node is fixed (cantilever) with the displacement and angle from the previous solution.
- If the node is at the front end of the traverse, the node is fixed in the center of the hole.

Each sub-element is given the same dimensions and properties as it would be given to the full drill string.

If the node length exceeds the maximum column-buckling load for the section, the node is further broken into fractional lengths to keep each section below the buckling threshold.

This short section is solved by solving each individual junction node for moments and forces, then displacing it to a point of zero force. If this position is beyond the hole wall, a restorative force is applied to keep it in the hole. This process is repeated for each node in the short beam until they reach their "relaxed" state.

The stiff string produces slightly different results when run "top down" or "bottom up", the difference is explained because of the mode of traversal is reversed. The length of beam selected for each stiff analysis has been selected to optimize speed while maintaining reliable consistent results.

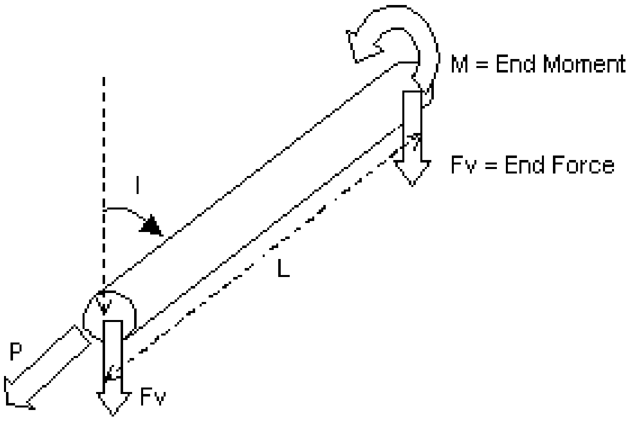

Figure 2.4: Inclined Beam Section [17]

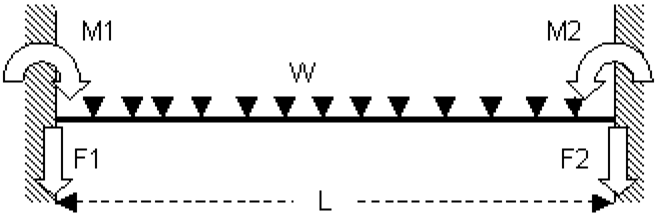

Figure 2.5: Idealized Beam Section with End Loads Caused by Weight W [17]

2.2.8 Loading and Unloading Models

In [23], Mitchell derives the loading method. The idea presented is that for compressive axial loads between 1.4 and 2.8 times the sinusoidal buckling force, there is enough strain energy in the pipe to sustain helical buckling, but not enough energy to spontaneously change from sinusoidal buckling to helical buckling. That is, if you could reach in and lift the pipe up into a helix, it would stay in the helix when you let go. This means that in an ideal situation, without external disturbances, the pipe would stay in a sinusoidal buckling mode until the axial force reached 2.8 times the sinusoidal buckling force. At this point, the pipe would transition to the helical buckling mode. This is the "loading" scenario. Once the pipe is in the helical buckling mode, the axial force can be reduced to 1.4 times the sinusoidal buckling force, and the helical mode will be maintained. If the axial force falls below 1.4 times the sinusoidal buckling force, the pipe will fall out of the helix into a sinusoidal buckling mode. This is the "unloading" scenario.

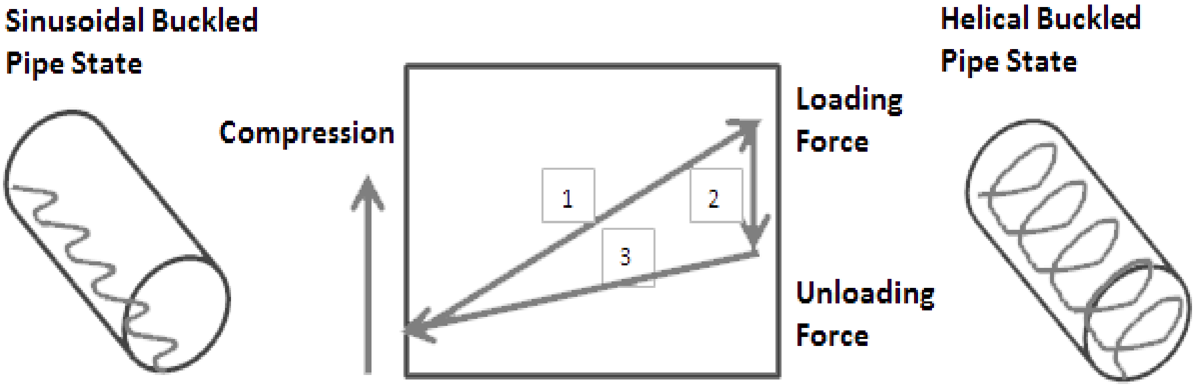

Figure 2.6: Loading and unloading scenarios

In the figure 2.6, in Stage 1 the compressive load is increased from the force required for sinusoidal buckling to the threshold force where the pipe snaps into a helical buckled state. This is the "loading" force. Stages 2 and 3 represent the reduction of the compressive load to another threshold force to snap out from helical buckled into a sinusoidal buckled state. This is the "unloading" force. Taking friction into consideration, we can imagine buckling friction acts a bit like glue. It gives resistance when the pipe is pushed into buckling (loading), and it also provides resistance to release the pipe from buckling (unloading). But when the pipe is rotating the "glue" bond is broken and gives no resistance. In the case where friction is effective, the transitions from sinusoidal to helical and vice versa are more explosive because the pipe picks up more spring energy because the friction prevents free pipe movement until the stored energy is enough to break the friction bond.

Loading Model

$$F_h = 2.828427F_s \tag{50}$$

Unloading Model

$$F_h = 1.414213F_s \tag{51}$$

Where,

$F_h = Compression\ force\ to\ induce\ onset\ of\ helical\ buckling$
$F_s = Compression\ force\ to\ induce\ onset\ of\ sinusodial\ buckling$

2.2.9 Buckling Limit Factor

Buckling limits commonly used are based on the theory that as the pipe is compressed inside the wellbore, the string goes initially into snaking or lateral buckling mode (also called sinusoidal buckling mode).

This condition allows the pipe to be compressed. After exceeding the threshold calculated by the researchers, the pipe snaps into helical buckling mode causing the wall force to increase which may result in a lockup state of the pipe. Usually, lockup is defined as the ratio between the changes in the downhole weight to the change in surface slack off weight less than 2%. In the past, various limits were published to define the regions of no buckling, sinusoidal buckling, and helical buckling.

Based on the work by Lubinski, Dawson and Paslay, and Paslay and Bogy, the compression force to induce the onset of sinusoidal buckling is given as:

$$F_s = 2[\frac{(sin\theta)EIW_{tm}}{r_{cl}}]^{\frac{1}{2}} \tag{52}$$

Using the curvilinear model, it can be given as:

$$F_s = 2\left(\sqrt{\frac{EIW_c}{r_{cl}}}\right) \tag{53}$$

In which the contact force between the pipe and wellbore is given as:

$$W_c = 2\left(\sqrt{W_t sin\theta + F_c\epsilon'^{)^2} + F_c^2 sin^2\theta\epsilon'^2}\right) \tag{54}$$

For constant curvature wellbores, the contact force can be expressed as:

$$W_c = \sqrt{(W_t n_z - F_c k^2)^2 + (W_t b_z)^2} \tag{55}$$

Compression force to induce onset of helical buckling is given as:

$$F_h = fF_s \tag{56}$$

Various buckling constants used for the onset of helical buckling by various authors are listed below, in table 2.1

Table 2.1: Helical buckling scaling factors [17]

Model	**Scaling Factor**
Chen and Cheatham 1990	-2.83
He and Kyllingstad 1995	-2.83
Lubinski and Woods 1953	-2.85
Lubinski and Logan 1962	-2.4
Qui, Miska and Volks 1998	-5.66
Qui, Miska and Volks 1998	-3.75
Wu and Juvkam Wold 1993	-3.66
Wu and Juvkam Wold 1995	-4.24

There is no consensus among the authors, and the validations carried out were with either 50 ft or less than 100 ft acrylic pipe with aluminum or steel rods. Acrylic pipe used in the lab for testing whether straight or slightly undulated does not translate closely to downhole conditions. Also, the models have been developed in tested in a discrete fashion. The model does not take into effect the pipe condition which may be completely different when analyzed piecewise. For example, the buckling condition may be different when the pipe is in J-type well as opposed to S-type well.

There were very limited field data available, and with the data available it has been found that the downhole weight change does not follow the theoretical prediction. In most of the cases it aligns well to the onset of the sinusoidal buckling and quickly goes into lockup state without the onset of helical buckling mode.

The Buckled Length: The length of buckled pipe is the length of pipe where the compressive axial force exceeds or equals the critical buckling force.

$$F_c \geq F_b \tag{57}$$

The total buckled length is the sum of all intervals that satisfy the inequality.

Key factors influencing buckling:

- Lateral clearance - hole wash out
- Localized pipe heating - flows behind pipe
- Temperature increase - drilling, production
- Formation sticking - axial restraints
- Incremental compressive load
- Wellbore interaction - friction and side loading
- Wellbore trajectory and tortuosity

The Buckling Limit Factor (BLF) is a multiplying factor used to adjust the constants used in the buckling equation. This helps to calibrate the model and adjust the buckling limit lines based on the wellbore tortuosity, borehole quality, or shape. The sinusoidal buckling force is modified as follows:

$$F_{s-modified} = f_{BLF} * 2 * \left(\sqrt{\frac{EIW_c}{r_{cl}}}\right) \tag{58}$$

Compression force to induce onset of helical buckling is given as:

$$F_h = fF_{s-modified} \tag{59}$$

Loading Model

$$F_h = 2.828427F_{s-modified} \tag{60}$$

Unloading Model

$$F_h = 1.414213F_{s-modified} \tag{61}$$

Suggested BLF with respect to the models are displayed in the table 2.2. The reference is based on the WellPlan™ model (He and Kyllingstad).

Table 2.2: Helical buckling Scaling factors and BLF [17]

Model	Scaling Factor	BLF
Chen and Cheatham 1990	-2.83	1
He and Kyllingstad 1995	-2.83	1
Lubinski and Woods 1953	-2.85	1.007
Lubinski and Logan 1962	-2.4	0.848
Qui, Miska and Volks 1998	-5.66	2
Qui, Miska and Volks 1998	-3.75	1.326
Wu and Juvkam Wold 1993	-3.66	1.295
Wu and Juvkam Wold 1995	-4.24	1.498

2.3 Hydraulics – Oliasoft

Drilling muds comes in a huge variety; thus, a generalized implementation of the mud properties is used. The density is calculated as a function of the pressure and temperature at location of interest as well as the rheology parameters. The Oliasoft WellDesign™ application performs calculation using the Herschel-Bulkley description of the mud shear stress as a function of the

shear rate:

$$\tau(\gamma) = \tau_0 + K \cdot \gamma^n \tag{62}$$

Where,

$\tau = shear\ stress$
$\gamma = shear\ rate$
$\tau_0 = yields\ stress$
$K = consistency\ index$
$n = flow\ behavior\ index$

Equation (63) covers the special rheology cases:

- Newtonian fluid — linear approximation of the shear stress; $\tau_0 = 0$ and $n = 1$

- Bingham Plastic fluid — linear approximation of shear stress, but with a yield stress $n = 0 \, and \, \tau_0 > 0$
- Power Law fluid — exponential behavior of the shear stress. Only shear thinning fluids are used in drilling; $0 \leq n \leq 1$

A variety of temperature profiles can be used by the calculation, from a simple linear geothermal profile, tabulated temperature data or temperature simulations of circulating fluids. The thermal expansion coefficient and pressure compressibility coefficient is used to determine the density of the mud. It is assumed that the mud is in its linear regime with respect to its compressibility β_p, and thermal expansion α_T, ie. β_p and α_T are constants with respect to pressure p and temperature T:

$$\rho(p) = \rho_0 \cdot e^{(p-p_0)\cdot\beta_p} \tag{63}$$

$$\rho(T) = \rho_0 \cdot e^{(T_0-T)\cdot\alpha_T} \tag{64}$$

where the subscript 0 denotes reference density, temperature, and pressure.

If the fluid is represented by a PVT matrix, equations (64) and (65) are used for interpolation in (p, T, ρ)–space. Oliasoft WellDesign™ also supplies some standardized fluids, like water, seawater, diesel, methanol etc. These have their own standard literature equations for determination of their density. When fluids are mixed, they are assumed be emulsions, thus, their combined density can be calculated by creating a weighted sum, using the volume fractions of the mixture.

2.3.1 Fluid mechanics flow equations

The calculation process for the pressure drop in the well is an iterative process. All regions with fixed geometry are treated separately and in succession as the result from one step is input to the next step. No general analytic solution for the equations exists, so a numeric process has been developed to converge on the correct pressure drop. When the pressure drops throughout the pipe and annulus have been found, all other engineering values can be calculated, e.g., the Equivalent Circulating Density (ECD).

2.3.2 Pressure loss calculation in annulus

Aadnøy [2] describes how to calculate the pressure drop in an annulus given that the drill string is free to move in the well bore, thus it depends on eccentricity, rotation and buckled state. The eccentricity is determined from the Torque and Drag (T&D) soft string model. The calculation uses the Herschel-Bulkley equation for the rheology; thus, it is a general description usable for any fluid. To calculate the pressure, drop in the annulus along a section of length δL, where the geometry is unchanged, the below sets of equations needs to be solved simultaneously. First the fluid shear stress τ at the wall is found from the mud flow equation, $Qannulus(\tau)$:

$$Q_{annulus}(\tau) = \frac{\pi(r_b+r_p)(r_b-r_p)^2}{2K^{\frac{1}{n}}r^2} \cdot (\tau - \tau_0)^{\frac{1+n}{n}} \cdot \left(\tau + \frac{n}{1+n}\tau_0\right) \tag{65}$$

Where,

$r_p = pipe\ radius$

$r_b = radius\ of\ the\ hole$

Then the Reynolds number for a yield power law fluid is calculated:

$$R = \frac{12v^2\rho(T,p)}{\tau} \tag{66}$$

Where,

- the superficial velocity v is calculated form the flow rate and the local geometry.
- The absolute pressure also be known at this point, which gives the correct density $\rho(T, p)$ of the mud.

The “generalized flow index”, N, is a generalization of the “flow index” n, also found in the power law rheology model. When the “flow index” is replaced with its generalized counterpart the friction factor equation is the same. N depends upon the n and the yield strength τ_0 of the fluid:

$$N = \frac{n_\tau}{3-2n_\tau} \tag{67}$$

$$n_\tau = \frac{3n}{1+2n}\left(1 - \frac{\tau_0}{\tau(1+n)} - \frac{n\tau_0^2}{\tau^2(1+n)}\right) \tag{68}$$

From the generalized flow index the transitions from laminar to transitional and transitional to turbulent flow can be calculated:

$$R_{lam}^{max} = 2100 \cdot N^{0.331}\left(1 + 1.402\frac{r_p}{r_b} - 0.977\frac{r_p^2}{r_b^2}\right) \forall N \in [0.1, 1] \tag{69}$$

$$R_{turb}^{min} = 2900 \cdot N^{-0.039\cdot(R_{lam}^{max})^{0.307}} \qquad \forall N \in [0.15, 0.4] \tag{70}$$

These 2 equations both have empirical constants (see discussion in [2]), which were determined in the general flow index ranges denoted for each Reynolds limit. The formulas are not extrapolated outside their valid range, and if the N is outside this range the standard equations (82) and (83) (also recommended by API 10A and RP13D) is used. The empirical constants for the annulus were also determined using a configuration where $\frac{r_p}{r_b} = 0.5$, but for any useful application this has been slightly extended to allow $\in [0.3, 0.7]$. Using these limits, the flow regime can be determined and a different set of equations

apply depending on the flow type. The friction factor f for the flow at this velocity is calculated:

$$Laminar\ flow: f_{lam} = K_f \cdot \frac{24}{R} \tag{71}$$

$$Turbulent\ flow: \frac{1}{\sqrt{f_{turb}}} = K_f \cdot \frac{4}{N^{0.75}} log_{10}\left(R \cdot f_{turb}^{\left(1-\frac{N}{2}\right)}\right) - \frac{0.4}{N^{1.2}} \tag{72}$$

Transitional flow is calculated as an extrapolation between the friction factor for laminar flow and turbulent flow:

$$f_{trans} = f_{lam} + \frac{R - R_{lam}^{max}}{R_{turb}^{min} - R_{lam}^{max}}(f_{turb} - f_{lam}) \tag{73}$$

The empirical constant K in equation (lam og turb) is found from:

$$K_f = \begin{cases} 1\ \forall\varepsilon = 0 \\ 1 - C_1\frac{\varepsilon}{N}\kappa^{0.08454} - C_2\varepsilon^2\sqrt{N}\kappa^{0.1852} + C_3\varepsilon^3\sqrt{N}\kappa^{0.2527}\ \forall\varepsilon > 0 \end{cases} \tag{74}$$

$$C_1 = 0.072, C_2 = \frac{3}{2}, C_3 = 0.96 \quad \forall\varepsilon > 0 \wedge R < R_{lam}^{max} \tag{75}$$

$$C_1 = 0.048, C_2 = \frac{2}{3}, C_3 = 0.0258 \quad \forall\varepsilon > 0 \wedge R > R_{turb}^{min} \tag{76}$$

$$\kappa = \frac{r_p}{r_b} \tag{77}$$

Finally, the pressure loss for the section can be calculated from the friction factor, f:

$$\frac{dp}{dl} = C_p \cdot \frac{f\rho(T,p)v^2}{r_b - r_p} \tag{78}$$

$C_p = 1$ if the drill string is not buckled. This applies to any type of buckling (sinusodial, partially helical or fully helical, see [16]). If the string is buckled the empirical correction for the pressure loss is calculated as:

$$C_p = \begin{cases} 1 & \forall \frac{F}{F_s} < 1 \\ 0.2287N - 0.0580\frac{F}{F_s} + 0.014844\omega + 0.4289 & \forall \frac{F}{F_s} \geq 1 \wedge R < R_{lam}^{max} \\ -1.0267 - 0.0096\frac{F}{F_s} + 0.00468\omega + 1.4222 & \forall \frac{F}{F_s} \geq 1 \wedge R \in [R_{lam}^{max}, R_{turb}^{min}] \\ -1.7821N - 0.0132\frac{F}{F_s} + 0.016656\omega + 2.7983 & \forall \frac{F}{F_s} \geq 1 \wedge R > R_{turb}^{min} \end{cases}$$

where (79)

$F = tension\ in\ the\ drill\ string$
$F_s = sinusodial\ buckling\ limit$
$\omega = rotation\ frequency$

2.3.3 Pressure loss calculation in pipe

Flow in pipe (circular conduit) is calculated in a similar way. The formulas used are found in [1]. The following equation replaces the corresponding equations from the previous section. First the generalized flow index, N is calculated as:

$$N = \left(\frac{(1-2n)\tau+3n\tau_0}{n(\tau-\tau_0)} + \frac{2n(1+n)((1+2n)\tau^2+n\tau_0\tau)}{n(1+n)(1+2n)\tau^2+2n^2(1+n)\tau\tau_0+2n^3\tau_0^2}\right)^{-1} \quad (80)$$

The Reynolds number limits for laminar to transitional and from transitional to turbulent flow in a pipe is given by:

$$R_{lam}^{max} = 3250 - 1150N \quad (81)$$

$$R_{turb}^{min} = 4150 - 1150N \quad (82)$$

With the given flow in the pipe, the fluid shear stress can be calculated from the following equation:

$$Q_{pipe}(\tau) = \frac{\pi r_p^3 n(\tau - \tau_0)^{1+\frac{1}{n}}}{(3n+1)K^{\frac{1}{n}}\tau^3}\left(\tau^2 + \frac{2n\tau_0\tau}{1+2n} + \frac{2n^2\tau_0^2}{(1+n)(1+2n)}\right) \tag{83}$$

With the now known shear stress in the fluid, its Reynolds number is given by:

$$R = \frac{8v^2\rho(T,p)}{\tau} \tag{84}$$

Setting $\varepsilon = 0$, the flow friction factor in the pipe can be calculated from equation (72), (73) or (74), using the results from equations (81) and (85). The pressure drop for the section is then calculated from equation (79) with $C = 1$.

2.3.4 Pipe and annulus velocity

In most situations the pipe is moving relative to the annulus. This means that the mud velocity ($vmud$) has to be calculated relative to its location. Inside the pipe the mud velocity is calculated relative to the pipe, which introduces a fixed offset, $vROP$ between apparent velocity and the velocity calculated from mud volume flow and cross section at any MD.

In the annulus the pipe movement causes a non-symmetric shear stress profile in the transverse direction in the mud since the wall of the bore is static. This is not considered in the published literature, since for all scenarios except surge and swab (SS), the mud velocity is much bigger than the pipe velocity, thus the approximation is sound. Since this is not the case in SS, Oliasoft WellDesign™ has introduced an approximation to the superficial velocity of the mud in the annulus. The flow velocity profile is proportional to τ^2. Integrating this renders the following approximation to the superficial flow velocity:

$$v_{apparent} = v_{mud} + \frac{v_{ROP}}{3} \tag{85}$$

Where,

$v_{apparent} = superficial\ flow\ velocity$:

$v_{mud} = mud\ velocity$

$v_{ROP} = pipe\ velocity$

2.3.5 Equivalent Circulating Density (ECD)

During drilling the equivalent circulating density in the wellbore should be between the well fracturing and the well collapse gradient in order to control wellbore instability issues. The ECD is determined from static mud weight and the annular frictions as given in Eq, 87

$$\rho_{ECD} = \rho(T, p) + \frac{p_{friction}(l_{MD})}{g \cdot h_{TVD}} \tag{86}$$

where

$l_{MD} = distance\ along\ trajectory\ to\ point\ MD$
$p_{friction}(l_{MD}) = frictional\ pressure\ loss\ down\ to\ point\ MD$
$g = gravitational\ constant$
$h_{TVD} = TVD\ between\ the\ Rotary\ Kelly\ Bushing\ (RKB) and\ point\ MD$

2.3.6 Drill bit calculation

The pressure drop is calculated according to the standard in the industry. The pressure drop coefficient is most probably manufacturer specific, see e.g. [19] for a discussion of its value. The following values are calculated:

$$P_{hyd} = \Delta p \cdot Q(\tau) \tag{87}$$

$$v_{nozzle} = \frac{Q(\tau)}{A_{nozzles}} \tag{88}$$

$$F_{impact} = \frac{Q^2(\tau)\rho}{A_{nozzles}} \tag{89}$$

$$P_{eff} = \frac{P_{hyd}}{\pi r_{bit}^2} \tag{90}$$

Where,

$\Delta p = pressure\ drop\ through\ nozzles\ of\ drill\ bit$
$P_{hyd} = hydraulic\ horse\ power$
$v_{nozzle} = average\ mud\ velocity\ in\ nozzles$
$F_{impact} = impact\ force\ of\ mud\ as\ it\ exits\ the\ nozzles$
$P_{eff} = hydraulic\ horse\ power\ intensity$
$r_{bit} = drill\ bit\ radius$

2.3.7 Hole cleaning

The transport of cuttings in the annulus is calculated using [20] and [21]. It is based upon finding the slip speed of the cuttings, and if the mud velocity is too slow to transport the cuttings, a cuttings bed will form, until the mud velocity is high enough (mud velocity increases with increasing cuttings bed cross sectional area). Below a certain inclination the cuttings bed will not be stable. In such a case the cross-sectional fraction of cuttings will accumulate until the mud velocity is high enough to transport the cuttings. This will necessarily cause a high increase in the mud pressure drop in the annulus. The cuttings volumetric flow rate, Q_{cut} is given by:

$$Q_{cut}(v_{ROP}) = v_{ROP}\pi r_p^2 \tag{91}$$

$$v_{ROP} = rate\ of\ penetration \tag{92}$$

In [21], an empirical equation for determining the mud's ability to transport the cuttings away from the drill bit was found from lab tests, determining an otherwise unsolvable problem on how to determine the cuttings to mud volumetric fraction, c_{volCut}:

$$c_{volCut} = 2.1v_{ROP} + 0.00505 \tag{93}$$

Reference [21] gives a complete cuttings transport calculation, but too many of the empirical constants are based on too low statistics to be trusted, in addition it is only applicable for $\alpha = 0\ and\ \alpha > 55°$. Thus, equation (94) is the only one used in the implementation. In [20] an additional 2 special numerical constants were constructed, which were analyzed from several earlier lab tests:

$$K_{corr} = \begin{cases} 1 + \frac{\alpha(359.479+\rho)(10-\omega)}{404334} & \forall\alpha \leq 45 \\ 1 + 2 \cdot \frac{(359.479+\rho)(10-\omega)}{17970.4} & \forall\alpha > 45 \end{cases} \tag{94}$$

$$A = \begin{cases} \frac{40}{R_{cut}} & \forall R_{cut} < 3 \\ \frac{22}{\sqrt{R_{cut}}} & \forall R_{cut} \in [3,300\rangle \\ 1.54 & \forall R_{cut} \geq 300 \end{cases} \tag{95}$$

There is a big discontinuity in A when $Rcut$ passed 3. This has not been resolved, thus $Rcut$ has an artificial low limit of 3. When the above values are determined the following sets of equations must be solved simultaneously:

$$\mu_{apparent} = \mu + \frac{0.25063\tau_0(r_b - r_p)}{v_{min}} \tag{96}$$

$$v_{slip} = A \cdot K_{corr}\sqrt{\frac{d_{cut}(\rho_{cut} - \rho)}{\rho}} \tag{97}$$

$$R_{cut} = \frac{v_{slip}d_{cut}\rho}{\mu_{apparent}} \tag{98}$$

$$v_{cut} = \frac{Q_{cut}(v_{ROP})}{c_{cut}\pi(r_b^2 - r_p^2)} \tag{99}$$

$$v_{min} = v_{cut} + v_{slip} \tag{100}$$

$$A_{bed} = \pi(r_b^2 - r_p^2) - \frac{Q_{annulus}(\tau)}{v_{min}(1 - c_{volCut})} \tag{101}$$

$$c_{cut} = \frac{1}{1 + \frac{Q_{annulus}(\tau) + Q_{cut}(v_{ROP})}{Q_{annulus}(\tau)} \cdot \left(1 - \frac{v_{slip}}{v_{min}}\right)} \tag{102}$$

Where,

$\alpha = inclination\ angle$
$d_{cut} = cuttings\ average\ diameter$
$v_{slip} = slip\ velocity$
$v_{cut} = cuttings\ velocity$
$v_{min} = minimum\ transport\ velocity$
$A_{bed} = cuttings\ bed\ cross - sectional\ area$
$c_{cut} = relative\ cross - section\ in\ annulus\ occupied\ by\ cuttings$

If the mud velocity is too low, $v_{mud} < v_{min}(1 - c_{volCut})$, the cuttings bed area is calculated, if not $A_{bed} = 0$

2.4 Hydraulics Model – Wellplan

The Hydraulics module can be used to simulate the dynamic pressure losses in the rig's circulating system and to provide analytical tools to optimize hydraulics. Several rheological models, including Newtonian, Bingham Plastic, Power Law, Generalized Herschel-Bulkley, and Herschel-Bulkley are provided. The rheological model one chooses provides the basis for the pressure loss calculations.

Hydraulics provides a quick means for you to determine the requirements you need to alter the existing fluid weight.

A Hole Cleaning model is also provided to assist for calculating the minimum flow rate you when you evaluate cuttings build-up in an actual well. You can also use this model as a tool to help evaluate mud systems.

2.4.1 Herschel-Bulkley Rheology Model

The Herschel-Bulkley model is a three-parameter model that has the Bingham Plastic Rheology Model and Power Law Rheology Model as special cases. This model is also known as the Yield Power Law (YPL) rheology model.

The shear stress (Fann reading) is modeled as a Zero Shear Yield Value plus a power law term. For n = 1, the YPL model reduces to the Bingham Plastic Rheology Model, where the plastic viscosity equals K, and the Bingham yield point equals the Zero Shear Yield Value. For Zero Shear Yield Value equals 0, it reduces to the standard Power Law model.

Parameters (Zero Shear Yield Value, n, K) are calculated by a non-linear fit to the YPL rheology equation if three or more Fann readings are provided. If only two Fann readings are provided, the Power Law model is assumed.

The rheology of drilling muds (oil or water based) and cements may be modeled accurately as YPL fluids. This model is the recommended model for drilling hydraulic calculations.

The Zero Shear Yield Value has been shown to correlate well to the tendency of weighted muds to "dynamically sag" under flowing conditions. Zero Shear Yield Value should not be confused with or compared to the standard yield point calculated from 600 and 300 rpm Fann data.

Extensive tests at the Amoco Catoosa Test Facility in a 1/2-scale flow loop confirm the accuracy of the YPL model for predicting annular and pipe pressure losses in laminar flow and the onset of turbulence. Empirical correlations from turbulent flow data extend the application of this model to turbulent flow and include the effects of pipe wall roughness.

First, calculate shear rates and shear stress based on Fann data. Curve fit the shear rates and shear stresses to the Herschel-Bulkley equation shown below:

$$\tau_0 + K\gamma^n \tag{103}$$

Where,

$K = Consistency\ index$
$n = Flow\ behavior\ index$
$\gamma = Shear\ rate$
$\tau = Shear\ stress$
$\tau_0 = Yield\ point$

2.4.1.1 Velocity Profile

The flow velocity profile of a YPL fluid in a pipe or between the inner and outer walls of a concentric annulus is similar and consists of a plug zone in the center of the flow channel if Zero Shear Yield Value is > 0 and a sheared zone between the plug zone and the pipe or annulus walls.

For laminar flow, the velocity and viscosity distribution across the cross-section of a pipe or annular gap can be calculated for a YPL fluid.

In the plug zone, the shear rate is zero and the viscosity is very high (theoretically infinite for a YPL fluid). Any weighted material within the plug zone should not settle. In the sheared zone, the viscosity of the mud decreases as the shear rate increases toward the pipe or annulus wall. It is this phenomenon of shear thinning toward the wall that contributes to dynamic sag of weighting material in high-angle holes.

2.4.1.2 Hydraulics

The pipe and annulus friction losses for a given interval are calculated using the YPL rheology model and the Amoco friction factor equations. For the annulus, the pressure loss is dependent upon the eccentricity.

2.4.1.3 Laminar Flow

A concentric annulus requires about twice the pressure gradient as a fully eccentric annulus in laminar flow.

2.4.1.4 Turbulent Flow

A concentric annulus requires about 25% more pressure gradient than a fully eccentric annulus in turbulent flow.

Amoco friction factor equations are used to predict the friction pressures. They are verified with extensive tests for validity.

2.4.2 ECD

Except for the pressure loss calculation models, the ECD of the Wellplan software is similar to the one used by the Oliasoft is given as:

$$\rho_{ECD} = \frac{p_h + p_f}{0.052(D_{TVD})} \tag{104}$$

$$p_h = 0.052(\rho D_{TVD}) \tag{105}$$

$$p_f = \sum\left(\frac{\Delta p_{as}}{\Delta L_{as}}\right)\Delta D_{TVD} \tag{106}$$

Where,

$D_{TVD} = True\ vertical\ depth\ at\ point\ of\ interest$

$\frac{\Delta p_{as}}{\Delta L_{as}} = Change\ in\ pressure\ per\ length\ along\ the\ annulus\ section.$

$This\ is\ a\ function\ of\ the\ selected\ pressure\ loss\ model.$

$p_h = Hydrostatic\ pressure\ change\ to\ ECD\ point$

$p_f = Frictional\ pressure\ change\ to\ ECD\ point$

$\rho_{ECD} = Equivalent\ circulating\ density$

2.4.3 Pressure Loss in Annulus and Pipe

Rheological Equation based on Power Law:

$$\tau = K\gamma^n \tag{107}$$

Flow Behavior Index:

$$n = 3.321928091 \log\left(\frac{\theta_{N_2}}{\theta_{N_1}}\right) \tag{108}$$

Consistency Factor:

$$K = \frac{510\theta_N}{(1.703N)^n} \tag{109}$$

Average Velocity in Pipe:

$$v_{ap} = \left(\frac{4}{\pi}\right)\left(\frac{Q}{d_{pi}^2}\right) \tag{110}$$

Average Velocity in Annulus:

$$v_{aa} = \left(\frac{4}{\pi}\right)\left(\frac{Q}{d_h^2 - d_{po}^2}\right) \tag{111}$$

Geometry Factor for Annulus:

$$G_a = \left[\frac{(2n+1)}{2n}\right]^n 8^{n-1} \tag{112}$$

Geometry Factor for Pipe:

$$G_p = \left[\frac{(3n+1)}{4n}\right]^n 8^{n-1} \tag{113}$$

Reynolds Number for Pipe:

$$R_p = \frac{\rho v_{ap}^{(2-n)}\left(d_{pi}^{n}\right)}{g_c G_p K} \tag{114}$$

Reynolds Number for Annulus:

$$R_a = \frac{\rho v_{aa}^{(2-n)}\left(d_h - d_{po}\right)^n}{g_c\left(\frac{2}{3}\right)G_a K} \tag{115}$$

Critical Reynolds Numbers:

$$R_i = 3470 - 1370n \tag{116}$$

$$R_t = 4270 - 1370n \tag{117}$$

Friction Factor for Pipe

Laminar flow:

$$f_p = \frac{16}{R_p} \tag{118}$$

Transition flow:

$$a = \frac{\log(n) + 3.93}{50} \tag{119}$$

$$b = \frac{1.75 - \log(n)}{7} \tag{120}$$

$$f_p = \left(\frac{16}{R_i}\right)\left[\frac{\left(R_p - R_i\right)}{800}\right]\left[\left(\frac{a}{R_t^b}\right) - \left(\frac{16}{R_i}\right)\right] \tag{121}$$

Turbulent flow:

$$a = \frac{\log(n) + 3.93}{50} \tag{122}$$

$$b = \frac{1.75 - \log(n)}{7} \tag{123}$$

$$f_p = \frac{a}{R_p^b} \tag{124}$$

Friction Factor Annulus

Laminar flow:

$$f_a = \frac{24}{R_a} \tag{125}$$

Transition flow:

$$a = \frac{\log(n) + 3.93}{50} \tag{126}$$

$$b = \frac{1.75 - \log(n)}{7} \tag{127}$$

$$f_a = \left(\frac{24}{R_i}\right)\left[\frac{(R_a - R_i)}{800}\right]\left[\left(\frac{a}{R_t^b}\right) - \left(\frac{24}{R_i}\right)\right] \tag{128}$$

Turbulent flow:

$$a = \frac{\log(n) + 3.93}{50} \tag{129}$$

$$b = \frac{1.75 - \log(n)}{7} \tag{130}$$

$$f_a = \frac{a}{R_a^b} \tag{131}$$

Pressure Loss in Pipe:

$$P_{lossp} = \frac{\rho}{g_c} v_p^2 f_p L_s \left(\frac{2}{d_{pi}}\right) \tag{132}$$

Pressure Loss in Annulus:

$$P_{lossa} = \frac{\rho}{g_c} v_a^2 f_a L_s \left(\frac{2}{d_h - d_{po}}\right) \tag{133}$$

Where:

$d_h = Annulus\ diameter$

$d_{pi} = Pipe\ inside\ diameter$

2.4.4 Bit Pressure Loss

Bit pressure loss represents the pressure loss through the bit.

$$\Delta P_{lossbit} = \frac{\rho v_f^2}{2g_c C_d^2} \tag{134}$$

Where,

$C_d = Nozzle\ Coefficient, 0.95$

$gc = Gravitational\ constant$

$\Delta P_{lossbit} = Bit\ pressure\ loss$

$v_f = Fluid\ velocity$

$\rho = Fluid\ density$

3 Software Simulation and Field Data Comparisons

In the field cases there has been focused on four different areas:

- Torque
- Drag
- Standpipe pressure
- ECD

There has been gathered input for the simulation software's from the same sources, so the input parameters would be as similar as possible. This is done so that any differences between the software's would be as valid as they can. Input parameters can be found in Appendix. Most important data is the hole geometry, string geometry, precise fluid properties and operational parameters.

Field cases consist of four different wells, with specified sections in each well. Valemon well consists of two drilling sections: 17 ½", 12 ¼" and two casing runs: 14x13 5/8", 9 7/8". Oseberg Sør consists of two drilling sections: 12" and 8 ½". Kvitebjørn consist of a liner run: 7". Gullfaks consists of a liner run: 9 5/8".

All well sections are executed finished, and simulated data are compared to actual data gathered during well operations.

3.1 Torque and Drag

3.1.1 Valemon B-13

The well selected from Valemon for the field case study is a recently drilled well in the North Sea. There are four different sections from the well for this field case study. 17 ½" drilling section, 13 3/8" casing section, 12 ¼" drilling section and 9 5/8" casing section. All depths refer to measured depths (MD), unless other is mentioned.

3.1.1.1 17 ½" Section – Torque & Drag simulation

This section is 2080 m long, from 1250 m to 3330 m Drilled with a 3D rotary drilling assembly.

3.1.1.2 Drag - Rotating Off Bottom (ROB)

The hookload when rotating off bottom can also be referred to the “free weight” of the drill string drilling BHA. Figure 3.1 shows the WP and OWD software simulated results compared with the field dataset. Results show the simulation runs for ROB hookload are similar to observed hookload. This is because rotational friction is the only force working on the drill string. If simulated ROB hookload differs from observed hookload, it is most probably inserted wrong or missing data in the string components, such as weights, lengths, and fluid density. In addition, the well path geometry plays an important role.

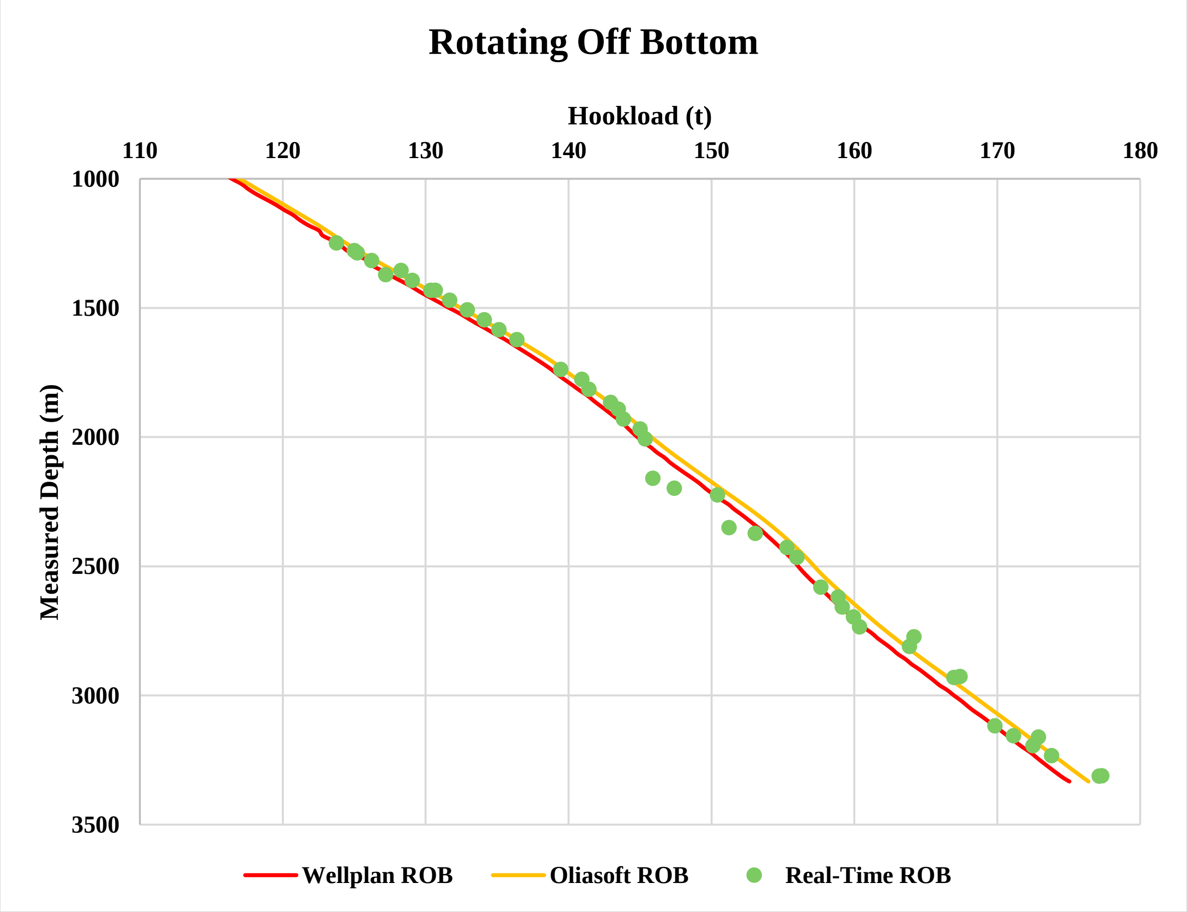

Figure 3.1: Simulated ROB hookload vs real-time ROB data

3.1.1.3 Drag - Running In to Hole/Tripping In (RIH)

Unlike ROB, tripping in and tripping out has no rotation in the drill string. It is possible to do these operations with rotation, but it has not been done in this study. Figure 3.2 shows the WP and OWD software simulated results compared with the field dataset. One may observe a small difference between OWD, and WP drag curves. The difference is about 1 ton down to 2800 m, then it grows to 3.5 tons at TD. OWD Buckling limit curve is a bit higher than WP throughout the wellbore. The actual running speed is not a constant value as it is assumed to be in the simulations, therefore observed hookload can vary a lot.

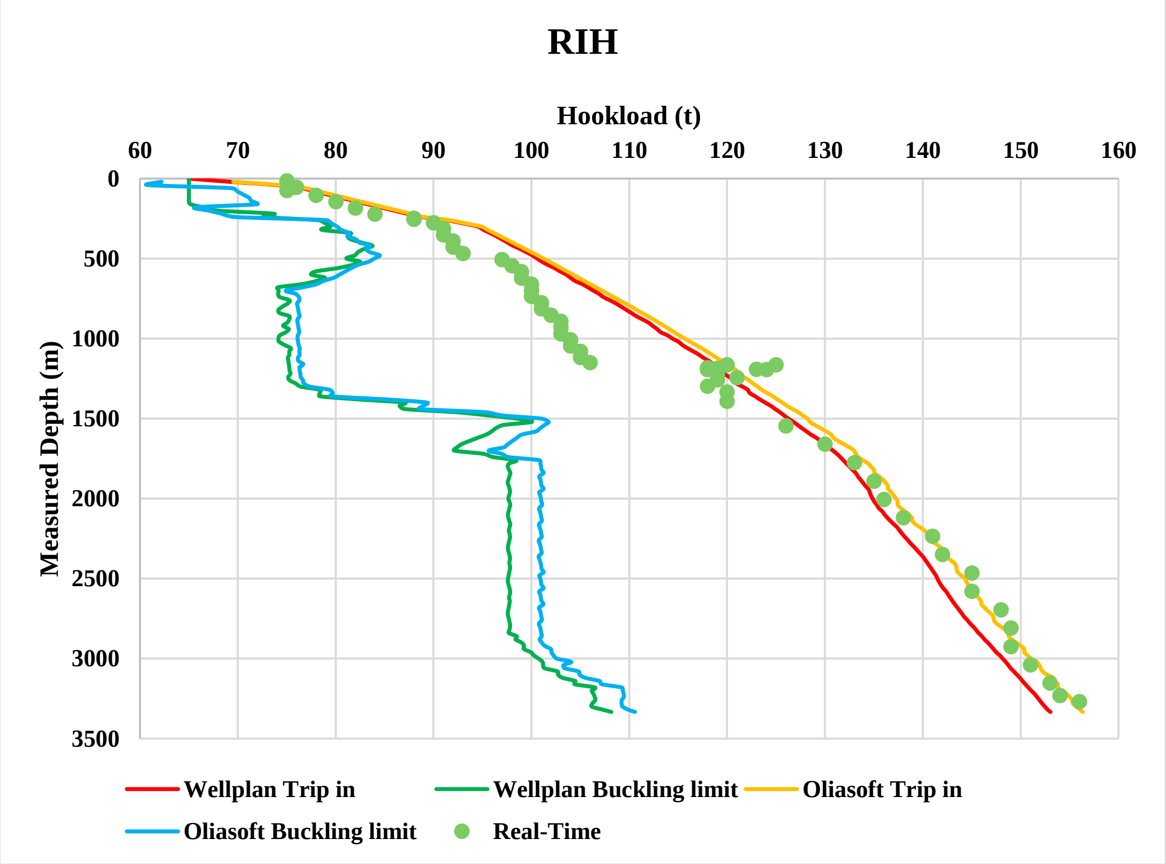

Figure 3.2: Simulated RIH hookload data vs real-time RIH hookload data

3.1.1.4 Drag - Pulling Out Of Hole/ Tripping Out (POOH)

Same concept as RIH, but it gets higher hookload because of the friction forces working in tensile direction. Figure 3.3 shows the WP and OWD software simulated results compared with the field dataset. Both OWD and WP drag curves follow one another closely, but they both start to increase more than the observed hookload at 1800m. Simulated yield curves follows the same trend as one another with a difference of 4 tons down to TD. The actual running speed is not a constant value as it is assumed to be in the simulations, therefore observed hookload can vary a lot.

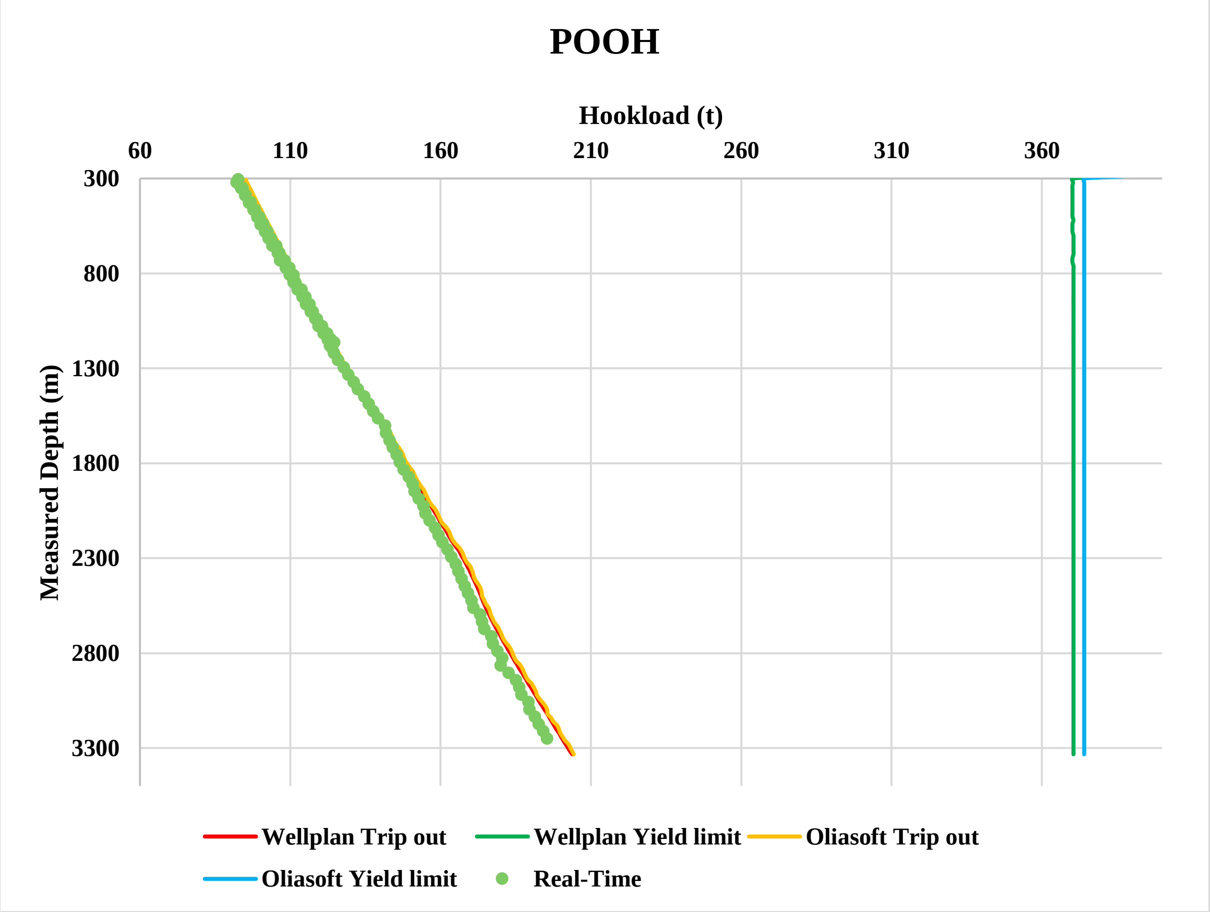

Figure 3.3: Simulated POOH hookload data vs real-time POOH hookload data

3.1.1.5 Torque - Rotating Off Bottom

Torque when rotating (default 100 RPM) off bottom with the drill string drilling BHA. Figure 3.4 shows the WP and OWD software simulated results compared with the field dataset. OWD torque values showing approximately 2 kNm higher torque from 2800m and down to TD, but both software's have the same trend. Observed torque values also follows the same trend but varying a few kNm, this can be explained by different parameters such as: Rotation speed is not constant, different WOB, varying flowrate and pipe stretch.

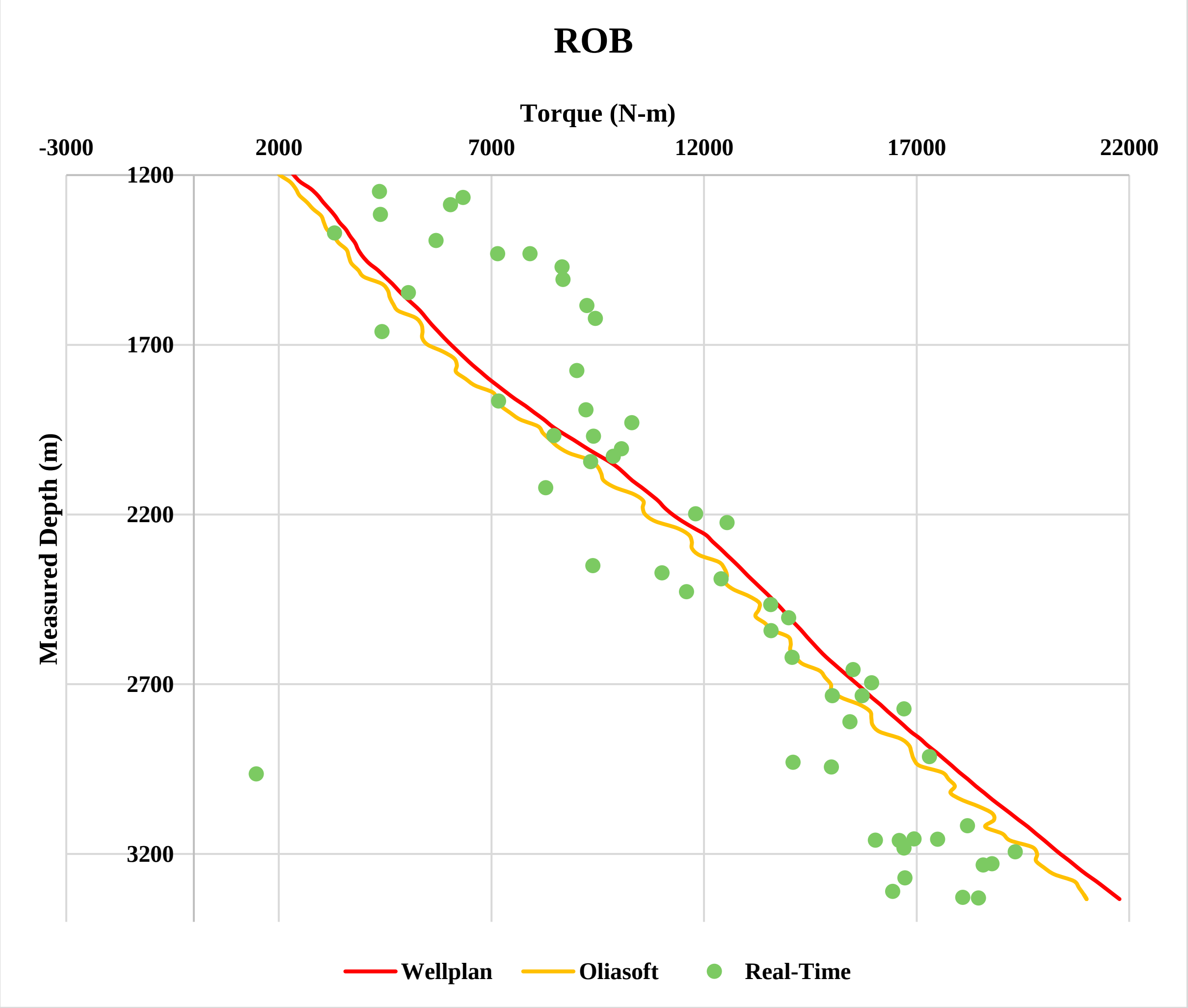

Figure 3.4: Simulated ROB torque data vs real-time ROB torque data.

3.1.2 14x13 5/8” Section – Drag simulation

14” x 13 5/8” Casing run from surface to 3322m MD.

3.1.2.1 Drag - Running Inn Hole/Tripping in

Figure 3.5 shows the WP and OWD software simulated results compared with the field dataset. Observed hookload shows higher from 2050m and down to TD. Actual casing weight can be higher than data sheet values. OWD buckling limit curve shows same trend as WP with a jump at 1300m to 1400m. Then it starts to deviate more than WP buckling limit curve at 2800m down to TD.

The actual running speed is not a constant value as it is assumed to be in the simulations, therefore observed hookload can vary.

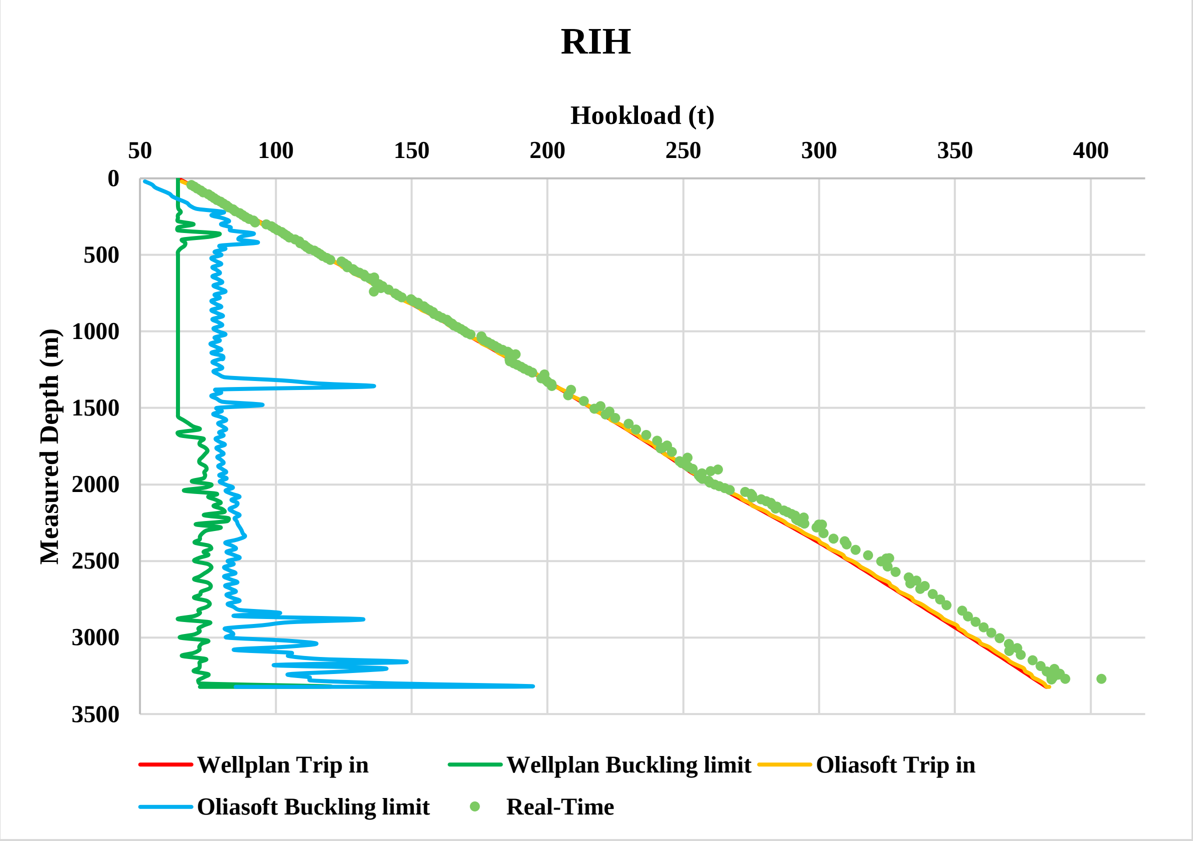

Figure 3.5: Simulated RIH hookload data vs real-time RIH hookload data

3.1.2.2 Drag - Pulling Out Of Hole/Tripping Out

Figure 3.6 shows the WP and OWD software simulated results compared with the field dataset. Both software's and observed drag curves follow one another closely throughout the wellbore. This also applies for the yield limit curve in both software\s.

The actual running speed is not a constant value as it is assumed to be in the simulations, therefore observed hookload can vary.

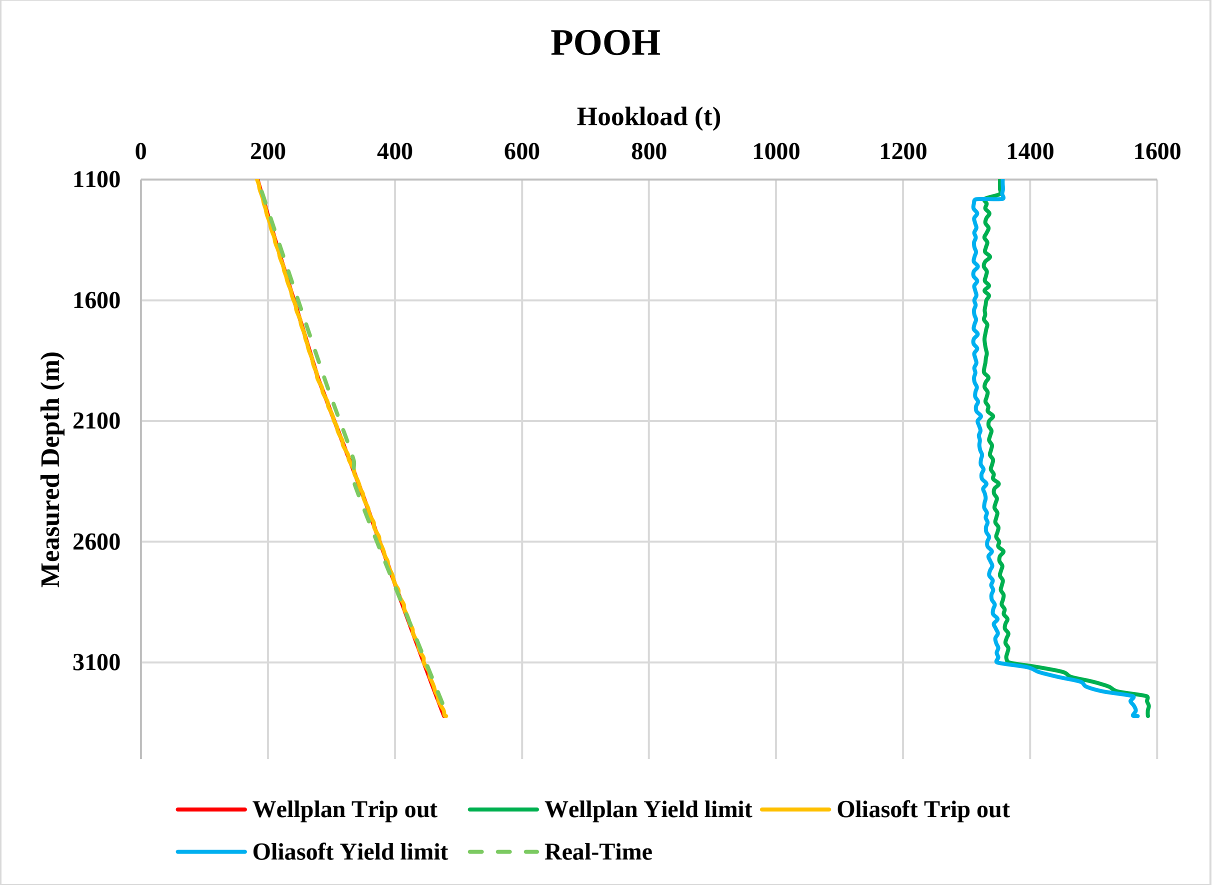

Figure 3.6: Simulated POOH hookload data vs real-time POOH hookload data

3.1.3 12 ¼” drilling Section

This section is 1258 m long, from 3330m to 4588m, drilled with a 3D rotary drilling assembly.

3.1.3.1 Drag - Rotating Off Bottom

Figure 3.7 shows the WP and OWD software simulated results compared with the field dataset. Both WP and OWD hookload data corresponds good with observed hookload data. WP drag curve is approximately 2 tons higher than OWD drag curve down to TD.

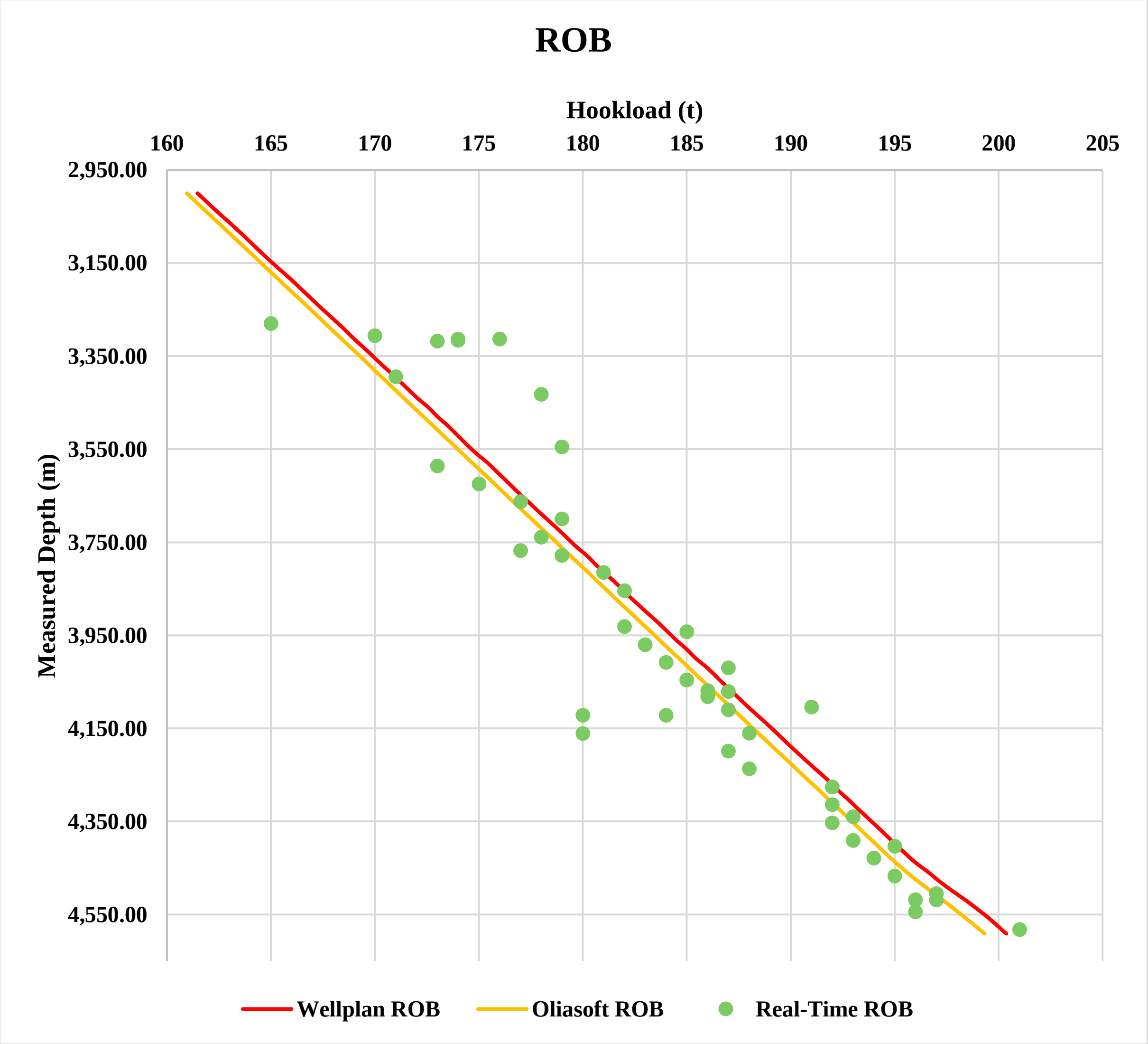

Figure 3.7: Simulated ROB hookload data vs real-time ROB hookload data

3.1.3.2 Drag - Running Inn Hole/Tripping inn

Figure 3.8 shows the WP and OWD software simulated results compared with the field dataset. Trendline of observed data has some similarities with WP and OWD data. From the plot one can see that there are several bigger increases in the observed data. This is because the pipe was filled with fluid(mud). This is not accounted for in the simulations. Buckling limit curve for both software's from the plot is almost identical.

The actual running speed is not a constant value as it is assumed to be in the simulations, therefore observed hookload can vary a lot.

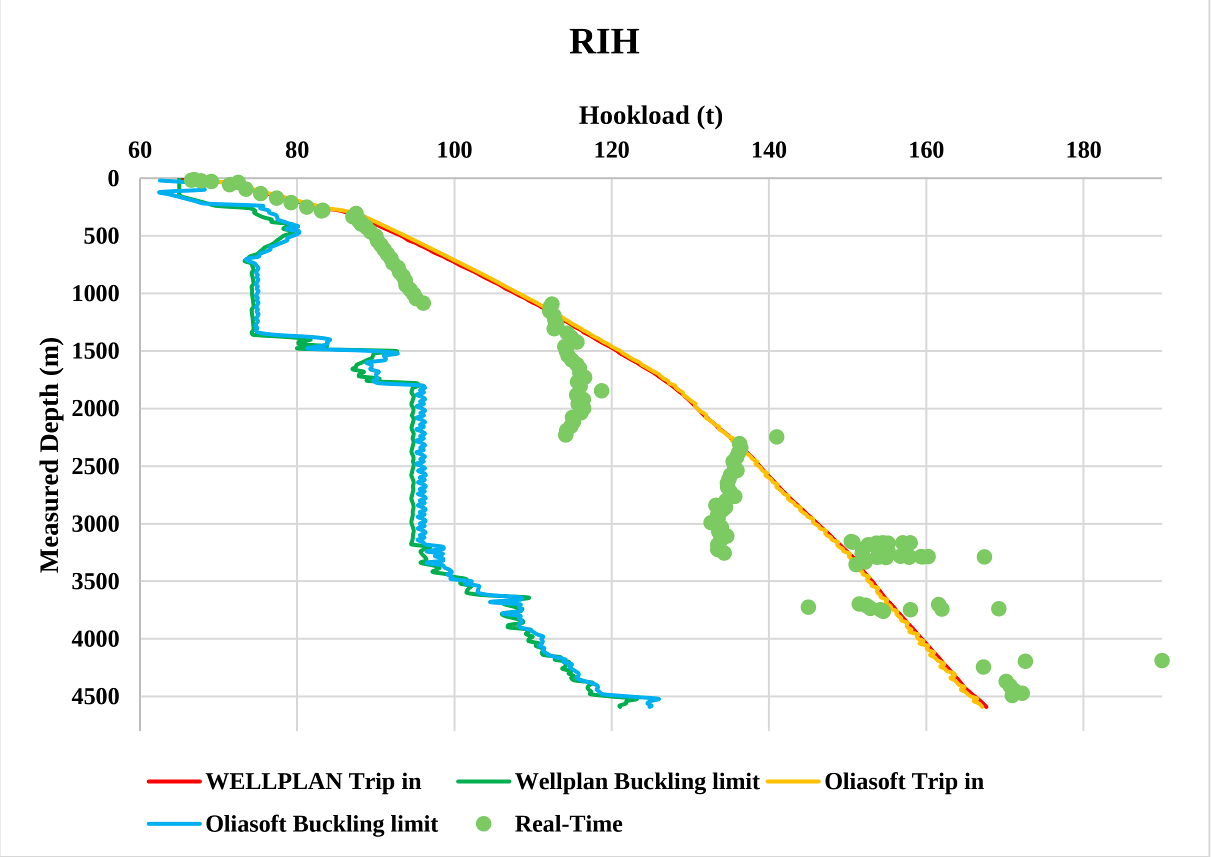

Figure 3.8: Simulated RIH hookload data vs real-time RIH hookload data

3.1.3.3 Drag - Pulling Out of Hole/Tripping Out

Figure 3.9 shows the WP and OWD software simulated results compared with the field dataset. Drag curve for OWD and WP are closely following each other throughout the wellbore. Observed data differs from simulated data at 4000m where it shows approximately 10 tons lower value. This can come from hydraulic drag.

Yield limit curves are identical after 1500m. From start to 1500m OWD has some deviations.

The actual running speed is not a constant value as it is assumed to be in the simulations, therefore observed hookload can vary.

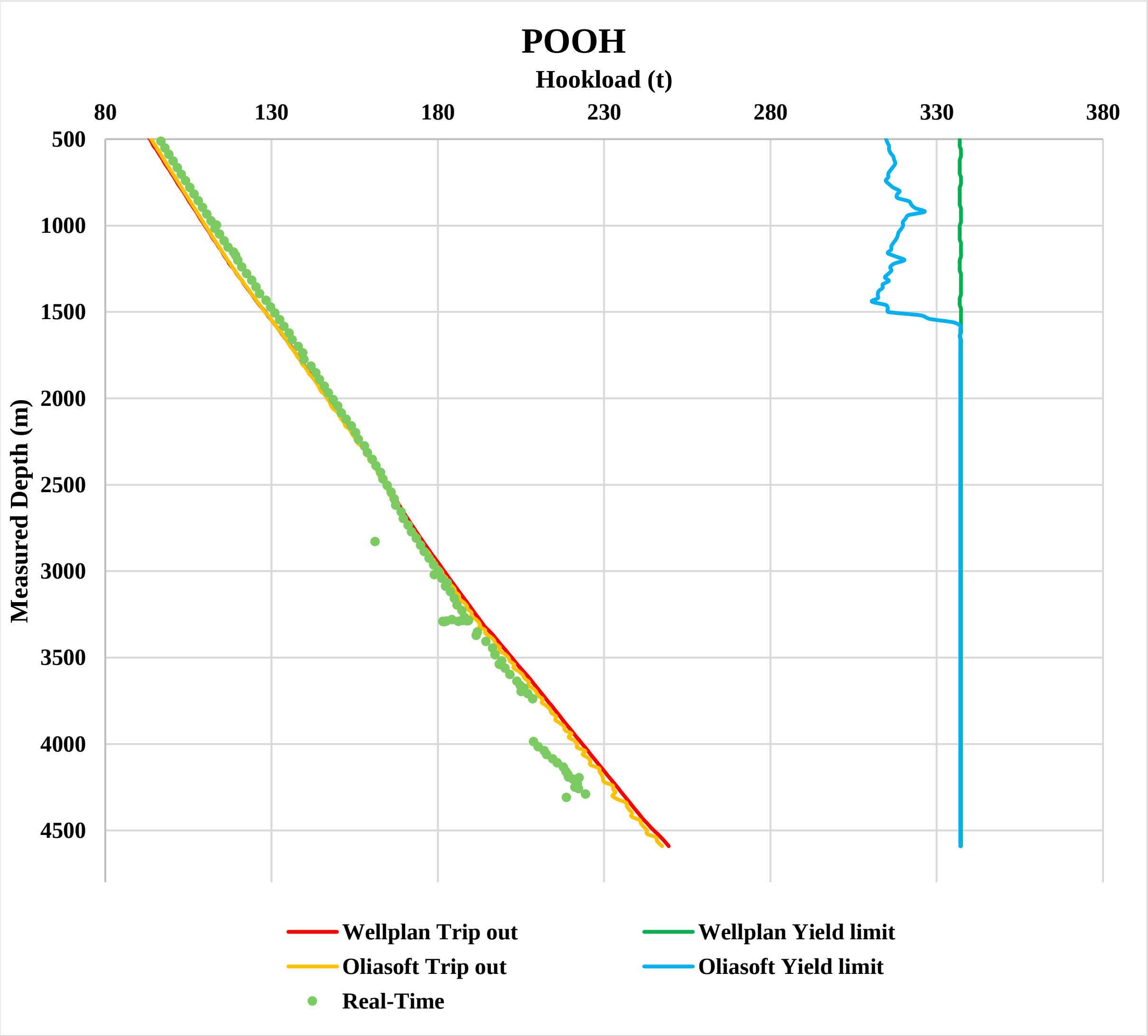

Figure 3.9: Simulated POOH hookload data vs real-time POOH hookload data

3.1.3.4 Torque - Rotating Off Bottom

Torque when rotating off bottom with the drill string drilling BHA. Figure 3.10 shows the WP and OWD software simulated results compared with the field dataset. High difference between WP and OWD. Observed data has big deviation in values, but the trend shows to be in between WP and OWD torque curves.

The deviation in observed data can come from parameters which are assumed constant in the two software's but are not. This can be rotation, flow and pipe stretch.

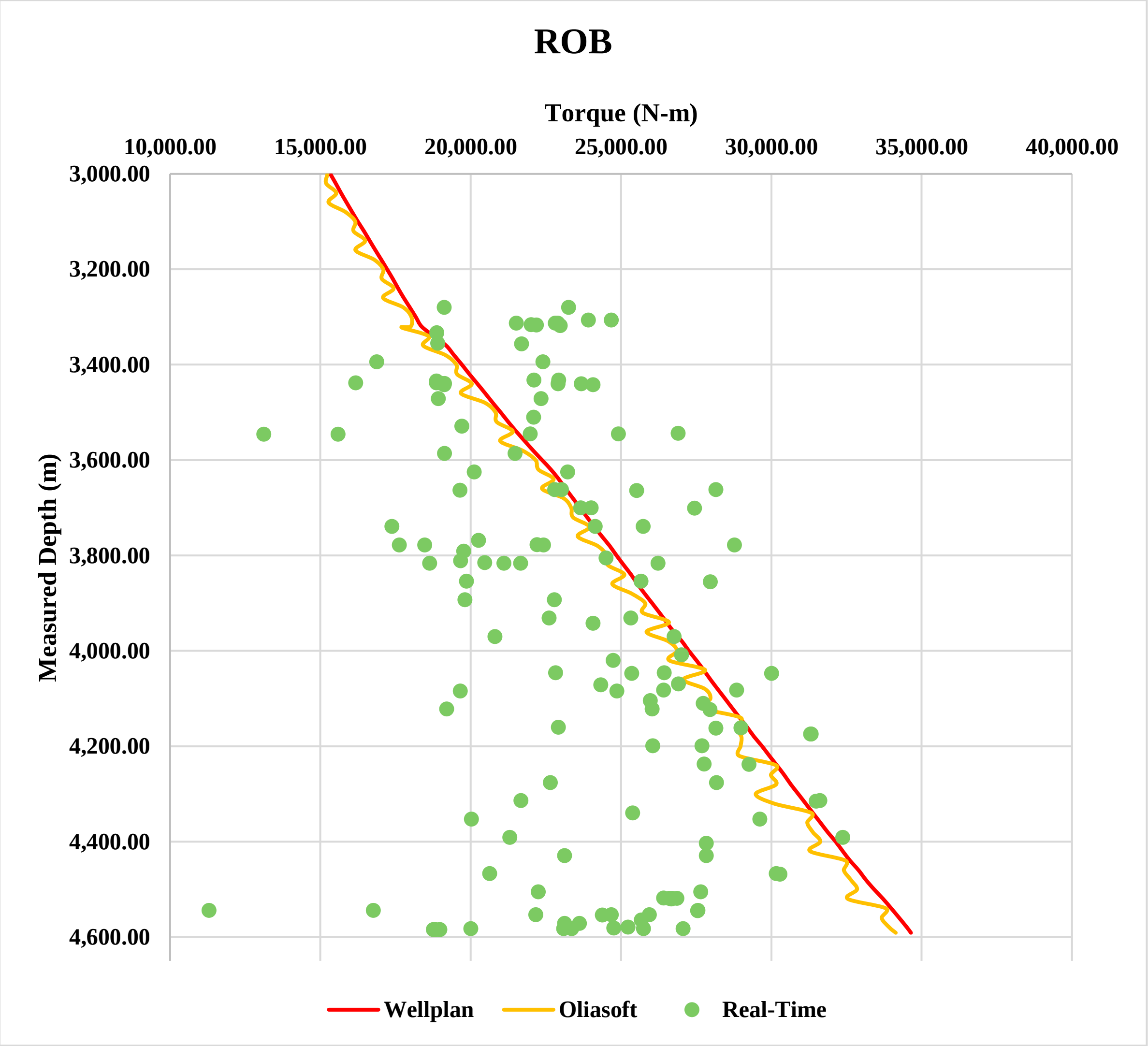

Figure 3.10: Simulated ROB torque data vs real-time ROB torque data

3.1.4 9 7/8" Section

9 7/8" casing run from RKB to 4582.6m MD.

3.1.4.1 Drag - Running Inn Hole/Tripping Inn

Figure 3.11 shows the WP and OWD software simulated results compared with the field dataset. OWD, and WP drag curves are similar, but observed data starts to increase and gets higher values at 3000m down to TD. Buckling limit curves shows large differences throughout the wellbore. This can come from different data input in each software's, but in this case, it is such a large difference between the two software's that further investigating needs to be done.

The actual running speed is not a constant value as it is assumed to be in the simulations, therefore observed hookload can vary.

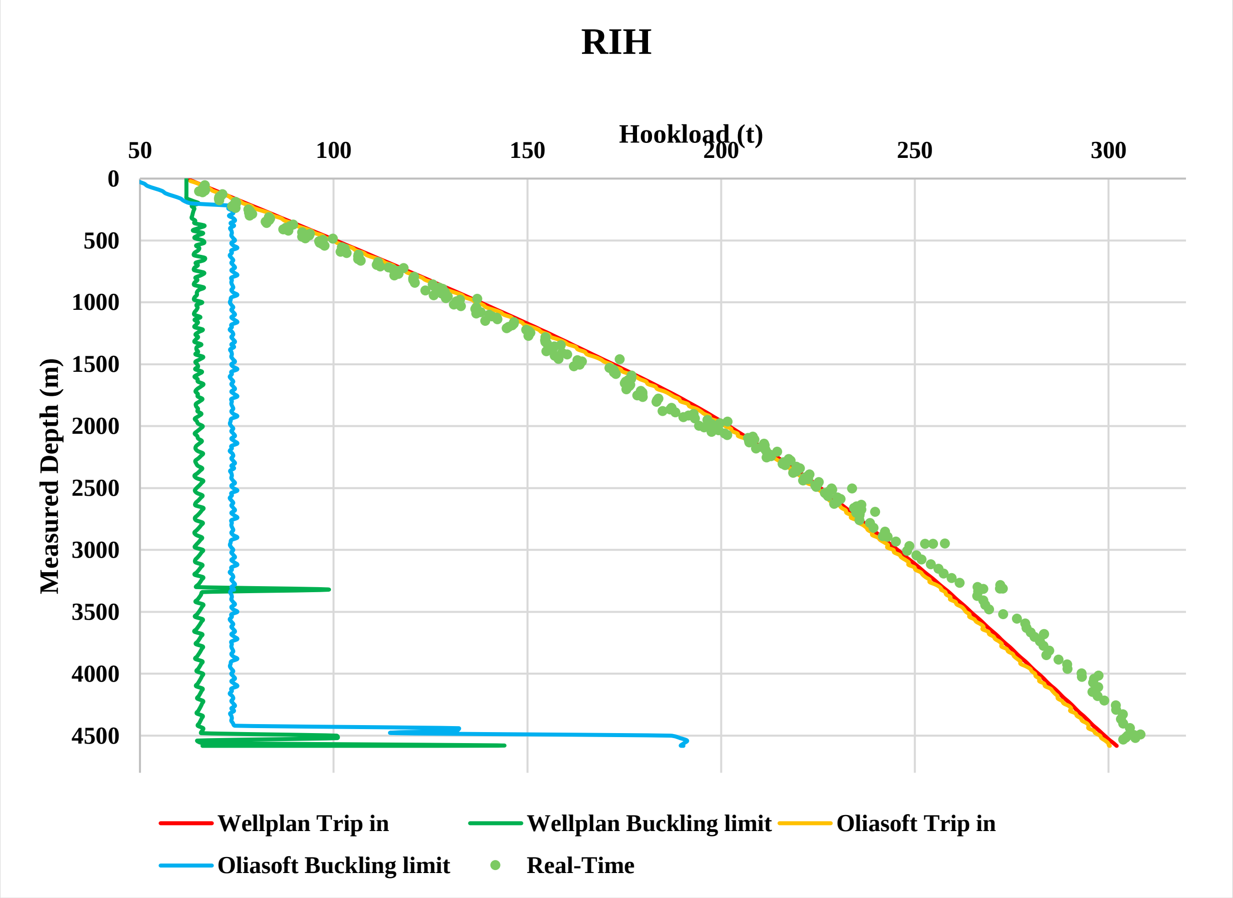

Figure 3.11: Simulated RIH hookload data vs real-time RIH hookload data

3.1.4.2 Drag - Pulling Out Of Hole/Tripping Out

Figure 3.12 shows the WP and OWD software simulated results compared with the field dataset. Simulated data are almost identical throughout the wellbore, while observed data follows a trend which increases slower. Yield limit curves in OWD and WP follows the same path, but OWD is approximately 10 tons higher.

The actual running speed is not a constant value as it is assumed to be in the simulations, therefore observed hookload can vary a lot.

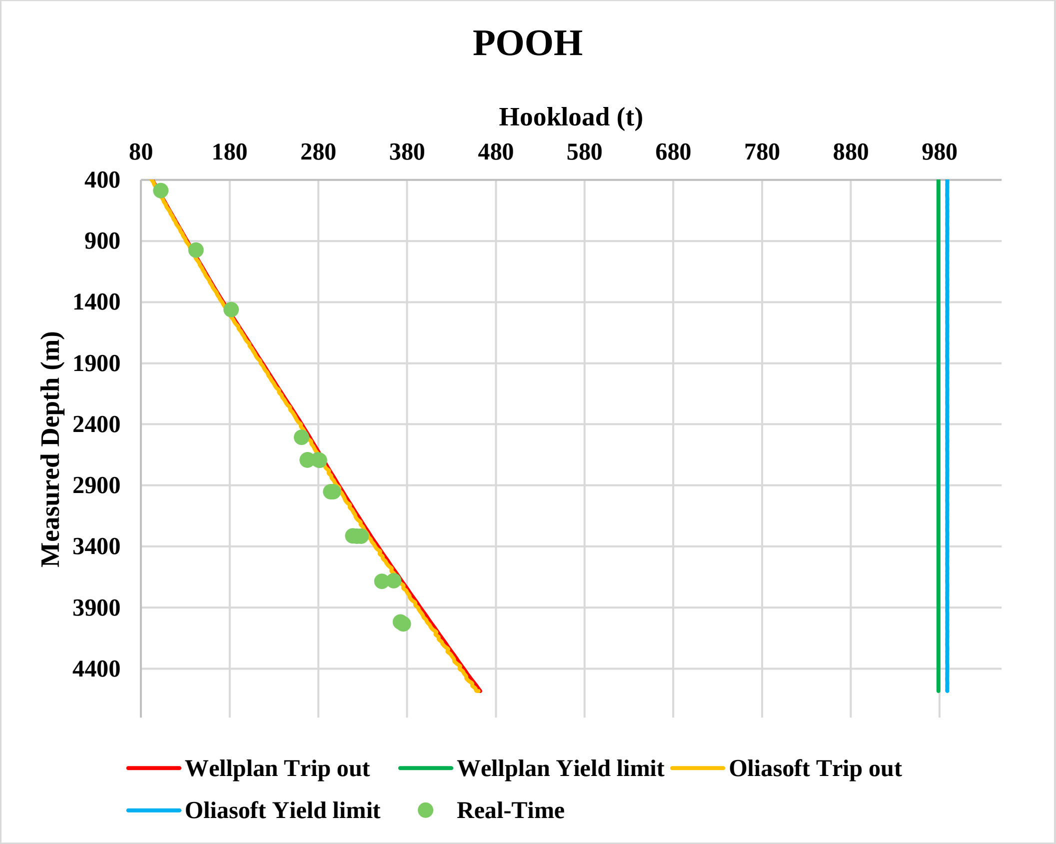

Figure 3.12: Simulated POOH hookload data vs real-time POOH hookload data

3.1.5 Oseberg Sør K-12 A

The well selected from Oseberg Sør for the field case study is a recently drilled well in the North Sea. There are four different sections from the well for this field case study. 12 ¼" and 8 ½" drilling sections All depths refer to measured depths (MD), unless other is mentioned.

3.1.6 12" Section

This section is 643m long, from 3117m to 3760m, drilled with a 3D rotary drilling assembly.

3.1.6.1 Drag - Rotating Off Bottom

Figure 3.13 shows the WP and OWD software simulated results compared with the field dataset. Results show that OWD and WP drag curves show similar trends with about 1 ton difference, but the observed data starts to increase faster from 3300m to 3500m, then decreases faster than simulated data down to TD. This can be caused by poor hole cleaning or formation related issues.

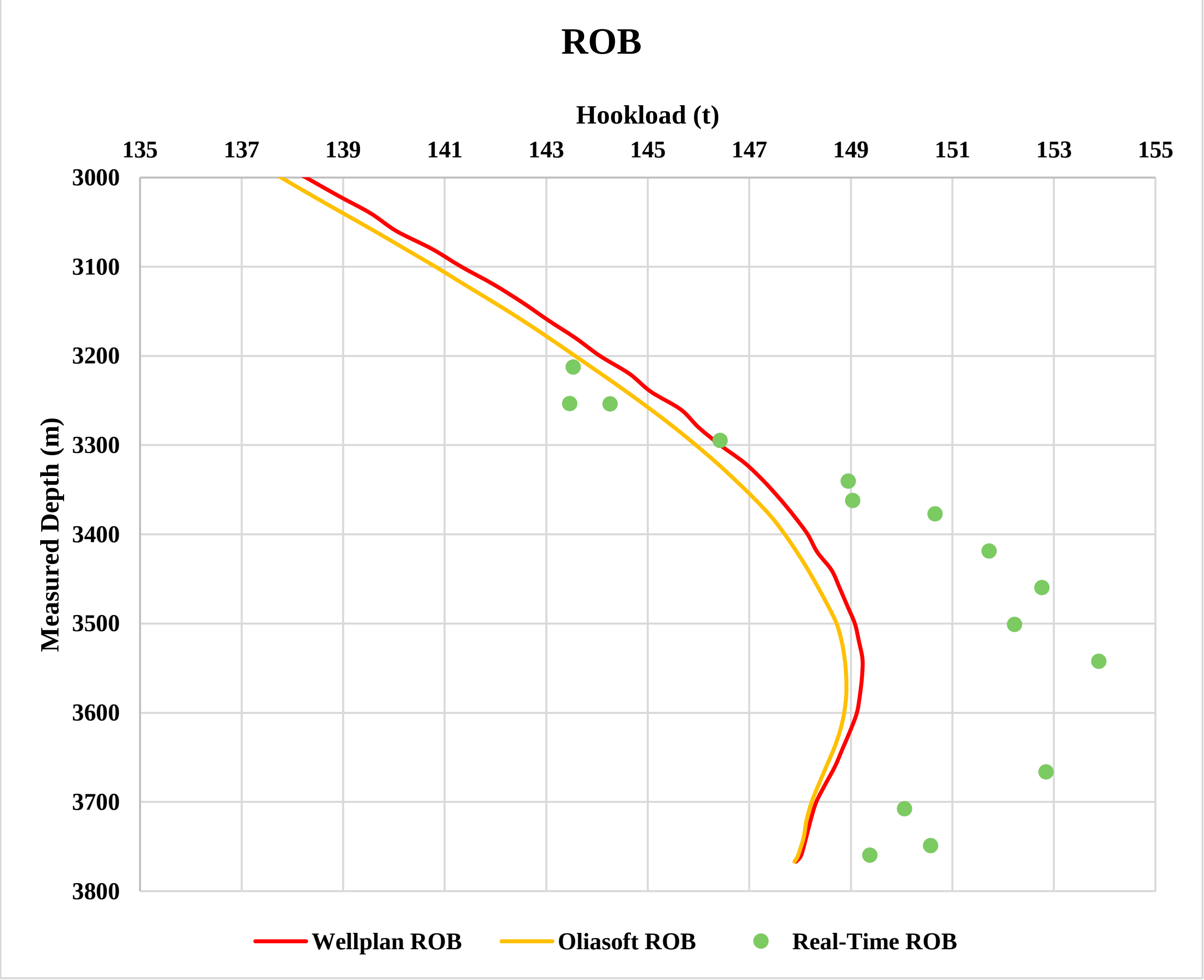

Figure 3.13: Simulated ROB hookload data vs real-time ROB hookload data

3.1.6.2 Drag - Running Inn Hole

Figure 3.14 shows the WP and OWD software simulated results compared with the field dataset. Simulated data follow one another closely throughout the wellbore. Observed data has a greater increase and therefore shows larger values in TD. Buckling limit curves are similar down to 3100m. From her and down to TD, OWD buckling limit curve is 4 tons higher than WP buckling limit curve.

The actual running speed is not a constant value as it is assumed to be in the simulations, therefore observed hookload can vary a lot.

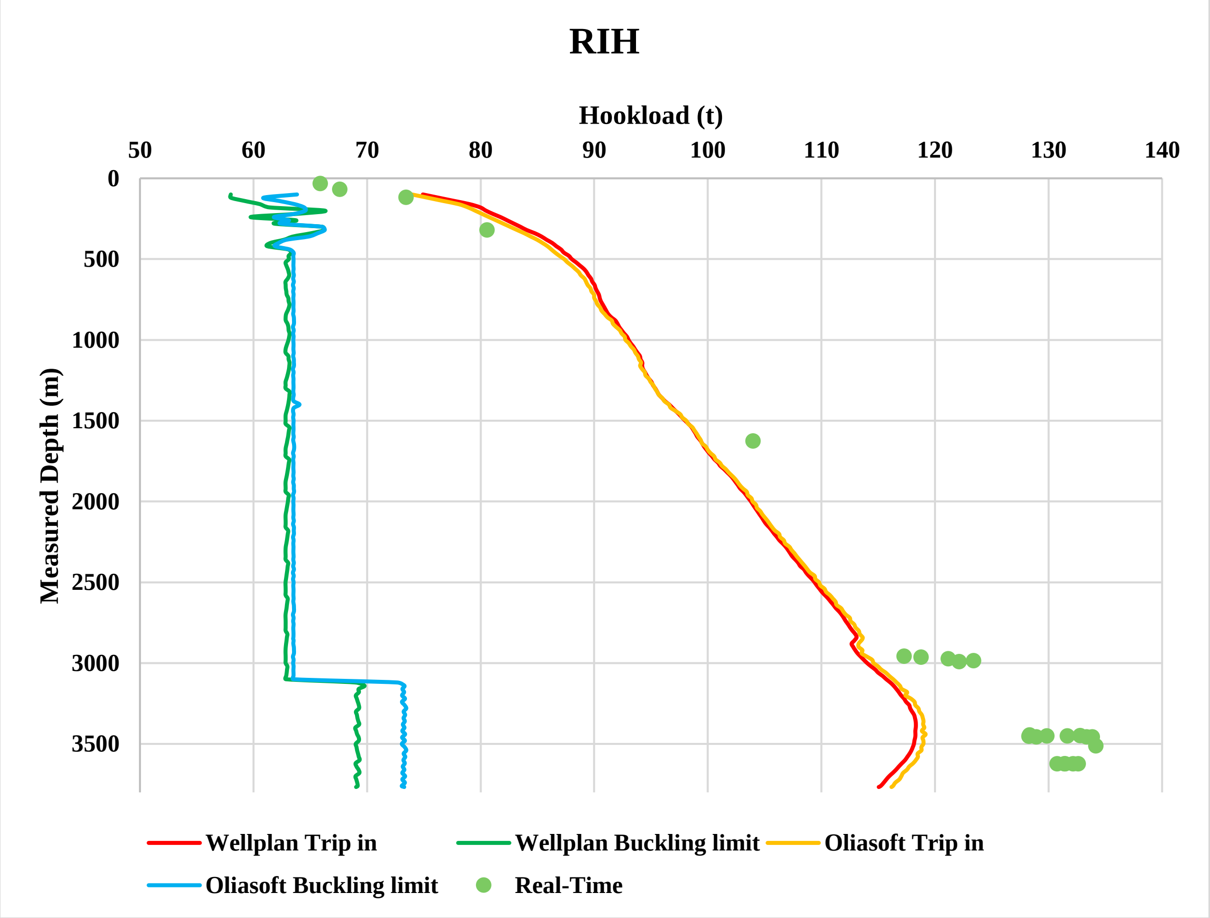

Figure 3.14: Simulated RIH hookload data vs real-time RIH hookload data

3.1.6.3 Drag - Pulling Out of Hole

Figure 3.15 shows the WP and OWD software simulated results compared with the field dataset. OWD, and WP drag curves shows similar trend while observed data deviates from simulated data at 3000m and down to TD. Yield limit curves has a difference in 4 tons throughout the wellbore.

The actual running speed is not a constant value as it is assumed to be in the simulations, therefore observed hookload can vary a lot.

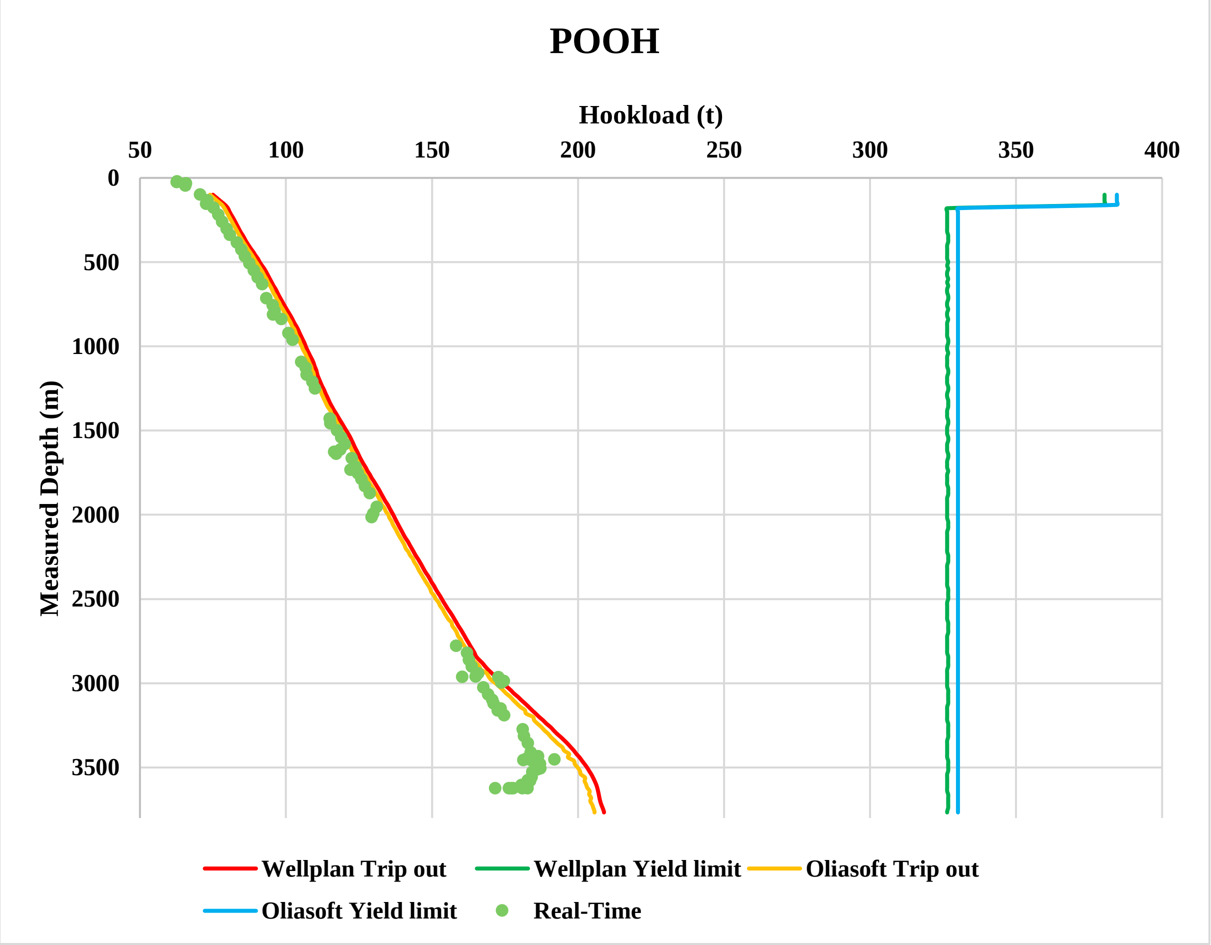

Figure 3.15: Simulated POOH hookload data vs real-time POOH hookload data

3.1.6.4 Torque – Rotating Off Bottom

Figure 3.16 shows the WP and OWD software simulated results compared with the field dataset. Simulated torque data shows a difference of 1 kNm throughout the plot. Observed data shows some deviation, but the trend is in a lower range than the simulated data. Deviation in observed data can come from parameters which is not constant through the operations, but is assumed to constant in the two software\s.

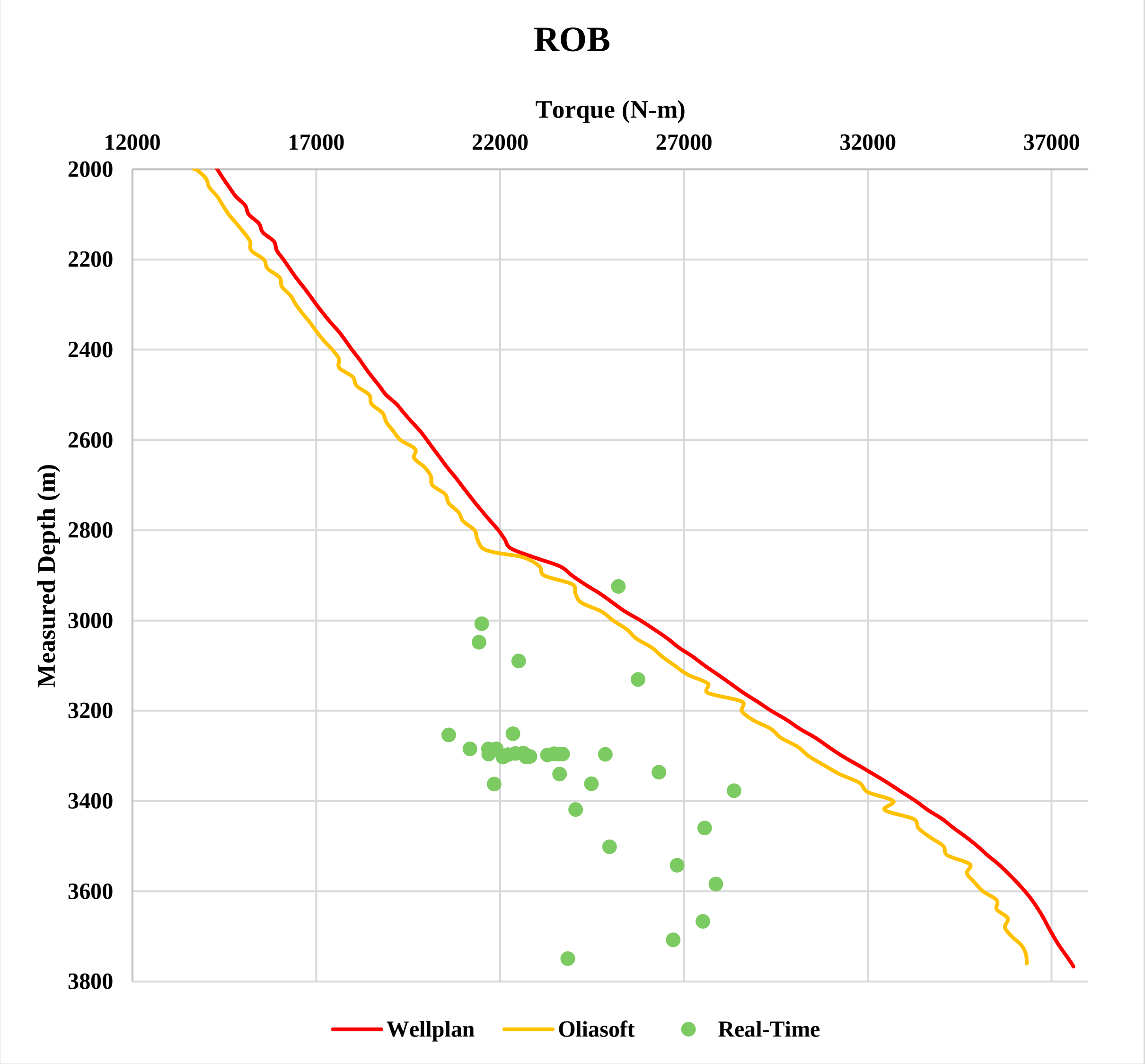

Figure 3.16: Simulated ROB torque data vs real-time ROB torque data

3.1.7 8 ½” drilling Section

This section is 1940m long, from 3762m to 5702m, drilled with a 3D rotary drilling assembly.

3.1.7.1 Drag - Rotating Off Bottom

Figure 3.17 shows the WP and OWD software simulated results compared with the field dataset. Simulated drag curves are as good as identical in this situation. Observed data differs quite a bit from simulated data and shows lower values.

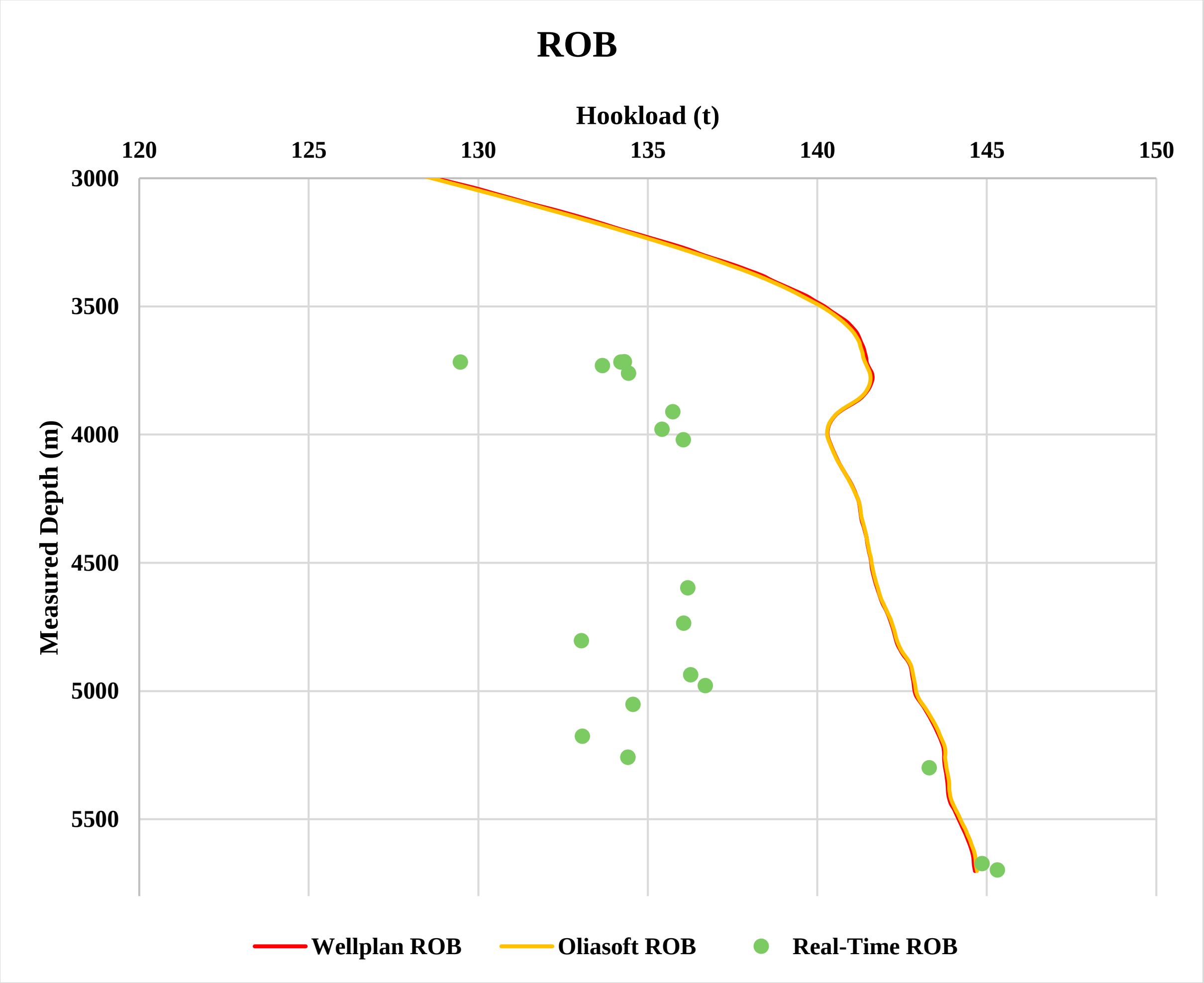

Figure 3.17: Simulated ROB hookload data vs real-time ROB hookload data

3.1.7.2 Drag - Running Inn Hole

Figure 3.18 shows the WP and OWD software simulated results compared with the field dataset. OWD, and WP drag curve follows one another closely throughout the wellbore. Observed data shows the same trend as simulated data, but with lower values down to 3700m and higher values from 4800m down to TD (note pipe filling every +/- 1100m). Buckling limit curves shows identical trends.

The actual running speed is not a constant value as it is assumed to be in the simulations, therefore observed hookload can vary a lot.

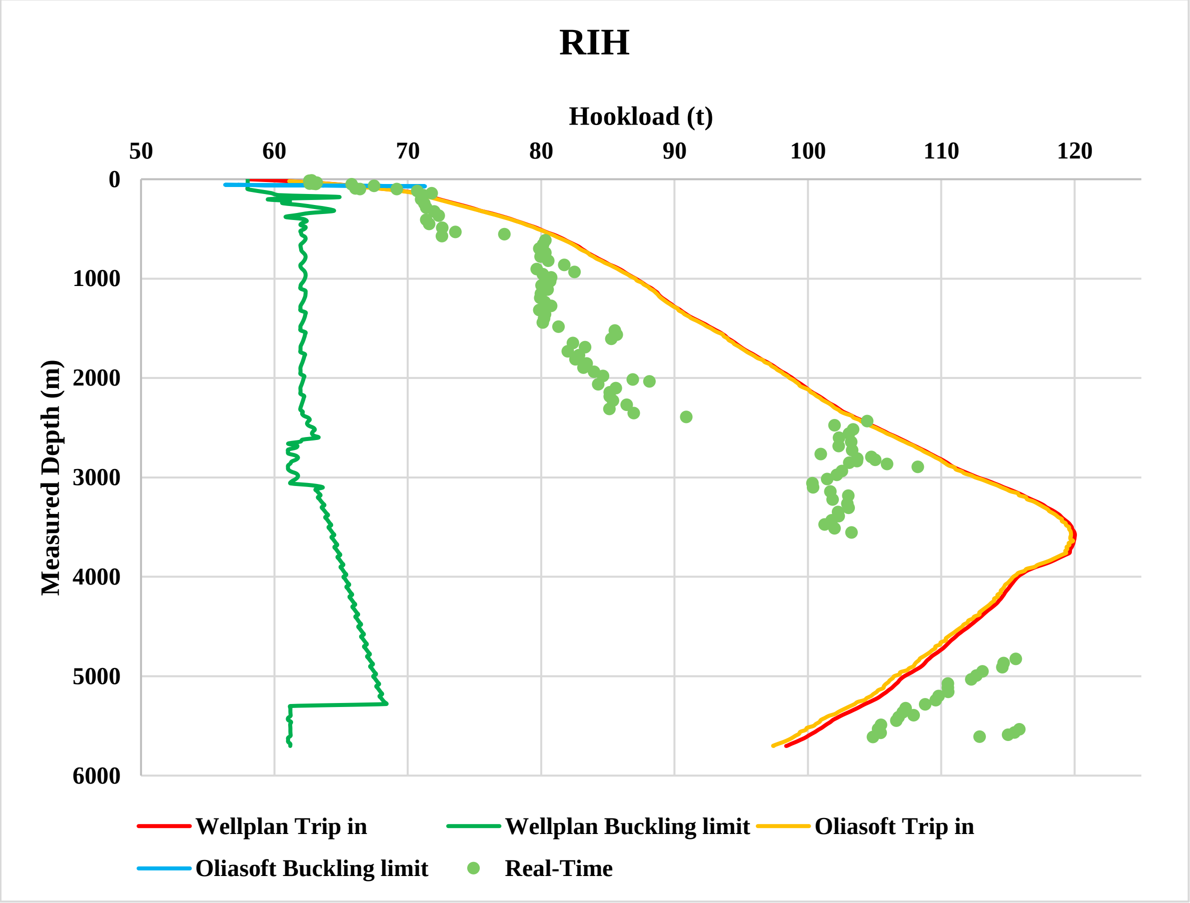

Figure 3.18: Simulated RIH hookload data vs real-time RIH hookload data

3.1.7.3 Drag - Pulling Out of Hole

Figure 3.19 shows the WP and OWD software simulated results compared with the field dataset. Simulated data shows good similarities, and observed data follows simulated data closely throughput the wellbore. Yield limit curves follows each other from the start and down to TD with a difference of 4 tons.

The actual running speed is not a constant value as it is assumed to be in the simulations, therefore observed hookload can vary a lot.

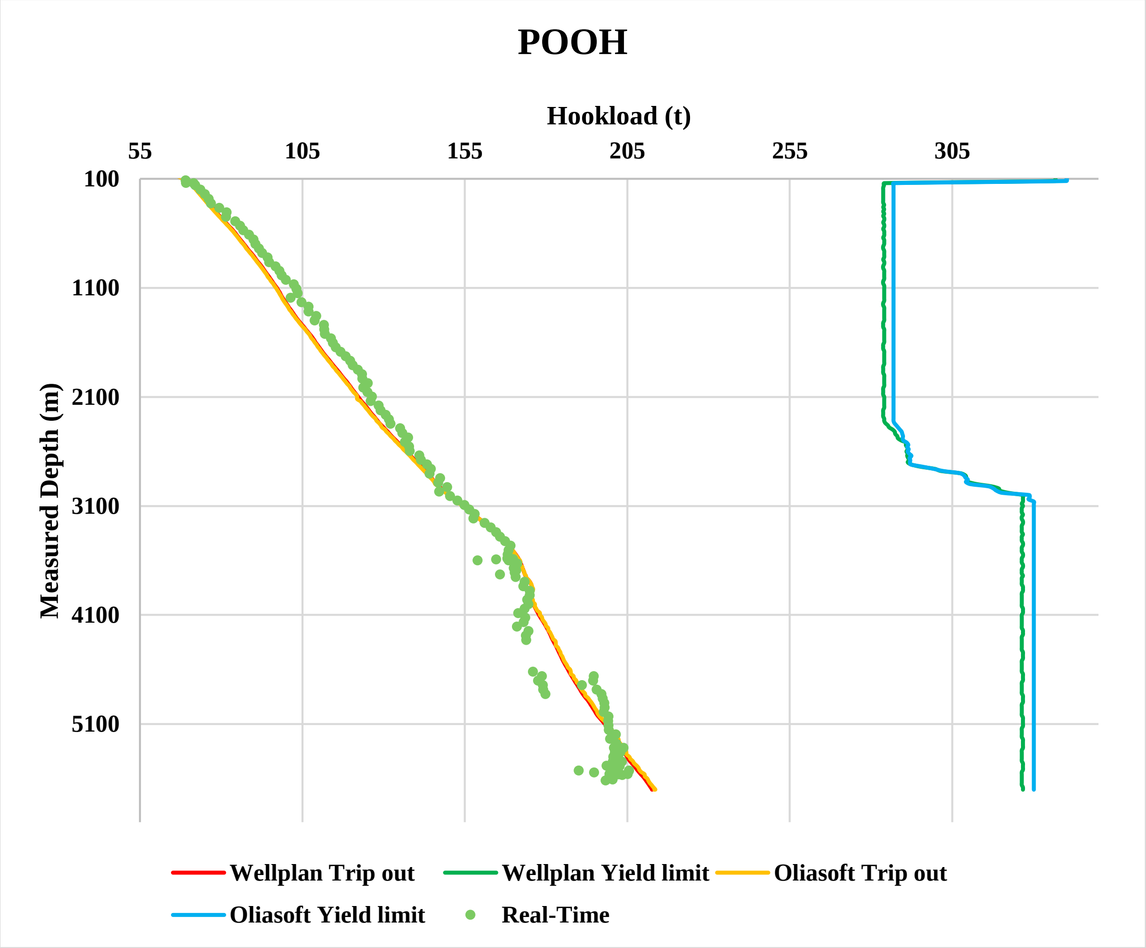

Figure 3.19: Simulated POOH hookload data vs real-time POOH hookload data

3.1.7.4 Torque – Rotating Off Bottom

Figure 3.20 shows the WP and OWD software simulated results compared with the field dataset. Here, the simulated torque curves follow one another as the bit move downwards with a difference of 800 Nm. Observed data shows a trend which has a smaller increase than both simulated torque curves. The deviation in observed data can come from non/constant parameters which is assumed constant in the two software's.

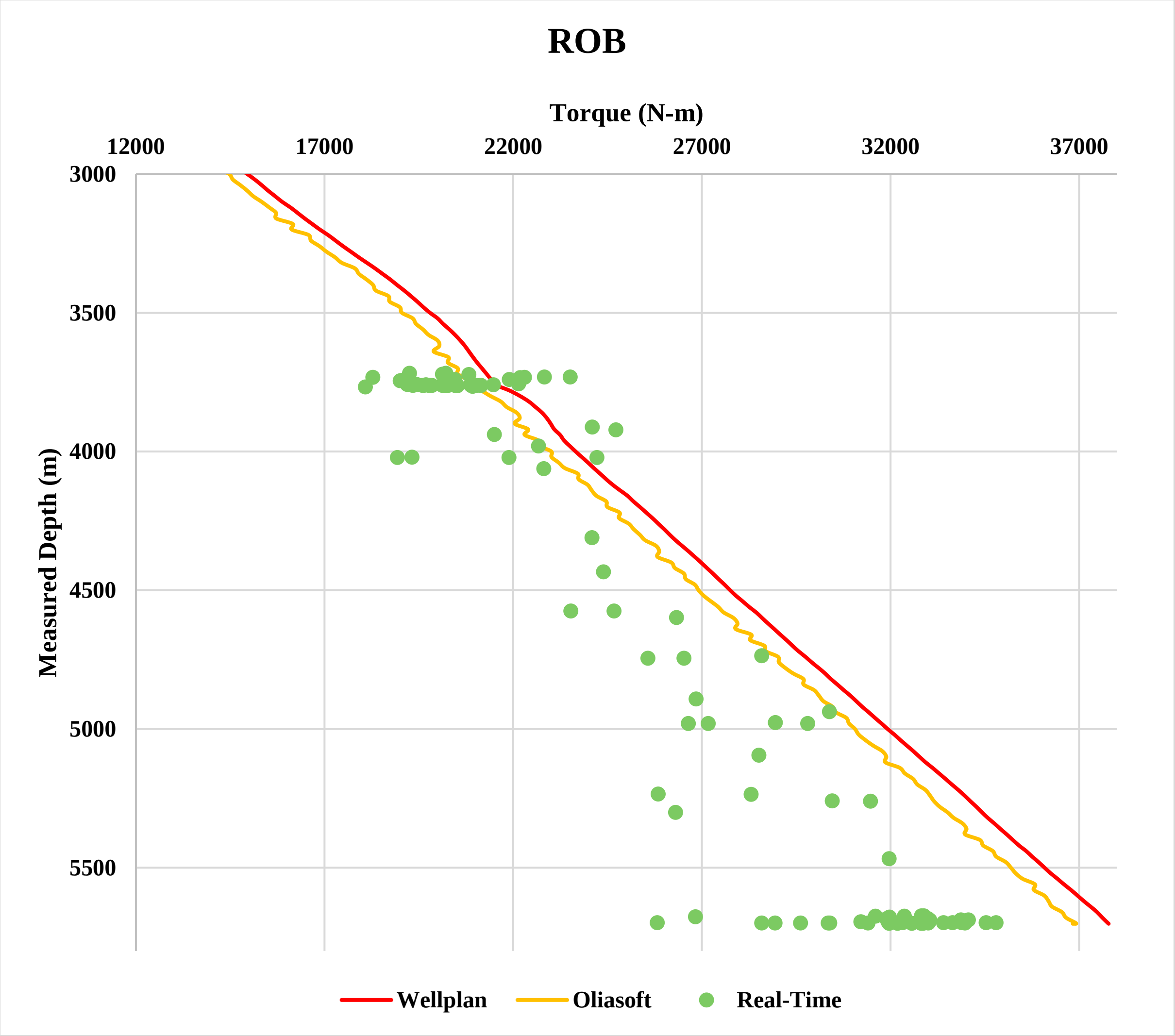

Figure 3.20: Simulated ROB torque data vs real-time ROB torque data

3.1.8 Kvitebjørn A-12 B

3.1.9 7” Liner Section

8 ½” section was drilled from 6465 m to 6947 m with a 3D rotary drilling assembly. Drilling BHA was pulled out of hole and a 7” liner was running in hole

3.1.9.1 Drag - Running Inn Hole

Figure 3.21 shows the WP and OWD software simulated results compared with the field dataset. Both OWD and WP drag curves shows the same trend. Observed data follows simulated data but has a slightly bigger increase from 5600m and down to TD. Buckling limit curves follow one another closely with the same trend.

The actual running speed is not a constant value as it is assumed to be in the simulations, therefore observed hookload can vary a lot.

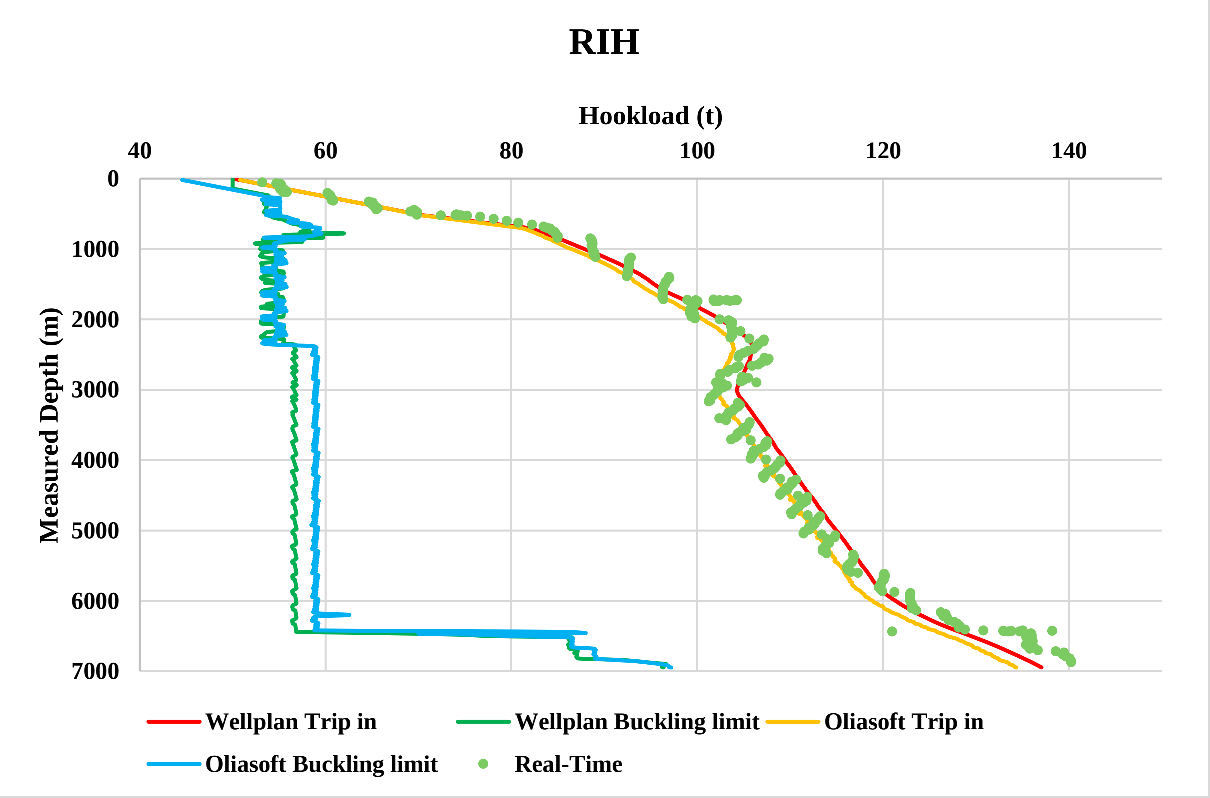

Figure 3.21: Simulated RIH hookload data vs real-time RIH hookload data

3.1.9.2 Drag - Pulling Out Of Hole

Figure 3.22 shows the WP and OWD software simulated results compared with the field dataset. Simulated drag curves show good similarities. Observed data has a bit lower value down to 4000m but shows the same trend as simulated data. Yield limit curves show good similarities.

Usualy there is not often a hookload for POOH when doing a liner run. In this case the hookload results is the drill string being pulled up without the liner. The liner is around 500m long, thus hookload for the last 500m is missing in the observed data curve.

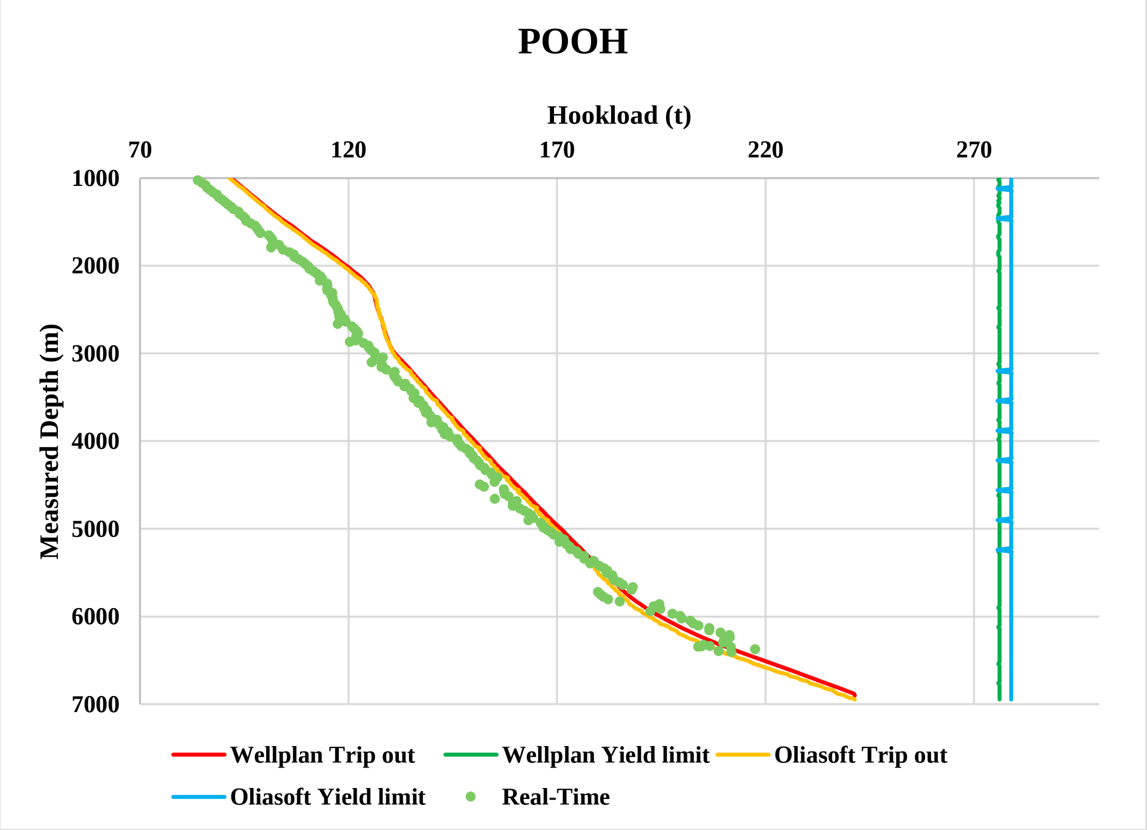

Figure 3.22: Simulated POOH hookload data vs real-time POOH hookload data

3.1.10 Gullfaks

3.1.11 9 5/8" Liner Section

12¼" section was drilled from 2045 m to 5772 m with a 3D rotary drilling assembly. A 9 5/8" liner was running in hole

3.1.11.1 Drag - Running Inn Hole

Figure 3.23 shows the WP and OWD software simulated results compared with the field dataset. Simulated drag curves follow each other closely. Observed data follows the same trend as simulated data, but with some lower value from 4000m and down to TD. Buckling limit curves shows a difference in approximately 10 tons down to 4600m. Then OWD buckling limit curves goes in the same pattern as WP buckling limit curve. Deviation in observed data in this case is from hole instability. Simulated and observed data corresponds very good in casing (down to 1800m).

The actual running speed is not a constant value as it is assumed to be in the simulations, therefore observed hookload can vary a lot.

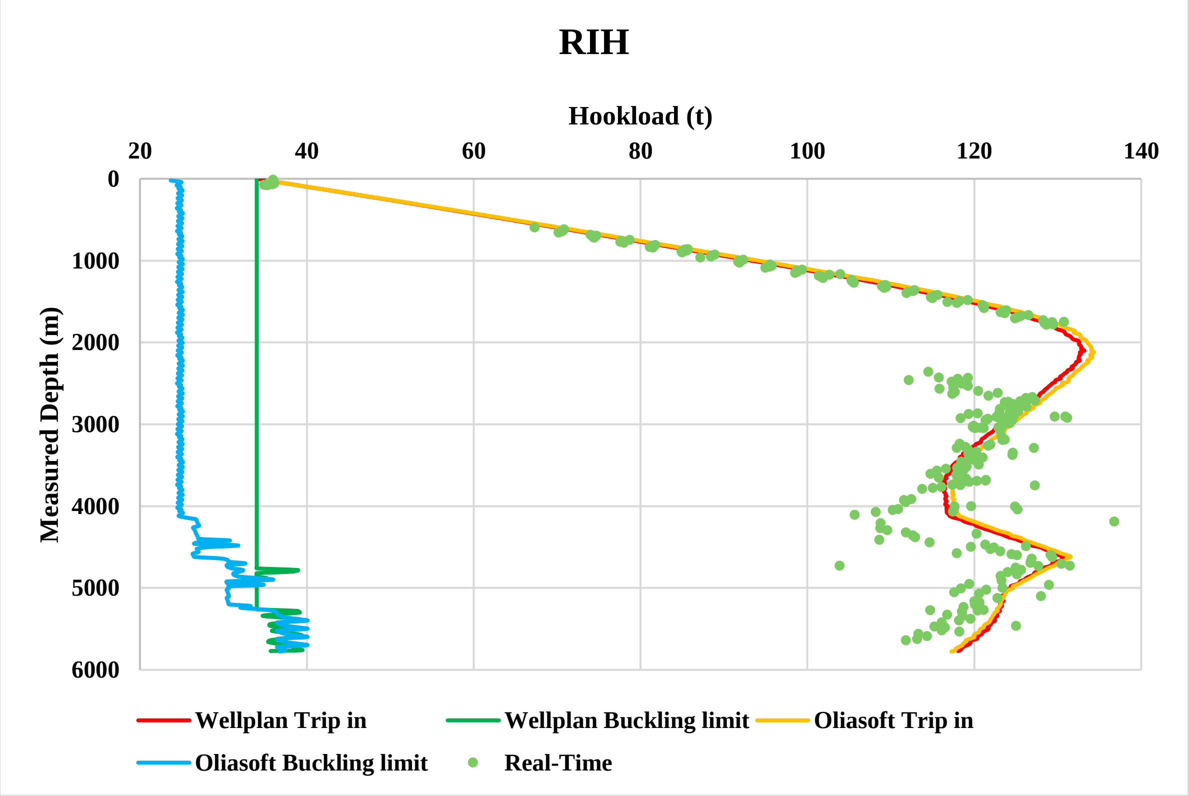

Figure 3.23: Simulated RIH hookload data vs real-time RIH hookload data

3.2 Hydraulics

3.2.1 Valemon

3.2.2 12 ¼" Section

3.2.2.1 Equivalent Circulating Density

Figure 3.24 shows the WP and OWD software simulated results compared with the field dataset. Simulated ECD data shows same trend with a difference in 0.01 sg. Observed data oscillates against 1.81 sg.

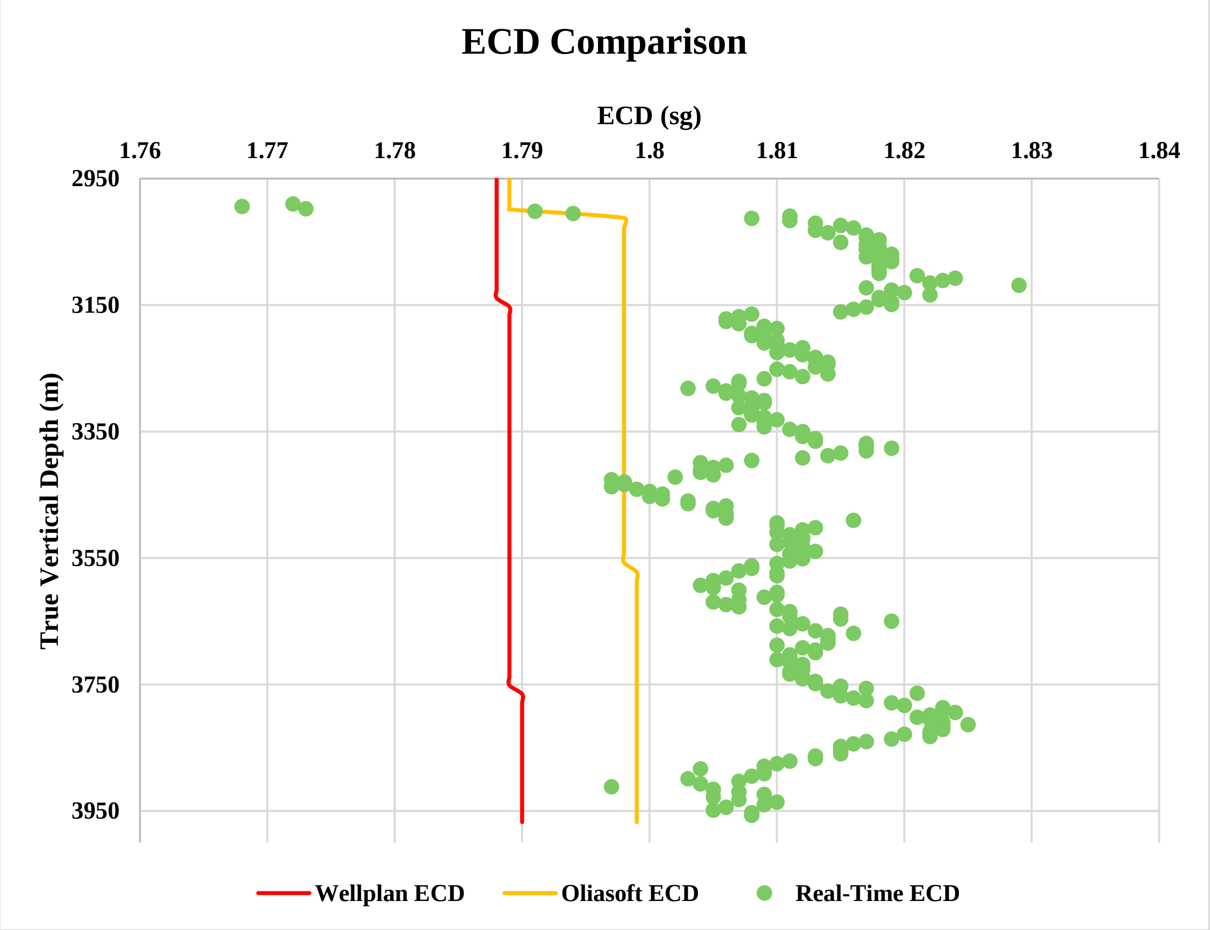

Figure 3.24: Simulated ECD data vs real-time ECD data

3.2.2.2 Standpipe Pressure

Figure 3.25 shows the WP and OWD software simulated results compared with the field dataset. Simulated SPP data shows the same trend, but with a difference of approximately 25 bars throughout the section. Observed data shows a similar trend as simulated data, but with a difference of 25 bars to OWD SPP curve and 50 bars to WP SPP curve. Deviation in observed SPP data can come from non-constant parameters which are assumed to be constant during simulations. These may be flow rate, RPM and ROP. Also, the cuttings load varies in size and density, but are assumed a constant values in the simulations.

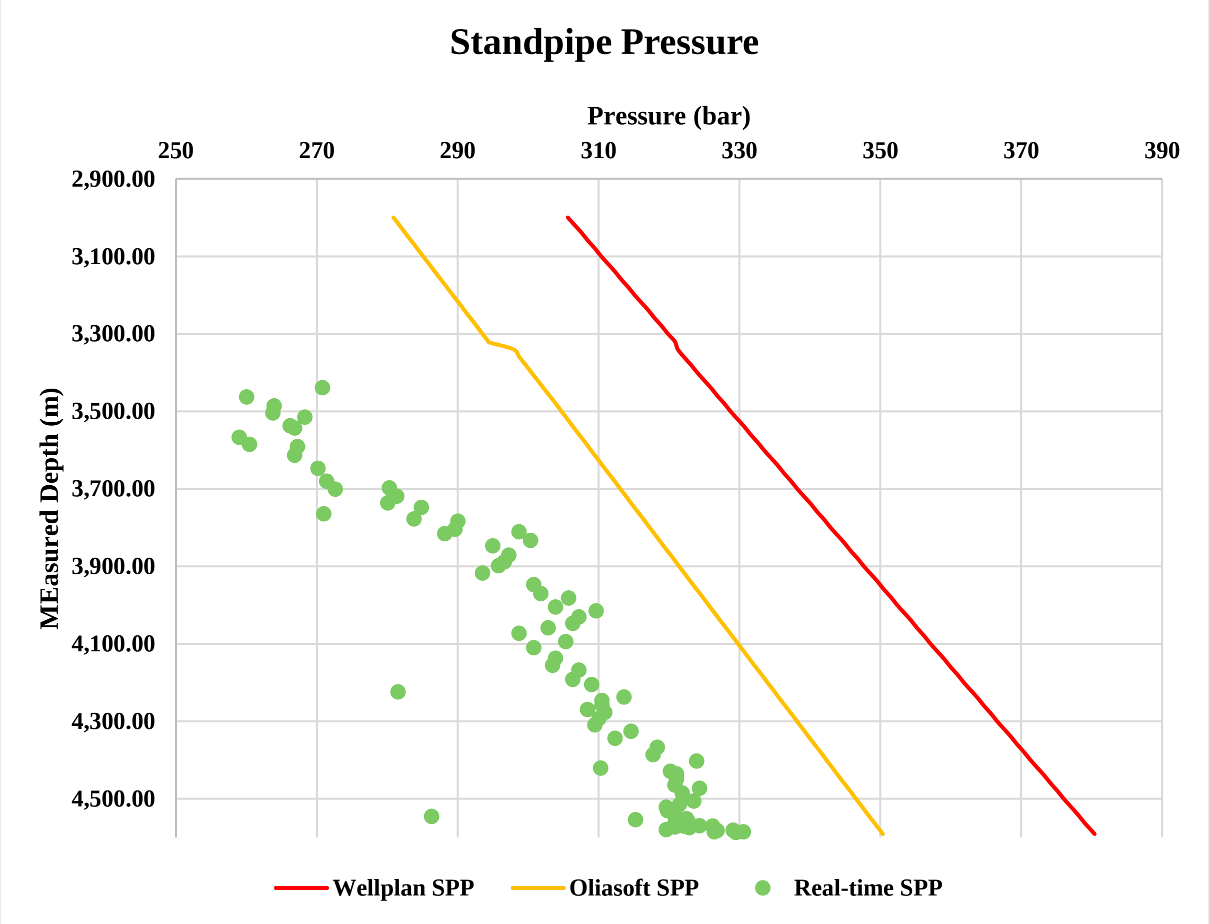

Figure 3.24: Simulated SPP data vs real-time SPP data

3.3 Oseberg Sør

3.3.1 12” Section

3.3.1.1 Equivalent Circulating Density

Figure 3.26 shows the WP and OWD software simulated results compared with the field dataset. OWD ECD curve follows the same pattern as WP ECD curve, but with 0.012sg lower throughout the section. Observed ECD data deviates a bit more and oscillates against 1.565sg before it goes up to 1.58sg at 2600m.

Deviation in observed ECD data can come from non-constant parameters which are assumed to be constant during simulations. These may be flow rate, RPM and ROP. Also, the cuttings load varies in size and density, but are assumed a constant values in the simulations.

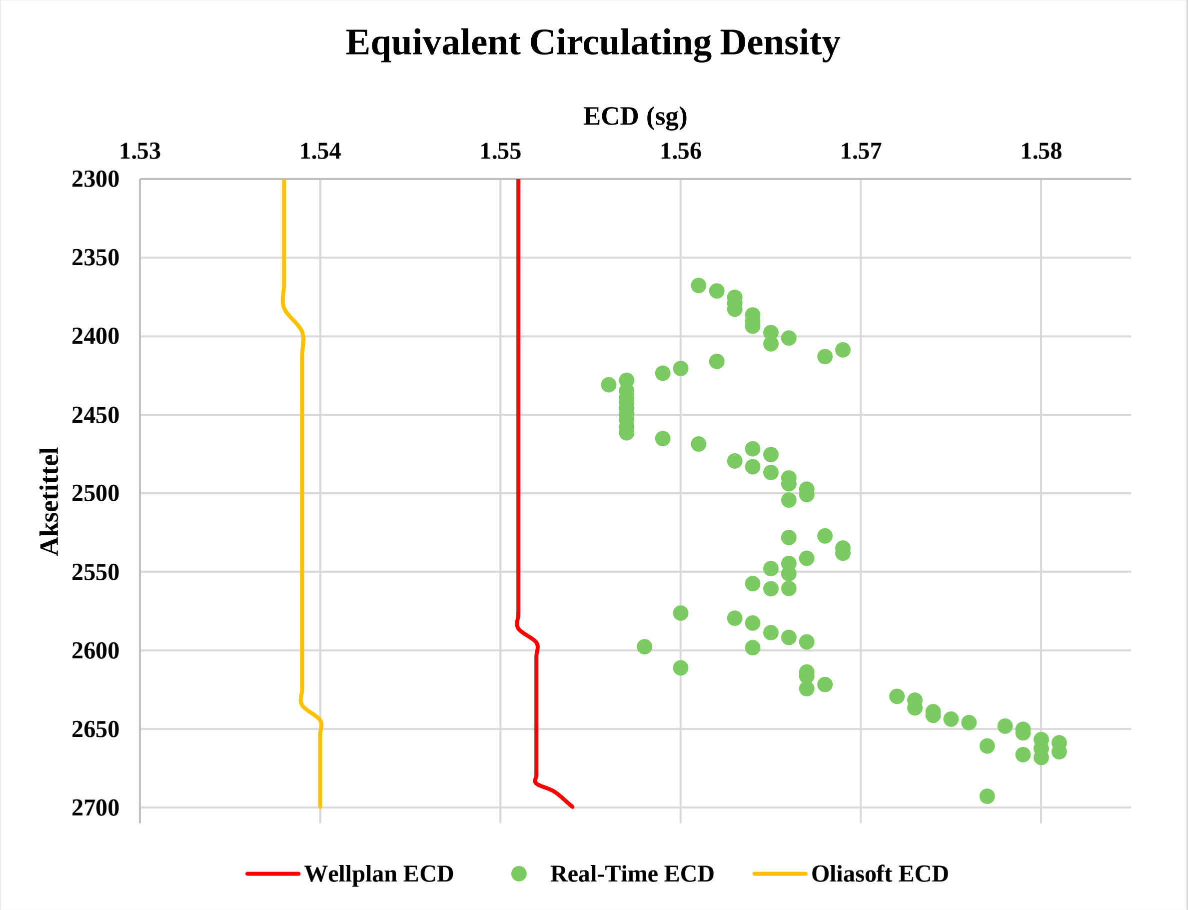

Figure 3.25: Simulated ECD data vs real-time ECD data

3.3.1.2 Standpipe Pressure

Figure 3.27 shows the WP and OWD software simulated results compared with the field dataset. OWD, and WP SPP curves follows the same trend, but with a difference of approximately 45 bars throughout the section. Observed data shows a trend with greater increase and goes from 170 bars to 320 bars in the interval 3200m to 3700m.

Deviation in observed SPP data can come from non-constant parameters which are assumed to be constant during simulations. These may be flow rate, RPM and ROP. Also, the cuttings load varies in size and density, but are assumed a constant values in the simulations.

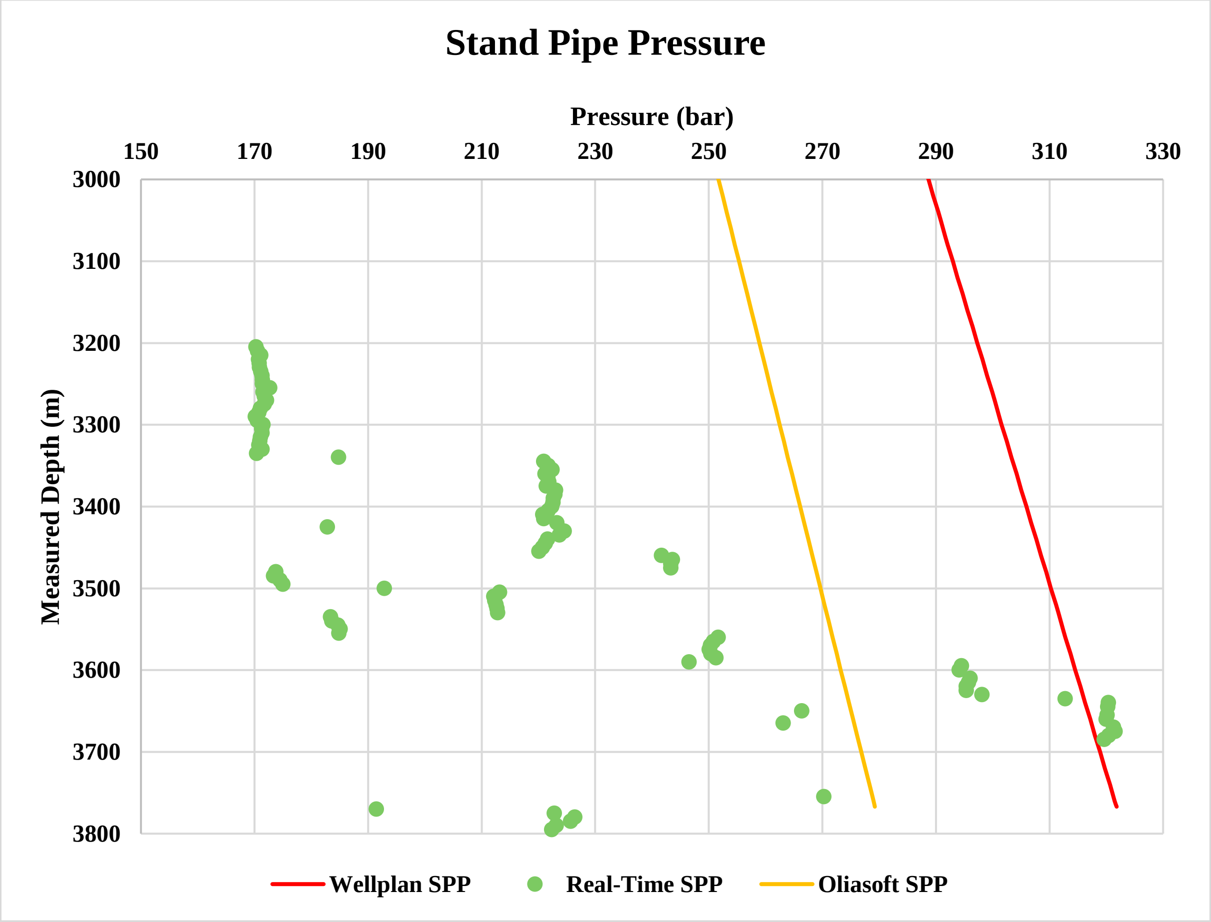

Figure 3.26: Simulated SPP data vs real-time SPP data

3.3.2 8 ½" Section

3.3.2.1 Equivalent Circulating Density

Figure 3.28 shows the WP and OWD software simulated results compared with the field dataset. Simulated ECD data shows the same trend, but WP with higher values throughout the section. Observed data also follows the same trend but are following the OWD ECD curve a bit closer than the WP ECD curve.

Deviation in observed ECD data can come from non-constant parameters which are assumed to be constant during simulations. These may be flow rate, RPM and ROP. Also, the cuttings load varies in size and density, but are assumed a constant values in the simulations.

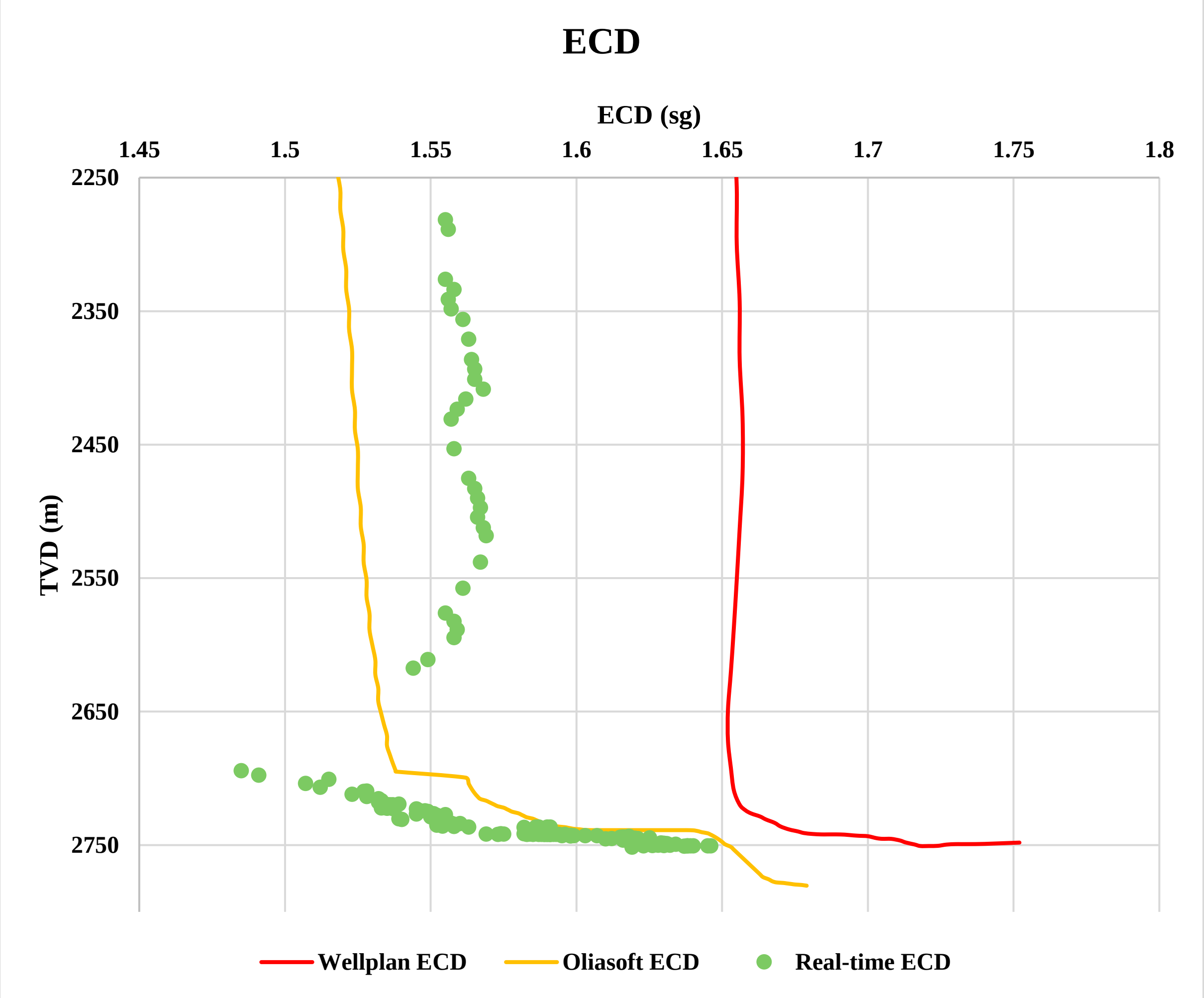

Figure 3.27: Simulated ECD data vs real-time ECD data

3.3.2.2 Standpipe Pressure

Figure 3.29 shows the WP and OWD software simulated results compared with the field dataset. Simulated data follows the same pattern, but with a difference of 30 to 40 bars throughout the section. Observed data shows similar trend as simulated data but makes a jump at 4300m from 230 bars up to 270 bars.

Deviation in observed SPP data can come from non-constant parameters which are assumed to be constant during simulations. These may be flow rate, RPM and ROP. Also, the cuttings load varies in size and density, but are assumed a constant values in the simulations.

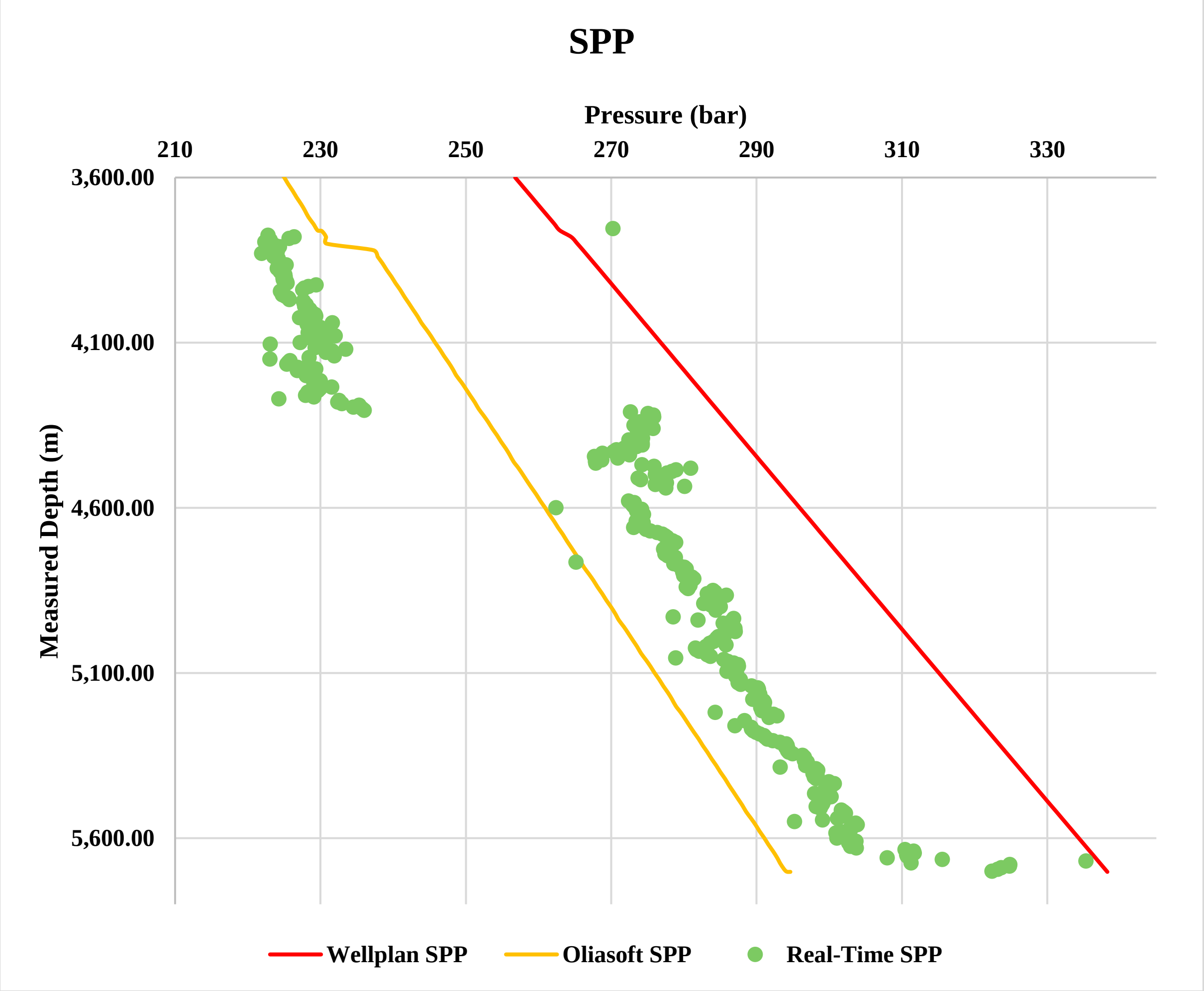

Figure 3.28: Simulated SPP data vs real-time SPP data

3.4 Summary of the Torque & Drag and Hydraulics

3.4.1 Torque & Drag

The drill string mechanics simulation study results with respect to the Torque and Drag will look at why differences between software's occurs, and why they deviate from observed data.

Results show that:

- The simulated drag data from the two software's are showing similar results and there is not much deviation.
- Rotation off bottom simulation values is almost the same from both software's, which is the mostly critical simulation results and calibration weights for further simulations.
- Simulated torque data has more differences, but similarities in trend.
- There are on some occasions differences in buckling limit and yield limit between the two software's. OWD has shown to be a bit more sensitive when it comes to ID (inner diameter) and OD (outer diameter) in casing and string components. This may be one of the reasons differences occur.
- Observed torque & drag data shows similar trend as simulated torque & drag data but has some differences. Reasons for this can be because of parameters which are assumed to be constant in during the simulations, while actual values vary. These parameters include tripping speed and friction factors. Torque & drag is directly affected by changes in these parameters which can be a reason why observed torque & drag data differs from simulated drag data.
- Other parameters which affect torque & drag is well path geometry, hole stability (formation properties), fluid properties and hole cleaning.

3.4.2 Pressure losses

For hydraulic simulations, all known software (Wellplan, DFG, MI) have different challenges. In this study WP has been used as a reference simulation software. Because of this uncertainty, there has been more focus on comparing simulated hydraulics data against actual hydraulics data gathered during well operations. WP doesn't have a perfect temperature simulation engine, which is giving lower simulated temperatures than actual temperatures, effecting mud rheology. It can affect the SPP and ECD data with higher values in the hydraulic simulations. It has been observed that OWD may have a better temperature simulation engine than WP. Anyway, this is still an ongoing process in the Equinor systems.

As mentioned earlier there are several parameters affecting the differences between simulated data and observed data. Cuttings loading such as density and size. These parameters vary throughout the wellbore and are difficult to determine. In the simulation software's these are assumed to be constant, while actual data are not constant. This could be one of the reasons observed data differs from simulated data.

Other parameters which are assumed constant in the simulation software's are flow rate, ROP, and RPM. Changes in these parameters happen regularly while drilling a well and are rarely constant during drilling. SPP and ECD is directly affected by the changes in these parameters which adds another reason why the difference in observed data and simulated data occurs.

There are also uncertainties around input data referring to string components. These may not be 100% accurate and thus affecting simulated results. Different string components has a certain pressure loss over its length. This is only accounted for the MWD (Measure While Drilling) string components in the simulation software's which can be wrong input for varies flow rates. Pressure loss over other string components is assumed to be zero. SPP is also affected by this.

4 Results Analysis and Verification

This chapter present the results analysis of the results obtained from the software and the measured field data. The main objective here is to verify the Oliasoft software to be qualified as a design and analysis tool. This can be done by evaluating the Oliasoft results deviation from the measured data and how the Oliasoft software results is comparable with the Landmark/WellPlan TM simulation results. Here, the benchmark for the Oliasoft software result is the WellPlan simulation. The main reason is that the issue with the field dataset is that the data may contain noises, which are due to vibrations. Software don't consider this effect. Moreover, the software simulation is based on ideal wellbore geometry and the friction factor is assumed to be the same for the whole drilling section. But the coefficient friction is a profile, which varies in depth section.

For the verification to reach to the conclusion, a excel comparison sheet has been used to simplify the results. The excel sheet is made in cooperation with Equinor employees. The different color codes are determined by the same Equinor employees, where green is acceptable, yellow is acceptable but needs investigation, gold is not acceptable and needs investigation and red is too big difference mainly caused by wrong input. All compared data is gathered from TD in well.

4.1.1 Rotating Off Bottom

One may observe from figure 4.1 that the difference between OWD and WP in percentage is below 1% for all cases. This is a verification that equal data input of well path geometry, fluid data and string data gives the same calculated weight of string which is an important basis for torque & drag calculations.

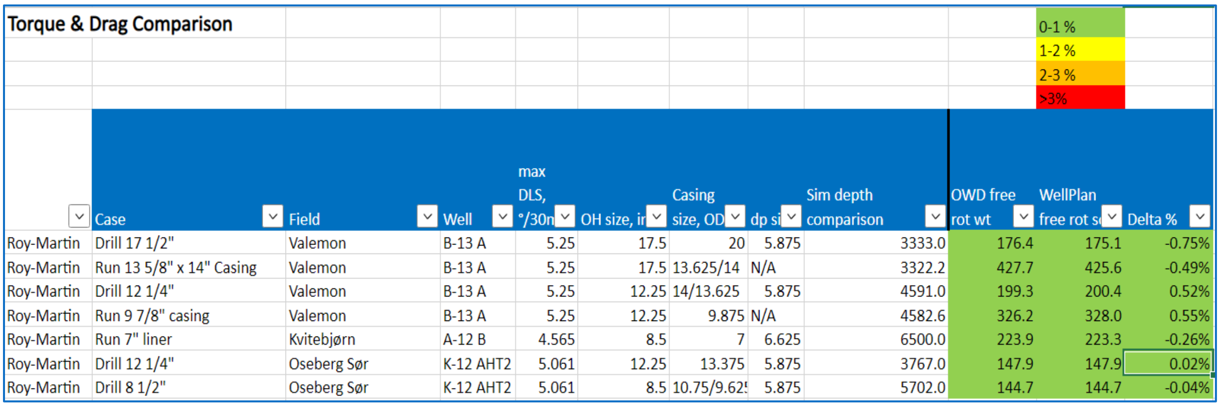

Torque & Drag Comparison

🟩 0-1 %
🟨 1-2 %
🟧 2-3 %
🟥 >3%

	Case	Field	Well	max DLS, °/30n	OH size, ir	Casing size, OD	dp si	Sim depth comparison	OWD free rot wt	WellPlan free rot s	Delta %
Roy-Martin	Drill 17 1/2"	Valemon	B-13 A	5.25	17.5	20	5.875	3333.0	176.4	175.1	-0.75%
Roy-Martin	Run 13 5/8" x 14" Casing	Valemon	B-13 A	5.25	17.5	13.625/14	N/A	3322.2	427.7	425.6	-0.49%
Roy-Martin	Drill 12 1/4"	Valemon	B-13 A	5.25	12.25	14/13.625	5.875	4591.0	199.3	200.4	0.52%
Roy-Martin	Run 9 7/8" casing	Valemon	B-13 A	5.25	12.25	9.875	N/A	4582.6	326.2	328.0	0.55%
Roy-Martin	Run 7" liner	Kvitebjørn	A-12 B	4.565	8.5	7	6.625	6500.0	223.9	223.3	-0.26%
Roy-Martin	Drill 12 1/4"	Oseberg Sør	K-12 AHT2	5.061	12.25	13.375	5.875	3767.0	147.9	147.9	0.02%
Roy-Martin	Drill 8 1/2"	Oseberg Sør	K-12 AHT2	5.061	8.5	10.75/9.62!	5.875	5702.0	144.7	144.7	-0.04%

Figure 4.1: Excel sheet containing ROB hookload data from OWD and WP and the percentage difference between them

4.1.2 Pulling Out Off the Hole

One may observe from figure 4.2 that the difference between OWD and WP in percentage is below 2% for all cases. This means OWD Torque and Drag simulations are within the acceptable range and can be used in Equinor system, when soft sting calculations are sufficient.

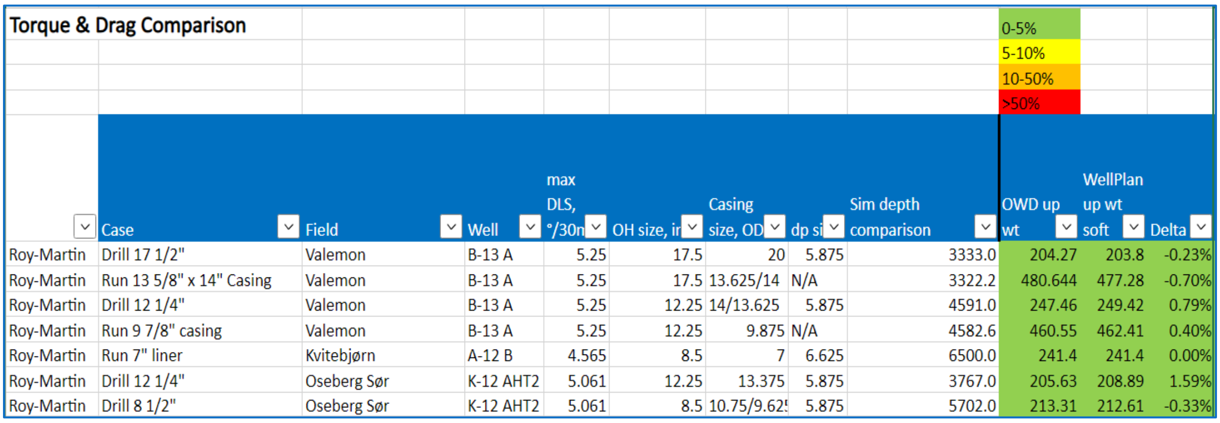

Torque & Drag Comparison

🟩 0-5%
🟨 5-10%
🟧 10-50%
🟥 >50%

	Case	Field	Well	max DLS, °/30n	OH size, in	Casing size, OD	dp si	Sim depth comparison	OWD up wt	WellPlan up wt soft	Delta
Roy-Martin	Drill 17 1/2"	Valemon	B-13 A	5.25	17.5	20	5.875	3333.0	204.27	203.8	-0.23%
Roy-Martin	Run 13 5/8" x 14" Casing	Valemon	B-13 A	5.25	17.5	13.625/14	N/A	3322.2	480.644	477.28	-0.70%
Roy-Martin	Drill 12 1/4"	Valemon	B-13 A	5.25	12.25	14/13.625	5.875	4591.0	247.46	249.42	0.79%
Roy-Martin	Run 9 7/8" casing	Valemon	B-13 A	5.25	12.25	9.875	N/A	4582.6	460.55	462.41	0.40%
Roy-Martin	Run 7" liner	Kvitebjørn	A-12 B	4.565	8.5	7	6.625	6500.0	241.4	241.4	0.00%
Roy-Martin	Drill 12 1/4"	Oseberg Sør	K-12 AHT2	5.061	12.25	13.375	5.875	3767.0	205.63	208.89	1.59%
Roy-Martin	Drill 8 1/2"	Oseberg Sør	K-12 AHT2	5.061	8.5	10.75/9.62!	5.875	5702.0	213.31	212.61	-0.33%

Figure 4.2: Excel sheet containing ROB hookload data from OWD and WP and the percentage difference between them

4.1.3 Running Into the Hole

One may observe from figure 4.3 that the difference between OWD and WP in percentage is below 3% for all cases. This means OWD Torque and Drag simulations are within the acceptable range and can be used in Equinor systems.

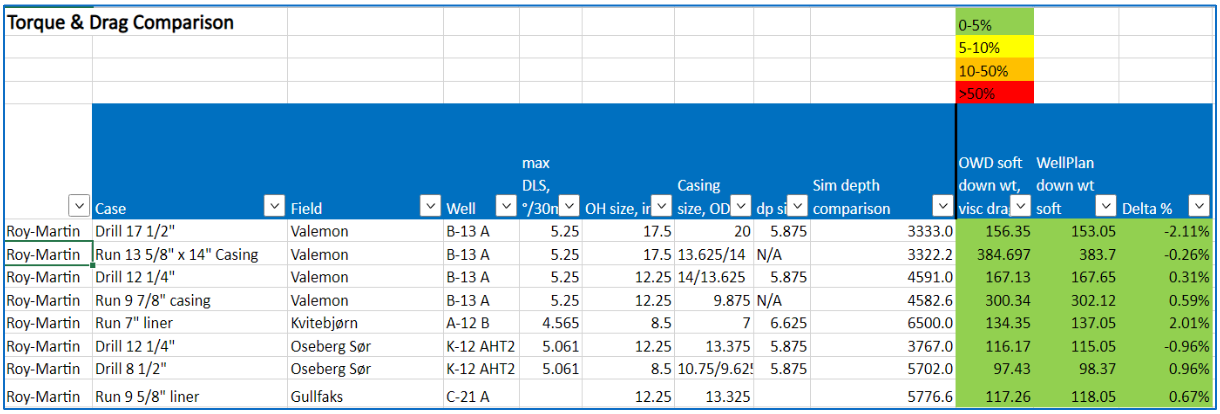

Torque & Drag Comparison

🟩 0-5%
🟨 5-10%
🟧 10-50%
🟥 >50%

	Case	Field	Well	max DLS, °/30n	OH size, in	Casing size, OD	dp si	Sim depth comparison	OWD soft down wt, visc dra	WellPlan down wt soft	Delta %
Roy-Martin	Drill 17 1/2"	Valemon	B-13 A	5.25	17.5	20	5.875	3333.0	156.35	153.05	-2.11%
Roy-Martin	Run 13 5/8" x 14" Casing	Valemon	B-13 A	5.25	17.5	13.625/14	N/A	3322.2	384.697	383.7	-0.26%
Roy-Martin	Drill 12 1/4"	Valemon	B-13 A	5.25	12.25	14/13.625	5.875	4591.0	167.13	167.65	0.31%
Roy-Martin	Run 9 7/8" casing	Valemon	B-13 A	5.25	12.25	9.875	N/A	4582.6	300.34	302.12	0.59%
Roy-Martin	Run 7" liner	Kvitebjørn	A-12 B	4.565	8.5	7	6.625	6500.0	134.35	137.05	2.01%
Roy-Martin	Drill 12 1/4"	Oseberg Sør	K-12 AHT2	5.061	12.25	13.375	5.875	3767.0	116.17	115.05	-0.96%
Roy-Martin	Drill 8 1/2"	Oseberg Sør	K-12 AHT2	5.061	8.5	10.75/9.62!	5.875	5702.0	97.43	98.37	0.96%
Roy-Martin	Run 9 5/8" liner	Gullfaks	C-21 A		12.25	13.325		5776.6	117.26	118.05	0.67%

Figure 4.3: Excel sheet containing ROB hookload data from OWD and WP and the percentage difference between them

4.1.4 Buckling limit

One may observe from figure 4.4 that in most cases, the difference between OWD and WP in percentage is below 5%. Other comparison results show differences are more than 10% which has been informed to Equinor employees and further investigations are ongoing. This means most of the buckling limit calculations used in the simulations are within the acceptable range and can use in Equinor systems. The largest differences are found in how centralizers affect the buckling of casings and liners.

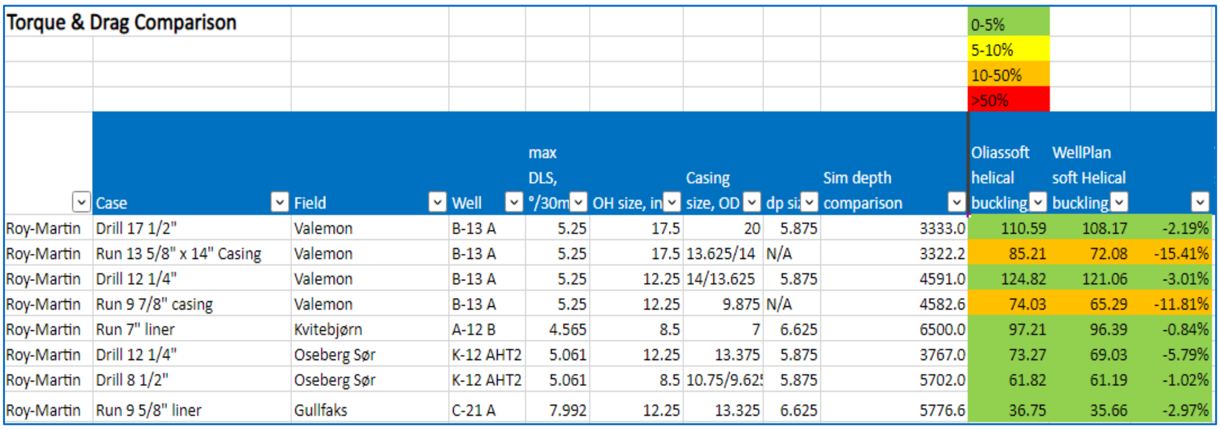

Torque & Drag Comparison

0-5%
5-10%
10-50%
>50%

	Case	Field	Well	max DLS, °/30m	OH size, in	Casing size, OD	dp si	Sim depth comparison	Oliassoft helical buckling	WellPlan soft Helical buckling	
Roy-Martin	Drill 17 1/2"	Valemon	B-13 A	5.25	17.5	20	5.875	3333.0	110.59	108.17	-2.19%
Roy-Martin	Run 13 5/8" x 14" Casing	Valemon	B-13 A	5.25	17.5	13.625/14	N/A	3322.2	85.21	72.08	-15.41%
Roy-Martin	Drill 12 1/4"	Valemon	B-13 A	5.25	12.25	14/13.625	5.875	4591.0	124.82	121.06	-3.01%
Roy-Martin	Run 9 7/8" casing	Valemon	B-13 A	5.25	12.25	9.875	N/A	4582.6	74.03	65.29	-11.81%
Roy-Martin	Run 7" liner	Kvitebjørn	A-12 B	4.565	8.5	7	6.625	6500.0	97.21	96.39	-0.84%
Roy-Martin	Drill 12 1/4"	Oseberg Sør	K-12 AHT2	5.061	12.25	13.375	5.875	3767.0	73.27	69.03	-5.79%
Roy-Martin	Drill 8 1/2"	Oseberg Sør	K-12 AHT2	5.061	8.5	10.75/9.62!	5.875	5702.0	61.82	61.19	-1.02%
Roy-Martin	Run 9 5/8" liner	Gullfaks	C-21 A	7.992	12.25	13.325	6.625	5776.6	36.75	35.66	-2.97%

Figure 4.4: Excel sheet containing ROB hookload data from OWD and WP and the percentage difference between them

4.1.5 Yield limit

One may observe from figure 4.5 that most of the difference between OWD and WP in percentage is below 2% for all cases. This means that the yield limit calculations used in simulations are within the acceptable range and can be used in Equinor systems.

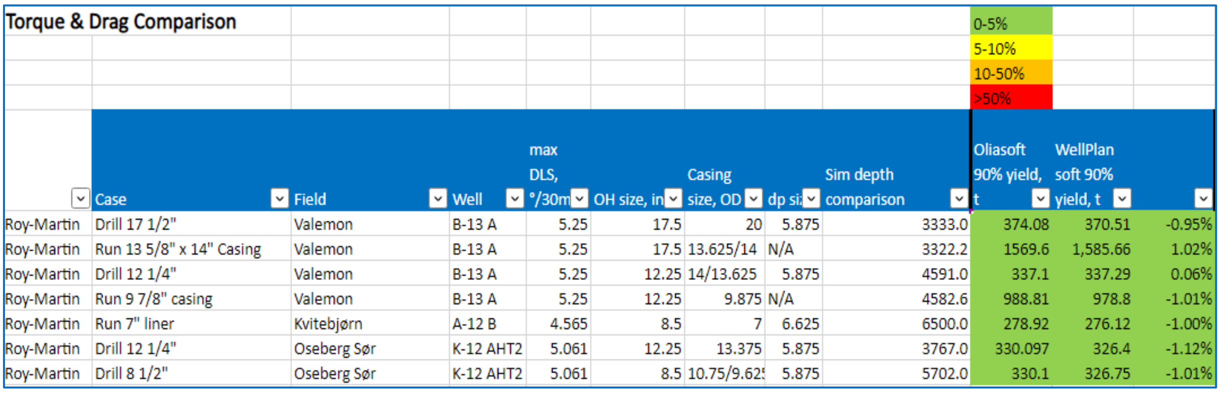

Torque & Drag Comparison

0-5%
5-10%
10-50%
>50%

	Case	Field	Well	max DLS, °/30m	OH size, in	Casing size, OD	dp si	Sim depth comparison	Oliasoft 90% yield, t	WellPlan soft 90% yield, t	
Roy-Martin	Drill 17 1/2"	Valemon	B-13 A	5.25	17.5	20	5.875	3333.0	374.08	370.51	-0.95%
Roy-Martin	Run 13 5/8" x 14" Casing	Valemon	B-13 A	5.25	17.5	13.625/14	N/A	3322.2	1569.6	1,585.66	1.02%
Roy-Martin	Drill 12 1/4"	Valemon	B-13 A	5.25	12.25	14/13.625	5.875	4591.0	337.1	337.29	0.06%
Roy-Martin	Run 9 7/8" casing	Valemon	B-13 A	5.25	12.25	9.875	N/A	4582.6	988.81	978.8	-1.01%
Roy-Martin	Run 7" liner	Kvitebjørn	A-12 B	4.565	8.5	7	6.625	6500.0	278.92	276.12	-1.00%
Roy-Martin	Drill 12 1/4"	Oseberg Sør	K-12 AHT2	5.061	12.25	13.375	5.875	3767.0	330.097	326.4	-1.12%
Roy-Martin	Drill 8 1/2"	Oseberg Sør	K-12 AHT2	5.061	8.5	10.75/9.62!	5.875	5702.0	330.1	326.75	-1.01%

Figure 4.5: Excel sheet containing ROB hookload data from OWD and WP and the percentage difference between them

4.1.6 Torque

One may observe from figure 4.6 that most of the difference between OWD and WP in percentage is below 4% for all cases. This means OWD Torque and Drag simulations are within the acceptable range and can be used in Equinor systems.

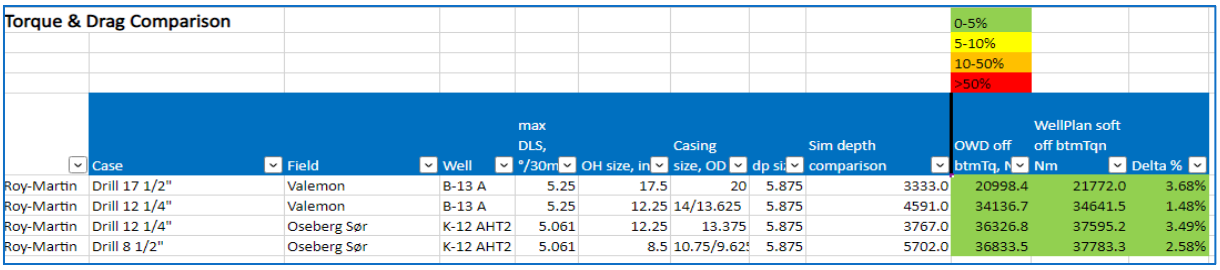

Torque & Drag Comparison

0-5%
5-10%
10-50%
>50%

	Case	Field	Well	max DLS, °/30m	OH size, in	Casing size, OD	dp si	Sim depth comparison	OWD off btmTq, N	WellPlan soft off btmTqn Nm	Delta %
Roy-Martin	Drill 17 1/2"	Valemon	B-13 A	5.25	17.5	20	5.875	3333.0	20998.4	21772.0	3.68%
Roy-Martin	Drill 12 1/4"	Valemon	B-13 A	5.25	12.25	14/13.625	5.875	4591.0	34136.7	34641.5	1.48%
Roy-Martin	Drill 12 1/4"	Oseberg Sør	K-12 AHT2	5.061	12.25	13.375	5.875	3767.0	36326.8	37595.2	3.49%
Roy-Martin	Drill 8 1/2"	Oseberg Sør	K-12 AHT2	5.061	8.5	10.75/9.62	5.875	5702.0	36833.5	37783.3	2.58%

Figure 4.6: Excel sheet containing ROB hookload data from OWD and WP and the percentage difference between them

4.1.7 Standpipe Pressure

One may observe from figure 4.7 that most of the difference between OWD and WP in percentage is below 10% for all cases. This means OWD hydraulic calculation for SPP used in simulations are within the acceptable range and can be used in Equinor systems.

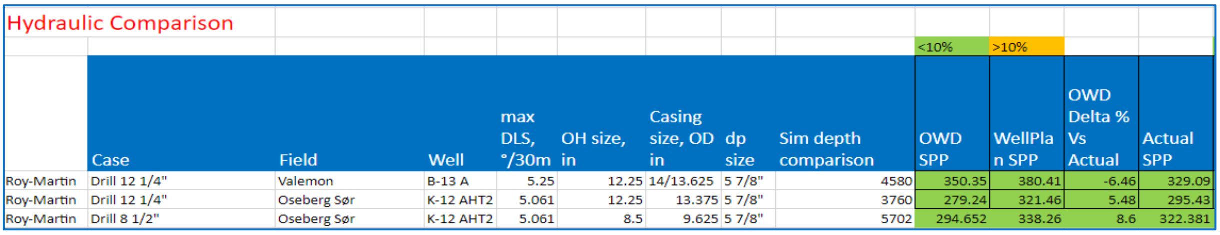

Hydraulic Comparison

<10%
>10%

	Case	Field	Well	max DLS, °/30m	OH size, in	Casing size, OD in	dp size	Sim depth comparison	OWD SPP	WellPlan SPP	OWD Delta % Vs Actual	Actual SPP
Roy-Martin	Drill 12 1/4"	Valemon	B-13 A	5.25	12.25	14/13.625	5 7/8"	4580	350.35	380.41	-6.46	329.09
Roy-Martin	Drill 12 1/4"	Oseberg Sør	K-12 AHT2	5.061	12.25	13.375	5 7/8"	3760	279.24	321.46	5.48	295.43
Roy-Martin	Drill 8 1/2"	Oseberg Sør	K-12 AHT2	5.061	8.5	9.625	5 7/8"	5702	294.652	338.26	8.6	322.381

Figure 4.7: Excel sheet containing ROB hookload data from OWD and WP and the percentage difference between them

4.1.8 Equivalent Circulating Density

One may observe from figure 4.8 that most of the difference between OWD and WP in percentage is below 2% for all cases. This means OWD hydraulic calculations for ECD used in simulations are within the acceptable range and can be used in Equinor systems.

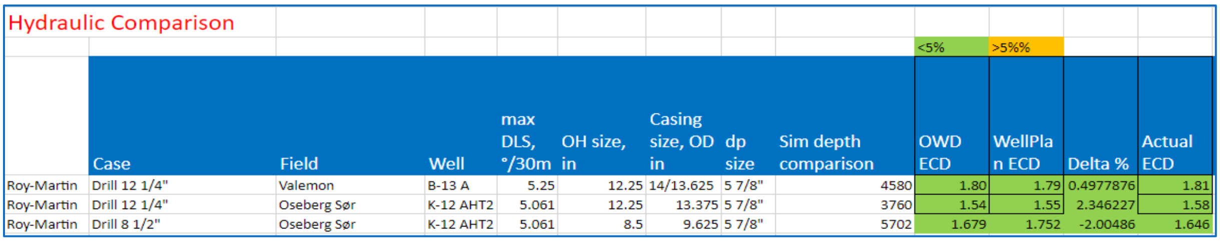

Hydraulic Comparison

<5%
>5%%

	Case	Field	Well	max DLS, °/30m	OH size, in	Casing size, OD in	dp size	Sim depth comparison	OWD ECD	WellPlan ECD	Delta %	Actual ECD
Roy-Martin	Drill 12 1/4"	Valemon	B-13 A	5.25	12.25	14/13.625	5 7/8"	4580	1.80	1.79	0.4977876	1.81
Roy-Martin	Drill 12 1/4"	Oseberg Sør	K-12 AHT2	5.061	12.25	13.375	5 7/8"	3760	1.54	1.55	2.346227	1.58
Roy-Martin	Drill 8 1/2"	Oseberg Sør	K-12 AHT2	5.061	8.5	9.625	5 7/8"	5702	1.679	1.752	-2.00486	1.646

Figure 4.8: Excel sheet containing ROB hookload data from OWD and WP and the percentage difference between them

5 Conclusion

This thesis work presents analysis of and verification of the mechanical and hydraulics modules of Oliasoft well design software. For this, the commonly and widely used Landmark/Wellplan^{TM} software is used as reference from which the Oliasoft Well Design (OWD) simulation result deviations will be evaluated for the verification of the OWD software qualifying the Equinor's acceptable requirement or not.

The overall analysis results with regards to the acceptance of the OWD Torque and Drag module and Hydraulics module showed that:

- Based on the rotating Off Bottom simulation, the OWD showed less than 1% deviation from the WP for all seven cases. This makes the OWD Torque and Drag module being within the acceptable range of the Equinor system.
- Based on the Pulling Out Off the Hole simulation scenario, the OWD exhibited less than 1% deviation from WP for the seven cases. One of the cases has shown 1.59% deviations. However, the overall results still show that the mechanical Torque and Drag of OWD is within the acceptable range of the Equinor system.
- Based on the Running Into the Hole simulation scenario, the OWD deviation from WP in is below 1% for all cases. This verify that the OWD Torque and Drag simulations are within the acceptable range set by the Equinor system.
- Based on the Buckling limit, results show that about five of the considered cases exhibited that the OWD percentile deviation from the WP is below 5%. On the other hand, one case has shown of the case studies has shown 15.4% deviation. This thesis advice Equinor to do further investigation regarding the Buckling limit module since the theory of buckling used different scaling factor, which are derived based on different load-deformation assumptions. However, in terms of case studies, about 75% of the case studies results obtained from the OWD deviation from the WP are within the acceptable range of the Equinor system.
- Based on the Yield limit, OWD showed less than 2% deviation from WP for all seven cases. This verify that the OWD Yield limit module is within the acceptable range of the Equinor system.
- Based on the Torque simulation, OWD showed less than 4% deviation from WP for all cases. This makes the OWD Torque module being within the acceptable range of the Equinor system.
- Based on the Standpipe Pressure simulation, OWD showed less than 9% deviation from the Real-Time data in all cases. This verify that the OWD Standpipe Pressure module are within acceptable range set by the Equinor system.
- Based on the Equivalent Circulating Density simulation, result show that OWD exhibited less than 3% deviation from the Real/Time data in all cases. This result makes the OWD Equivalent Circulating Density module within the acceptable range of the Equinor system.

6 References

1. Mirhaj, E. Kaarstad, and B.S. Aadnoy. Improvement of torque-and-drag modeling in long-reach wells. Modern Applied Science, 5(5):10–28, 2011. https://doi.org/10.5539/mas.v5n5p10
2. B.S. Aadnoy, M. Fazaelizadeh, and G. Hareland. A 3-dimensional analytical model for wellbore friction. Journal of Canadian Petroleum Technology, 49(10), 2010. SPE-141515- PA. https://doi.org/10.2118/141515-PA
3. B.S. Aadnoy and K Andersen. Friction analysis for long-reach wells. IADC/SPE Drilling Conference, Dallas, Texas, March 1998, 1998. SPE 39391. https://doi.org/10.2118/39391-MS
4. T Tveitdal. Torque & drag analyses of North Sea wells using new 3d model. Master's thesis, University of Stavanger, Faculty of Science and Technology, 2011.
5. E.E. Maidla and A.K. Wojtanowicz. Field method of assessing borehole friction for directional well casing. Middle East Oil Show, 7-10 March, Bahrain, page 85, 1987. SPE-15696-MS. https://doi.org/10.2118/15696-MS
6. R. F. Mitchell. Tubing buckling – the state of the art. Society of Petroleum Engineers, 23(4), December 2008. SPE-104267-PA. https://doi.org/10.2118/104267-PA
7. A. Lubinski. A study of the buckling of rotary drilling strings. Am Pet Inst., 224(1):123 –165, May 1950. http://www.ajer.org/v6(05).html
8. Nwonodi Roland Ifeanyi1, Adali Francis, and Tswenma Tsokwa. Predicting drillstring buckling. American Journal of Engineering Research, 6(5):301 – 311, May 2017. http://www.ajer.org/v6(05).html
9. R. F. Mitchell. Exact analytical solution for pipe buckling in vertical and horizontal wells. Society of Petroleum Engineers, 7(4), December 2002. SPE-72079-PA. https://doi.org/10.2118/72079-PA
10. A. Lubinski, W. S. Althouse, and J. L. Logan. Helical buckling of tubing sealed in packers. Society of Petroleum Engineers, 14(6), June 1962. SPE-178-PA. https://doi.org/10.2118/178-PA
11. Gao and W-J. Huang. A review of down-hole tubular string buckling in well engineering. Petroleum Science, 12(3):443 – 457, 2015. https://doi.org/10.1007/s12182-015-0031-z
12. C.A. Johancsik, D.B. Friesen, and R. Dawson. Torque and drag in directional wells prediction and measurement. Journal of Petroleum Technology, 36(6):987 – 992, 1984. SPE-11380-PA. http://dx.doi.org/10.2118/11380-PA
13. Mitchell, R.F. and Samuel, R. 2009. How Good Is the Torque/Drag Model? SPE Drilling & Completion **24** (1): 62-71. SPE-105068-PA. https://doi.org/10.2118/105068-PA

14. Mason, C.J. and Chen, D.C.K. 2007. Step Changes Needed to Modernize T&D Software. Paper SPE/IADC 104609 presented at the SPE/IADC Drilling Conference, Amsterdam, The Netherlands, 20-22 February. https://doi.org/10.2118/104609-MS
15. Aadnoy, B.S. 2006. Mechanics of Drilling. Aachen, Germany: Shaker Verlag.
16. Oliasoft Truls M. Larsen. Technical specification torque and drag “soft string model”. Online PDF. Torque & Drag | Oliasoft Documentation
17. Landmark’s technical specification for **WellPlan™**. 2019.
18. Aadnoy. B, Cooper. I, Miska.S, Mithell. R.F, Payne. M.L. Advanced Drilling and Well Technology. Society of Petroleum Engineers, 2009. ISBN: 987-1-55563-145-1
19. L. Robinson. Drill bit pressure loss. Americal association of drilling engineers, 2010. AADE-10DF-HO-26
20. R. Rubiandini. Equation for estimating mud minimum rate for cuttings transport in an inclined-until-horizontal well. Society of Petroleum Engineers, SPE/IADC Middle East Drilling Technology Conference, 8-10 November, Abu Dhabi, United Arab Emirates, 1999. SPE-57541. Doi: https://doi.org/10.2118/57541-MS.
21. T.I. Larsen, A.A. Pilehvari, and J.J. Azar. Development of a new cuttings transport model for high angle wellbores including horizontal wells. Society of Petroleum Engineers, 12(02), 1997. SPE-25872-PA. Doi: https://doi.org/10.2118/25872-PA
22. A.T Bourgoyne Jr, K.K. Millheim, M.E. Chenevert and F.S. Young Jr. Applied Drilling Engineering. Society of Petroleum Engineers, 1991. ISBN: 978-1-55563-001-0
23. R.F. Mitchell. Buckling Analysis in Deviated Wells: A Practical Method. Presented in the SPE Annual Technical Conference and Exhibition, 1996. SPE-36761-MS. Doi: https://doi.org/10.2118/36761-MS

7 Appendix

7.1 Valemon

7.1.1 B-13 A: Drill 17 ½” section

Hole Section

Section Type	Section Depth (m)	Section Length (m)	Shoe Depth (m)	ID (in)	Drift (in)	Eff. Hole Diameter (in)	Coefficient of Friction	Linear Capacity (L/m)	Volume Excess (%)
Riser	68.92	68.92		19			0.1	182.92	
Casing	1181.7	1112.78	1181.7	18.73	18.7	24	0.2	177.76	
Open Hole	3333	2151.3		17.5		17.5	0.2	155.18	0

String Details

Type	**Length (m)**	**Depth (m)**	**Body**		**Stabilizer / Tool Joint**				**Weight**	**Material**	**Grade**	**Class**
			OD (in)	**ID (in)**	**Avg Joint Length (m)**	**Length (m)**	**OD (in)**	**ID (in)**				
Drill Pipe	3035.575	3035	5.875	5.045	9.14	0.6	7	3.75	26.3	S-135_2 [SH]	S-135_2 [SH]	P
Heavy Weight	40	3075	6.625	4.5	9.14	1.22	7	4	70.31	S-135_2 [SH]	1340 MOD [SH]	
Jar	9.75	3085.	8.25	3	9.75				154.36	S-135_2 [SH]	4145H MOD (2) [SH]	
Heavy Weight	200	3285.33	5.875	4	9.14	0.6	7	4	55.36	CS_1340 MOD	1340 MOD	
Sub	0.9	3286.23	6.96	3	0.9				71.84	S-135_2 [SH]	4145H MOD (2)	
Drill Collar	18	3304.23	9.5	3	9.14				208.4	S-135_2 [SH]	4145H MOD (2)	
Sub	0.9	3305.13	9.5	3	0.9				100.73	S-135_2 [SH]	4145H MOD (2)	
Stabilizer	1.94	3307.07	9.5	3	1.94				192.5	SAE 4145	SAE 4145	
MWD	6.4	3313.47	9	3	6.4				200	SAE 4145 [SH]	SAE 4145 [SH]	
Stabilizer	1.5	3314.97	9.5	3.5	1.5				192.45	S-135_2 [SH]	4145H MOD (2)	
MWD	8.4	3323.37	9.5	6.25	8.4				177.26	SAE 4145 [SH]	SAE 4145 [SH]	
Stabilizer	1.83	3325.2	9.5	3	1.83				192.45	S-135_2 [SH]	4145H MOD (2)	
Rotary Steerable System	7.5	3332.7	11	3	7.5				177.26	CS_API 5CT	V-150	
Bit	0.305	3333	17.5		0.3				565			

Fluid Rheology Data

Temperature (°C)	Pressure (bar)	Base Density (sg)	Ref Fluid Properties	PV (Mulnf) (cp)	N’	K’ (Pa*s^n')	YP (Tau0) (lbf/100ft²)	Fann Data	
								Speed (rpm)	Dial (°)
50	1.01	1.46	Yes	40.32	0.85	0.1136	12.08	600	94
								300	57
								200	43
								100	30
								6	13
								3	12

T&D Settings

Measured Depth of Bit	3333.00 m	Bending Stress Magnification	Yes
Block Weight	65.00 tonne	Stiff String Analysis	No
Enable Sheave Friction Correction	No	Viscous Torque and Drag	Yes
Pump Rate	0.0 L/min	Contact Force Normalization Length	m
Mechanical Efficiency (Single Sheave)		Lines Strung	
		Side Force	N
Offset from Wellhead	m	Angle at Wellhead	°

Run Parameters

Start MD	0.00 m	End MD	3333.00 m
Step Size	20.00 m		

Normal Analysis Operational Parameters

Drilling	WOP/Overpull (tonne)	Torque at Bit (N-m)
Rotating On Bottom	15.00	13000.0
Slide Drilling	NA	NA

Backreaming	NA	NA
Rotating Off Bottom	Y	
Tripping	Speed (m/min)	RPM (rpm)
Tripping In	18.29	0
Tripping Out	18.29	0

Friction Factors

Section Type	Coefficient of Friction
Casing	0.20
Open Hole	0.20
Riser	0.10

Hyd Cuttings Loading Calculation Option

Rate of Penetration	50.00 m/hr	Rotary Speed	150 rpm
Cuttings Diameter	0.240 in	Cuttings Density	2.145 sg
Bed Porosity	36.00 %	MD Calculation Interval	20.00 m

HYD Pump Pressure Information

Maximum Surface Pressure	0.00 bar	Pump Rate	5200.0 L/min
Maximum Pump Power	0.000 kW	Maximum Allowable Pump Rate	0.0 L/min
Use Roughness	N		
Pipe Roughness	NA	Annulus Roughness	NA
Booster Pump		Injection Depth	NA
Injection Temperature	NA	Injection Rate	NA
Include Tool Joint Pressure Losses			
Include Back Pressure		Back Pressure	bar
Sea Floor Returns	N	Sea Water Density	NA

7.1.2 B-13 A: Drill 12 ¼" section

Hole Section

Section Type	Section Depth (m)	Section Length (m)	Shoe Depth (m)	ID (in)	Drift (in)	Eff. Hole Diameter (in)	Coefficient of Friction	Linear Capacity (L/m)	Volume Excess (%)
Riser	68.92	68.92		18.75			0.1	178.14	
Casing	1400	1331.08	1400	12.4	12.25	17.5	0.2	77.91	
Casing	3322.2	1922.2	3322.2	12.375	12.25	17.5	0.2	77.6	
Open Hole	4591	1268.8		12.25		12.25	0.3	76.04	0

String Details

Type	Length (m)	Depth (m)	Body		Stabilizer / Tool Joint				Weight	Material	Grade	Class
			OD (in)	ID (in)	Avg Joint Length (m)	Length (m)	OD (in)	ID (in)				
Drill Pipe	4270.197	4270.2	5.875	5.153	12.5	0.671	7	4.25	27.05	S-135_2 [SH]	S-135_2 [SH]	1
Heavy Weight	**40**	**4310.2**	**5.875**	**4**	**12**	**1.219**	**7**	**4**	**49.17**	**CS_1340 MOD**	**1340 MOD**	
Sub	1	4311.2	7.92	3.25	1				100.73	S-135_2 [SH]	4145H MOD	
Jar	**9.75**	**4320.95**	**8.28**	**3.25**	**9.75**				**135.29**	**CS_API 5D/7**	**4145H MOD**	
Heavy Weight	234	4554.95	5.825	4	12	1.219	7	4	49.17	CS_1340 MOD	1340 MOD	
Sub	**0.914**	**4555.86**	**7.92**	**3**	**0.91**				**147**	**CS_API 5D/7**	**4145H MOD**	
Sub	0.914	4556.78	7.92	3	0.91				147	CS_API 5D/7	4145H MOD	
Drill Collar	**15**	**4571.78**	**8**	**2.812**	**9.14**				**152.76**	**S-135_2 [SH]**	**4145H MOD (2)**	
MWD	7.498	4579.27	8.25	5.9	7.5				92.39	SAE 4145	SAE 4145	
MWD	**5.486**	**4584.76**	**8.25**	**2.81**	**5.49**				**155.56**	**SAE 4145**	**SAE 4145**	
Stabilizer	1.5	4586.26	9	3	1.5				192.45	4145H MOD (2) [SH]	4145H MOD (2) [SH]	
Rotary Steerable System	**4.45**	**4590.71**	**9.25**	**3**	**4.45**				**150**	**CS_API 5D/7**	**4145H MOD**	
Bit	0.29	4591	12.25		0.29				462.31			

Fluid Data

Fluid	**OBM WARP 1,75**	**Type**	**Mud**
Mud Base Type	**Synthetic**	**Base Fluid**	**ACCOLADE**
Rheology Model	**Herschel-Bulkley**	**Foamed**	

Compressibility Data

Oil (Vol)/Water (Vol)	**57.00 %/12.00 %**	**Reference Temperature**	**50.000**

Salt Content (wt)	**10.00**	**Average Solid Gravity**	**3.700**

Rheology Data

Temperature (°C)	Pressure (bar)	Base Density (sg)	Ref Fluid Properties	PV (Mulnf) (cp)	N'	K' (Pa*s^n')	YP (Tau0) (lbf/100ft²)	Fann Data	
								Speed (rpm)	Dial (°)
50	**1.01**	**1.76**	**Yes**	**51.5**	**0.9**	**0.1031**	**3.112**	**600**	**105**
								300	58
								200	**41**
								100	23
								6	**5**
								3	3.5

T&D Settings

Measured Depth of Bit	**4591.00 m**	**Bending Stress Magnification**	**Yes**
Block Weight	**65.00 tonne**	**Stiff String Analysis**	**No**
Enable Sheave Friction Correction	**No**	**Viscous Torque and Drag**	**No**
Pump Rate	**0.0 L/min**	**Contact Force Normalization Length**	**9.45 m**
Mechanical Efficiency (Single Sheave)	**97.00**	**Lines Strung**	**12**
		Side Force	**N**
Offset from Wellhead	**m**	**Angle at Wellhead**	**°**

Run Parameters

Start MD	**0.00 m**	**End MD**	**4591.00 m**
Step Size	**20.00 m**		

Normal Analysis Operational Parameters

Drilling	WOP/Overpull (tonne)	Torque at Bit (N-m)
Rotating On Bottom	**10.00**	**5000.0**
Slide Drilling	**NA**	**NA**
Backreaming	**NA**	**NA**
Rotating Off Bottom	**Y**	
Tripping	**Speed (m/min)**	**RPM (rpm)**
Tripping In	**18.29**	**0**
Tripping Out	**18.29**	**0**

Friction Factors

Section Type	Coefficient of Friction
Casing	**0.20**
Casing	0.20
Open Hole	**0.30**
Riser	0.10

HYD Cuttings Loading Calculation Option

Rate of Penetration	**25.00 m/hr**	**Rotary Speed**	**180 rpm**
Cuttings Diameter	**0.240 in**	**Cuttings Density**	**2.600 sg**
Bed Porosity	**36.00 %**	**MD Calculation Interval**	**20.00 m**

HYD Pump Pressure Information

Maximum Surface Pressure	**0.00 bar**	**Pump Rate**	**4000.0 L/min**
Maximum Pump Power	**0.000 kW**	**Maximum Allowable Pump Rate**	**5150.8 L/min**
Use Roughness	**N**		
Pipe Roughness	**NA**	**Annulus Roughness**	**NA**
Booster Pump		**Injection Depth**	**NA**
Injection Temperature	**NA**	**Injection Rate**	**NA**
Include Tool Joint Pressure Losses			
Include Back Pressure		**Back Pressure**	**bar**
Sea Floor Returns	**N**	**Sea Water Density**	**NA**

7.1.3 B-13 A: Run 13 5/8”x14” casing

Hole Section

Section Type	Section Depth (m)	Section Length (m)	Shoe Depth (m)	ID (in)	Drift (in)	Eff. Hole Diameter (in)	Coefficient of Friction	Linear Capacity (L/m)	Volume Excess (%)
Riser	68.92	68.92		19			0.1	182.92	
Casing	**1181.7**	**1112.78**	**1181.7**	**18.7**	**18.7**	**22**	**0.15**	**177.19**	
Open Hole	3333	2151.3		17.5		17.5	0.15	155.18	0

String Details

Type	**Length (m)**	**Depth (m)**	**Body**		**Stabilizer / Tool Joint**				**Weight**	**Material**	**Grade**	**Class**
			OD (in)	**ID (in)**	**Avg Joint Length (m)**	**Length (m)**	**OD (in)**	**ID (in)**				
Casing	1406	1406	14	12.4	12.19		15.337	12.667	114	SM125S (Active)	SM125S (ACTIVE)	

Casing	**1926**	**3332**	**13.625**	**12.375**	**12.19**		**14.754**	**12.444**	**88.2**	**SM125S (Active)**	**SM125S (ACTIVE)**	
Casing Shoe	1	3333	14	10.5	1				88	SM125S (Active)	SM125S (ACTIVE)	

Fluid Data

Fluid	**Versatec 1.46 (actual B13)**	**Type**	**Mud**
Mud Base Type	**Synthetic**	**Base Fluid**	**ACCOLADE**
Rheology Model	**Herschel-Bulkley**	**Foamed**	

Compressibility Data

Oil (Vol)/Water (Vol)	**55.00 %/24.00 %**	**Reference Temperature**	**21.111**
Salt Content (wt)	**10.00**	**Average Solid Gravity**	**3.670**

Rheology Data

Temperature (°C)	Pressure (bar)	Base Density (sg)	Ref Fluid Properties	PV (MuInf) (cp)	N'	K' (Pa*s^n')	YP (Tau0) (lbf/100ft²)	Fann Data	
								Speed (rpm)	Dial (°)
40	**1.01**	**1.46**	**Yes**	**51.39**	**0.81**	**0.1878**	**10.328**	**600**	**111**
								300	67
								200	**51**
								100	34
								6	**12**
								3	11

Settings

Measured Depth of Bit	**3333.00 m**	**Bending Stress Magnification**	**No**
Block Weight	**64.00 tonne**	**Stiff String Analysis**	**Yes**
Enable Sheave Friction Correction	**No**	**Viscous Torque and Drag**	**Yes**
Pump Rate	**0.0 L/min**	**Contact Force Normalization Length**	**9.45 m**
Mechanical Efficiency (Single Sheave)	**97.00**	**Lines Strung**	**12**
		Side Force	**N**
Offset from Wellhead	**m**	**Angle at Wellhead**	**°**

Run Parameters

Start MD	**0.00 m**	**End MD**	**3322.20 m**
Step Size	**20.00 m**		

Normal Analysis Operational Parameters

Drilling	WOP/Overpull (tonne)	Torque at Bit (N-m)
Rotating On Bottom	**NA**	**NA**
Slide Drilling	**NA**	**NA**
Backreaming	**NA**	**NA**
Rotating Off Bottom	**N**	
Tripping	**Speed (m/min)**	**RPM (rpm)**
Tripping In	**18.29**	**0**
Tripping Out	**18.29**	**0**

Friction Factors

	Cased Hole	Open Hole
Back Reaming	0.00	0.00
Rotating off Botton	0.00	0.00
Tripping In	0.15	0.10
Tripping Out	0.15	0.20

7.1.4 B-13 A: Run 9 5/8" casing

Hole Section

Section Type	Section Depth (m)	Section Length (m)	Shoe Depth (m)	ID (in)	Drift (in)	Eff. Hole Diameter (in)	Coefficient of Friction	Linear Capacity (L/m)	Volume Excess (%)
Riser	68.99	68.99		19			0.2	182.92	
Casing	**1400**	**1331.01**	**1400**	**12.4**	**12.4**		**0.2**	**77.91**	
Casing	3322.2	1922.2	3322.2	12.375	12.375		0.2	77.6	
Open Hole	**4582.6**	**1260.4**				**12.25**	**0.25**	**76.04**	**0**

String Details

Type	**Length (m)**	**Depth (m)**	**Body**		**Stabilizer / Tool Joint**				**Weight**	**Material**	**Grade**	**Class**
			OD (in)	**ID (in)**	**Avg Joint Length (m)**	**Length (m)**	**OD (in)**	**ID (in)**				
Casing	4581.6	4581.6	9.875	8.625	12.27		11.054	8.693	66.4	SM125S (Active)	SM125S (ACTIVE)	
Casing Shoe	**1**	**4582.6**	**10.25**	**8.625**	**1**				**60.48**	**Q-125 (Active)**	**Q-125 (ACTIVE)**	

Fluid Data

Fluid	**WARP 1.76 sg**	**Type**	**Mud**
Mud Base Type	**Synthetic**	**Base Fluid**	**ACCOLADE**
Rheology Model	**Herschel-Bulkley**	**Foamed**	

Compressibility Data

Oil (Vol)/Water (Vol)	**58.00 %/13.00 %**	**Reference Temperature**	**21.111**
Salt Content (wt)	**10.00**	**Average Solid Gravity**	**3.950**

Rheology Data

Temperature (°C)	Pressure (bar)	Base Density (sg)	Ref Fluid Properties	PV (Mulnf) (cp)	N'	K' (Pa*s^n')	YP (Tau0) (lbf/100ft²)	Fann Data	
								Speed (rpm)	Dial (°)
50	**1.01**	**1.76**	**Yes**	**47.49**	**0.93**	**0.0769**	**3.19**	**600**	**98**
								300	53
								200	**37**
								100	21
								6	**4.5**
								3	3.5

Settings

Measured Depth of Bit	**4582.60 m**	**Bending Stress Magnification**	**No**
Block Weight	**62.00 tonne**	**Stiff String Analysis**	**Yes**
Enable Sheave Friction Correction	**No**	**Viscous Torque and Drag**	**Yes**
Pump Rate	**0.0 L/min**	**Contact Force Normalization Length**	**9.45 m**
Mechanical Efficiency (Single Sheave)	**97.00**	**Lines Strung**	**12**
		Side Force	**N**
Offset from Wellhead	**m**	**Angle at Wellhead**	**°**

Run Parameters

Start MD	**0.00 m**	**End MD**	**4582.60 m**
Step Size	**20.00 m**		

Normal Analysis Operational Parameters

Drilling	WOP/Overpull (tonne)	Torque at Bit (N-m)
Rotating On Bottom	**NA**	**NA**
Slide Drilling	**NA**	**NA**
Backreaming	**NA**	**NA**
Rotating Off Bottom	**Y**	
Tripping	**Speed (m/min)**	**RPM (rpm)**
Tripping In	**18.29**	**0**
Tripping Out	**18.29**	**0**

Friction Factors

Section Type	Coefficient of Friction
Casing	**0.20**
Casing	0.20
Open Hole	**0.25**
Riser	0.20

Geothermal Gradient Data

Ambient Temperature	15.000 °C	Mudline Temperature	4.000 °C
Temperature @ Depth	120.000 °C @ 4332.96 m	Gradient	2.81 °C/100m

7.2 Oseberg Sør

7.2.1 K-12 AHT2: Drill 12 ¼" Section

Hole Section

Section Type	Section Depth (m)	Section Length (m)	Shoe Depth (m)	ID (in)	Drift (in)	Eff. Hole Diameter (in)	Coefficient of Friction	Linear Capacity (L/m)	Volume Excess (%)
Riser	162	162		18.75			0.1	178.14	
Casing	**2886**	**2724**	**2886**	**12.347**	**12.25**	**14.75**	**0.25**	**77.25**	
Open Hole	3751	865		12.25		12.25	0.35	76.04	0

String Details

Type	Length (m)	Depth (m)	Body		Stabilizer / Tool Joint				Weight	Material	Grade	Class
			OD (in)	ID (in)	Avg Joint Length (m)	Length (m)	OD (in)	ID (in)				
Drill Pipe	3585.011	3585.01	5.875	5.153	13.72	0.75	7	4.25	26.04	S-135_2 [SH]	S-135_2 [SH]	P
Heavy Weight	**86.4**	**3671.41**	**5.875**	**4**	**9.4**	**1.499**	**7**	**4**	**57.01**	**CS_1340 MOD**	**1340 MOD**	
Jar	10	3681.41	8	3	10				154.36	CS_API 5D/7	4145H MOD	
Heavy Weight	**38.4**	**3719.81**	**5.875**	**4**	**9.4**	**1.499**	**7**	**4**	**57.01**	**CS_1340 MOD**	**1340 MOD**	
Stabilizer	2.2	3722.01	8	2.813	2.2				149.92	CS_API 5D/7	4145H MOD	

Sub	0.914	3722.93	7.92	3	0.91				147	CS_API 5D/7	4145H MOD	
Sub	0.6	3723.53	9.5	3	0.6				216	SS07 [SH]	SS07 [SH]	
MWD	5.55	3729.08	8.25	3.125	5.55				179.42	SS07 [SH]	SS07 [SH]	
Sub	2.75	3731.83	6.625	2.812	2.75				201.59	SS07 [SH]	SS07 [SH]	
MWD	3.7	3735.53	9.53	2.95	3.7				315.83	SS07 [SH]	SS07 [SH]	
MWD	7	3742.53	9.69	4	7				316.5	SS07 [SH]	SS07 [SH]	
MWD	2.3	3744.83	9.524	2.68	2.3				207.64	SS07 [SH]	SS07 [SH]	
Stabilizer	1.825	3746.65	9.5	3.5	1.82				324.56	SS07 [SH]	SS07 [SH]	
MWD	1.5	3748.15	9	2.5	1.5				440	SAE 4145 [SH]	SAE 4145 [SH]	
MWD	2.5	3750.65	9.5	3	2.5				443	SAE 4145 [SH]	SAE 4145 [SH]	
Bit	0.35	3751	12.25		0.35				80.64			

String Nozzles

Component	MD (m)	Port Open	Diverted Flow	Amount Diverted (%)	Nozzle (32nd")	TFA (in²)
Polycrystalline Diamond Bit	3,767	NA	NA	NA	1.0X15.0 2.0X16.0 3.0X18.0	1.311

Fluid Data

Fluid	1,50 sg CARBO-SEA	Type	Mud
Mud Base Type		Base Fluid	
Rheology Model	Herschel-Bulkley	Foamed	

Compressibility Data

Oil (Vol)/Water (Vol)	57.00 %/21.00 %	Reference Temperature	21.111
Salt Content (wt)	10.00	Average Solid Gravity	3.675

Rheology Data

Temperature (°C)	Pressure (bar)	Base Density (sg)	Ref Fluid Properties	PV (MuInf) (cp)	N'	K' (Pa*s^n')	YP (Tau0) (lbf/100ft²)	Fann Data	
								Speed (rpm)	Dial (°)
50	1	1.51	Yes	41.62	0.83	0.1351	7.489	600	92
								300	55
								200	41
								100	26
								6	9
								3	8

Geothermal Gradient Data

Ambient Temperature	15.000 °C	Mudline Temperature	4.000 °C
Temperature @ Depth	110.000 °C @ 2748.10 m	Gradient	4.10 °C/100m

Settings

Measured Depth of Bit	3751.00 m	Bending Stress Magnification	Yes
Block Weight	58.00 tonne	Stiff String Analysis	No
Enable Sheave Friction Correction	No	Viscous Torque and Drag	No
Pump Rate	0.0 L/min	Contact Force Normalization Length	9.45 m
Mechanical Efficiency (Single Sheave)	97.00	Lines Strung	12
		Side Force	N
Offset from Wellhead	m	Angle at Wellhead	°

Run Parameters

Start MD	0.00 m	End MD	3751.00 m
Step Size	20.00 m		

Normal Analysis Operational Parameters

Drilling	WOP/Overpull (tonne)	Torque at Bit (N-m)
Rotating On Bottom	15.00	6000.0
Slide Drilling	NA	NA
Backreaming	NA	NA
Rotating Off Bottom	Y	
Tripping	Speed (m/min)	RPM (rpm)
Tripping In	30.00	0
Tripping Out	30.00	0

Friction Factors

Section Type	Coefficient of Friction
Riser	0.10
Casing	0.25
Open Hole	0.35

Cuttings Loading Calculation Option

Rate of Penetration	**25.00 m/hr**	**Rotary Speed**	**120 rpm**
Cuttings Diameter	**0.125 in**	**Cuttings Density**	**2.600 sg**
Bed Porosity	**36.00 %**	**MD Calculation Interval**	**30.00 m**

Pump Pressure Information

Maximum Surface Pressure	**350.00 bar**	**Pump Rate**	**4200.0 L/min**
Maximum Pump Power	**2500.000 kW**	**Maximum Allowable Pump Rate**	**L/min**
Use Roughness	**N**		
Pipe Roughness	**NA**	**Annulus Roughness**	**NA**
Booster Pump	**N**	**Injection Depth**	**NA**
Injection Temperature	**NA**	**Injection Rate**	**NA**
Include Tool Joint Pressure Losses			
Include Back Pressure		**Back Pressure**	**bar**
Sea Floor Returns	**N**	**Sea Water Density**	**NA**

7.2.2 K-12 AHT2: Drill 8 ½” Section

Hole Section

Section Type	Section Depth (m)	Section Length (m)	Shoe Depth (m)	ID (in)	Drift (in)	Eff. Hole Diameter (in)	Coefficient of Friction	Linear Capacity (L/m)	Volume Excess (%)
Riser	162	162		18.75			0.1	178.14	
Casing	**322**	**160**	**322**	**9.66**	**9.504**		**0.2**	**47.28**	
Casing	1544	1222	1544	8.535	8.5		0.2	36.91	
Casing	**3762**	**2218**	**3762**	**8.535**	**8.5**		**0.2**	**36.91**	
Open Hole	5702	1940		8.5		8.5	0.3	36.61	0

String Details

Type	**Length (m)**	**Depth (m)**	**Body**		**Stabilizer / Tool Joint**				**Weight**	**Material**	**Grade**	**Class**
			OD (in)	**ID (in)**	**Avg Joint Length (m)**	**Length (m)**	**OD (in)**	**ID (in)**				
Drill Pipe	3371.19	3371	5.875	5.153	13.72	0.75	7	4.25	26.04	S-135_2 [SH]	S-135_2 [SH]	P
Drill Pipe	**2200**	**5571**	**5**	**4.276**	**13.72**	**0.646**	**6.625**	**3.25**	**22.92**	**S-135_2 [SH]**	**S-135_2 [SH]**	**P**
Heavy Weight	45	5616	5	3	9.4	1.448	6.625	3	52.27	1340 MOD [SH]	1340 MOD [SH]	
Jar	**10**	**5626**	**6.5**	**2.75**	**10**				**91.79**	**CS_API 5D/7**	**4145H MOD [SH]**	
Heavy Weight	27	5653	5	3	9.4	1.448	6.625	3	52.27	1340 MOD [SH]	1340 MOD [SH]	
Stabilizer	**2.2**	**5655**	**6.75**	**2.25**	**2.2**				**83.27**	**CS_API 5D/7**	**4145H MOD**	
Sub	1	5656	6.72	2.16	1				108.25	CS_API 5D/7	4145H MOD	
Sub	**2**	**5658**	**7**	**2.812**	**2**				**110**	**SS07 [SH]**	**SS07 [SH]**	
MWD	8	5666	6.75	2.875	8				94.08	SS07 [SH]	SS07 [SH]	
Sub	**2.2**	**5668**	**5**	**2.25**	**2.2**				**67.2**	**SS07 [SH]**	**SS07 [SH]**	
MWD	2.4	5670	7.024	1.744	2.4				111.55	SS07 [SH]	SS07 [SH]	
Stabilizer	**2.5**	**5673**	**7**	**2.5**	**2.5**				**67.2**	**SS07 [SH]**	**SS07 [SH]**	
MWD	4.9	5678	7.28	1.75	4.9				109.53	SS07 [SH]	SS07 [SH]	
MWD	**8.5**	**5686**	**5.2**	**2.5**	**8.5**				**114.23**	**SS07 [SH]**	**SS07 [SH]**	
Stabilizer	1.31	5688	7	2.785	1.31				84	SS07 [SH]	SS07 [SH]	
MWD	**6.7**	**5694**	**7**	**2.5**	**6.7**				**114.23**	**SS07 [SH]**	**SS07 [SH]**	
MWD	2.2	5697	7.024	1.744	2.2				111.55	SS07 [SH]	SS07 [SH]	
Stabilizer	**1.3**	**5698**	**7**	**2.5**	**1.3**				**67.2**	**SS07 [SH]**	**SS07 [SH]**	
MWD	1.1	5699	7.2	3	1.1				400	SAE 4145 [SH]	SAE 4145 [SH]	
Stabilizer	**2.2**	**5701**	**7**	**2.5**	**2.2**				**124.99**	**SS07 [SH]**	**SS07 [SH]**	
Bit	0.3	5702	8.5		0.3				200			

String Nozzles

Component	MD (m)	Port Open	Diverted Flow	Amount Diverted (%)	Nozzle (32nd")	TFA (in²)
Polycrystalline Diamond Bit	**5,702**	**NA**	**NA**	**NA**	**6.0X13.0**	**0.778**

Fluid Data

Fluid	**OV2 Askepott 8,5" 1,36 sg DELTA-TEQ**	**Type**	**Mud**
Mud Base Type		**Base Fluid**	
Rheology Model	**Herschel-Bulkley**	**Foamed**	

Compressibility Data

Oil (Vol)/Water (Vol)	**62.00 %/20.00 %**	**Reference Temperature**	**30.000**
Salt Content (wt)	**16.00**	**Average Solid Gravity**	**2.600**

Rheology Data

Temperature (°C)	Pressure (bar)	Base Density (sg)	Ref Fluid Properties	PV (Mulnf) (cp)	N'	K' (Pa*s^n')	YP (Tau0) (lbf/100ft²)	Fann Data	
								Speed (rpm)	Dial (°)
50	**1.01**	**1.37**	**Yes**	**41.53**	**0.86**	**0.1148**	**7.755**	**600**	**92**
								300	54
								200	**40**
								100	26
								6	**9**
								3	8

Geothermal Gradient Data

Ambient Temperature	15.000 °C	Mudline Temperature	4.000 °C
Temperature @ Depth	110.000 °C @ 2748.10 m	Gradient	4.10 °C/100m

Settings

Measured Depth of Bit	**5702.00 m**	**Bending Stress Magnification**	**Yes**
Block Weight	**58.00 tonne**	**Stiff String Analysis**	**No**
Enable Sheave Friction Correction	**No**	**Viscous Torque and Drag**	**No**
Pump Rate	**0.0 L/min**	**Contact Force Normalization Length**	**9.45 m**
Mechanical Efficiency (Single Sheave)	**97.00**	**Lines Strung**	**12**
		Side Force	**N**
Offset from Wellhead	**m**	**Angle at Wellhead**	**°**

Run Parameters

Start MD	**0.00 m**	**End MD**	**5702.00 m**
Step Size	**20.00 m**		

Normal Analysis Operational Parameters

Drilling	WOP/Overpull (tonne)	Torque at Bit (N-m)
Rotating On Bottom	**10.00**	**4000.0**
Slide Drilling	**NA**	**NA**
Backreaming	**NA**	**NA**
Rotating Off Bottom	**Y**	
Tripping	**Speed (m/min)**	**RPM (rpm)**
Tripping In	**30.00**	**0**
Tripping Out	**30.00**	**0**

Friction Factors

Section Type	Coefficient of Friction
Casing	**0.20**
Riser	0.10
Casing	**0.20**
Casing	0.20
Open Hole	**0.30**

Cuttings Loading Calculation Option

Rate of Penetration	**30.00 m/hr**	**Rotary Speed**	**140 rpm**
Cuttings Diameter	**0.125 in**	**Cuttings Density**	**2.600 sg**
Bed Porosity	**36.00 %**	**MD Calculation Interval**	**20.00 m**

Pump Pressure Information

Maximum Surface Pressure	**0.00 bar**	**Pump Rate**	**2150.0 L/min**
Maximum Pump Power	**0.000 kW**	**Maximum Allowable Pump Rate**	**0.0 L/min**
Use Roughness	**N**		
Pipe Roughness	**NA**	**Annulus Roughness**	**NA**
Booster Pump	**N**	**Injection Depth**	**NA**
Injection Temperature	**NA**	**Injection Rate**	**NA**
Include Tool Joint Pressure Losses			
Include Back Pressure		**Back Pressure**	**bar**
Sea Floor Returns	**N**	**Sea Water Density**	**NA**

Run Parameters

Start MD	**0.00 m**	**End MD**	**5702.00 m**
Step Size	**20.00 m**		

7.3 Kvitebjørn

7.3.1 A-12 B: Run 7" liner

Hole Section

Section Type	Section Depth (m)	Section Length (m)	Shoe Depth (m)	ID (in)	Drift (in)	Eff. Hole Diameter (in)	Coefficient of Friction	Linear Capacity (L/m)	Volume Excess (%)
Riser	30	30		18.75			0.1	178.14	
Casing	**425**	**395**	**425**	**9.56**	**9.5**	**12.25**	**0.18**	**46.31**	
Casing	6465.6	6040.6	6465.6	8.553	8.397	12.25	0.18	37.07	
Open Hole	**6947**	**481.4**				**8.5**	**0.3**	**36.61**	**0**

String Details

Type	**Length (m)**	**Depth (m)**	**Body**		**Stabilizer / Tool Joint**				**Weight**	**Material**	**Grade**	**Class**
			OD (in)	**ID (in)**	**Avg Joint Length (m)**	**Length (m)**	**OD (in)**	**ID (in)**				
Drill Pipe	6206.87	6206.87	5	4.276	13.6	0.318	6.625	3.5	21.83	S-135_2 [SH]	S-135_2 [SH]	P
Heavy Weight	**188.13**	**6395**	**5**	**2.75**	**9.14**	**0.762**	**6.625**	**2.75**	**55.3**	**CS_1340 MOD**	**1340 MOD**	
Casing	550	6945	7	6.004	12.19		7.787		35	P-110 (Active)	P-110 (ACTIVE)	
Casing Shoe	**1**	**6946**	**7**	**5.675**	**1**				**45**	**L-80 [SH]**	**L-80 [SH]**	

Fluid Data

Fluid	**Warp 1.85sg**	**Type**	**Mud**
Mud Base Type	**Oil**	**Base Fluid**	**ESCAID110**
Rheology Model		**Foamed**	

Compressibility Data

Oil (Vol)/Water (Vol)	**57.00 %/12.00 %**	**Reference Temperature**	**20.000**
Salt Content (wt)	**8.00**	**Average Solid Gravity**	**4.100**

Rheology Data

Temperature (°C)	Pressure (bar)	Base Density (sg)	Ref Fluid Properties	m’	N’	PV (MuInf) (cp)	YP (Tau0) (lbf/100ft²)	Fann Data	
								Speed (rpm)	Dial (°)
50	**1.01**	**1.85**	**Yes**	**0.62**	**0.62**	**31.84**	**1.132**	**600**	**72**
								300	38
								200	**27**
								100	15
								6	**2.5**
								3	2

Geothermal Gradient Data

Ambient Temperature	26.667 °C	Mudline Temperature	4.444 °C
Temperature @ Depth	119.287 °C @ 4451.00 m	Gradient	2.73 °C/100m

Settings

Measured Depth of Bit	**6946.00 m**	**Bending Stress Magnification**	**No**
Block Weight	**48.00 tonne**	**Stiff String Analysis**	**Yes**
Enable Sheave Friction Correction	**No**	**Viscous Torque and Drag**	**Yes**
Pump Rate	**0.0 L/min**	**Contact Force Normalization Length**	**9.60 m**
Mechanical Efficiency (Single Sheave)	**97.00**	**Lines Strung**	**12**
		Side Force	**N**
Offset from Wellhead	**m**	**Angle at Wellhead**	**°**

Run Parameters

Start MD	**0.00 m**	**End MD**	**6946.00 m**
Step Size	**20.00 m**		

Normal Analysis Operational Parameters

Drilling	WOP/Overpull (tonne)	Torque at Bit (N-m)
Rotating On Bottom	**NA**	**NA**
Slide Drilling	**NA**	**NA**
Backreaming	**NA**	**NA**
Rotating Off Bottom	**Y**	
Tripping	**Speed (m/min)**	**RPM (rpm)**
Tripping In	**18.29**	**0**
Tripping Out	**18.29**	**0**

Friction Factors

	Cased Hole	Open Hole
Rotating on Bottom	0.18	0.30
Slide Drilling	0.22	0.30
Back Reaming	0.22	0.30
Rotating off Botton	0.02	0.20
Tripping In	0.15	0.20
Tripping Out	0.15	0.20

7.4 Gullfaks:

7.4.1 C-21 A: Run 9 5/8” liner

Hole Section

Section Type	Section Depth (m)	Section Length (m)	Shoe Depth (m)	ID (in)	Drift (in)	Eff. Hole Diameter (in)	Coefficient of Friction	Linear Capacity (L/m)	Volume Excess (%)
Riser	84.1	84.102		13			0.05	85.63	

Casing	**1761.1**	**1676.998**	**1761.1**	**12.375**	**12.25**		**0.2**	**77.6**	
Casing	2045	283.9	2045	10.772	10.625		0.25	58.8	
Open Hole	**5772.6**	**3727.6**				**12.25**	**0.25**	**76.04**	**0**

String Details

Type	**Length (m)**	**Depth (m)**	**Body**		**Stabilizer / Tool Joint**				**Weight**	**Material**	**Grade**	**Class**
			OD (in)	**ID (in)**	**Avg Joint Length (m)**	**Length (m)**	**OD (in)**	**ID (in)**				
Drill Pipe	1150.5	1150.5	6.625	5.901	9.14	0.482	8	4.25	31.54	S-135_2 [SH]	S-135_2 [SH]	P
Heavy Weight	**500**	**1650.5**	**6.625**	**4.75**	**9.6**	**1.524**	**8.25**	**4.75**	**69.66**	**CS_API 5D/7**	**4145H MOD**	
Casing	4121.1	5771.6	9.625	8.535	12.19		10.575		53.5	P-110 (Active)	P-110 (ACTIVE)	
Casing Shoe	**1**	**5772.6**	**9.675**	**8**	**1**				**60.48**	**L-80 [SH]**	**L-80 [SH]**	

Fluid Data

Fluid	**1.66 sg OBM WARP**	**Type**	**Mud**
Mud Base Type	**Synthetic**	**Base Fluid**	**ACCOLADE**
Rheology Model	**Herschel-Bulkley**	**Foamed**	

Compressibility Data

Oil (Vol)/Water (Vol)	**57.00 %/12.00 %**	**Reference Temperature**	**20.000**
Salt Content (wt)	**8.00**	**Average Solid Gravity**	**4.000**

Rheology Data

Temperature (°C)	Pressure (bar)	Base Density (sg)	Ref Fluid Properties	PV (MuInf) (cp)	N’	K’ (Pa*s^n’)	YP (Tau0) (lbf/100ft²)	Fann Data	
								Speed (rpm)	Dial (°)
50	**1**	**1.66**	**Yes**	**34.38**	**0.92**	**0.0617**	**1.54**	**600**	**72**
								300	39
								200	**27**
								100	15
								6	**2.5**
								3	2

Geothermal Gradient Data

Ambient Temperature	10.000 °C	Mudline Temperature	20.000 °C
Temperature @ Depth	175.011 °C @ 4176.43 m	Gradient	4.00 °C/100m

Settings

Measured Depth of Bit	**5772.60 m**	**Bending Stress Magnification**	**No**
Block Weight	**34.00 tonne**	**Stiff String Analysis**	**Yes**
Enable Sheave Friction Correction	**No**	**Viscous Torque and Drag**	**Yes**
Pump Rate	**0.0 L/min**	**Contact Force Normalization Length**	**9.45 m**
Mechanical Efficiency (Single Sheave)	**97.00**	**Lines Strung**	**12**
		Side Force	**N**
Offset from Wellhead	**m**	**Angle at Wellhead**	**°**

Run Parameters

Start MD	**400.00 m**	**End MD**	**5770.00 m**
Step Size	**20.00 m**		

Normal Analysis Operational Parameters

Drilling	WOP/Overpull (tonne)	Torque at Bit (N-m)
Rotating On Bottom	**NA**	**NA**
Slide Drilling	**NA**	**NA**
Backreaming	**NA**	**NA**
Rotating Off Bottom	**Y**	
Tripping	**Speed (m/min)**	**RPM (rpm)**
Tripping In	**5.00**	**0**
Tripping Out	**5.00**	**0**

Friction Factors

Section Type	Coefficient of Friction
Casing	**0.20**
Casing	0.25
Open Hole	**0.25**
Riser	0.05